UNIVERSITA' DEGLI STUDI DI MILANO-BICOCCA
Facoltà di Medicina e Chirurgia
Scuola di Dottorato in Scienze Mediche Sperimentali e Cliniche
Corso di Dottorato in Neuroscienze - ciclo XXV -

IN VITRO BLOOD BRAIN BARRIER MODELS AS A SCREENING TOOL FOR BRAIN TARGETED NANOBASED DRUG DELIVERY SYSTEMS

Coordinatore: Chiar. mo Prof. Guido Cavaletti
Tutor: Chiar. mo Prof. Guido Cavaletti

Ilaria Nadia Cambianica

Anno Accademico 2011-2012

CONTENTS

ABSTRACT

The blood brain barrier (BBB) is a selective biological barrier located at the brain capillaries, that protects the central nervous system (CNS) by monitoring exchanges between blood and brain. The BBB controls and regulates the composition of the CNS environment and it still constitutes the main obstacle for drug delivery to the brain (Weiss N. et al., 2009). The significant scientific and industrial interest in the physiology and pathology of the BBB led to the development of vast number of *in vitro* BBB models. Even though no "ideal" model exists yet, some of the currently available ones are very useful to investigate permeability, transport mechanisms and cellular and molecular events which occur at the BBB level. New strategies for brain targeted drug delivery exploit endogenously expressed transporters to elicit drug passage across the BBB. Among them, nanoparticles represent a promising tool, since they are biocompatible and biodegradable, and they can be functionalized to target the BBB (De Boer A.G. and Gaillard P.J., 2007) (Beija M et al., 2012; Caruthers S.D. et al., 2007; Moghimi S.M. et al., 2005).

In this study we settled in vitro BBB models to identify, with high-throughput screening, the most promising nanoliposomes (NL) for combined BBB crossing and binding of amyloid peptides, for joint therapy and diagnosis of Alzheimer's disease (AD).

Firstly, we characterized two *in vitro* models of BBB, based on immortalized cell lines of human and rat origin, the hCMEC/D3 and RBE4 cells, respectively. We tested the trans-endothelial electrical resistance (TEER) and the endothelial permeability (PE) of small hydrophilic compounds: our results, in agreement with data reported in literature, lead us to conclude that these cellular models are suitable for their employment as high-throughput screening tools.

Subsequently, we tested NL mono-functionalized with three different peptides, the apolipoproteinE derived peptide (the ApoE monomer (mApoE), amino acids 141-150), its tandem dimer (dApoE) $(141\text{-}150)_2$, and the Human Immunodeficency Virus type 1 (HIV-1) transactivator of transcription (TAT) peptide. We evaluated their uptake and PE; we selected the TAT functionalization as the best performing concerning cellular uptake, and the mApoE functionalization when considering both the internalization and PE. Once assessed the dynamics of mono-functionalized NL interactions with endothelial cells, we investigated mApoE- and dApoE-NL loading a curcumin-derivative (Re F. et al., 2011) to bind Aβ. We clearly demonstrated that the mApoE-functionalization allows a better drug cellular internalization, whereas dApoE-NL enhances drug PE at the highest extent.

We then considered mApoE- and dApoE-NL exposing the Aβ targeting ligands phosphatidic acid (PA) or cardiolipin (CL), demonstrating that PA-mApoE-NL showed the highest cellular uptake and PE. We also studied TAT-NL exposing curcumin derivative3 (Airoldi C. et al., 2011) for Aβ binding, clearly indicating that TAT functionalization increased cellular uptake and PE of curcumin derivative3-NL. We also studied intracellular fate of NL double functionalized, exposing Aβ targeting ligands, and no co-localization was detected with acidic cellular compartments, suggesting that NL may escape from lysosomal degradative pathway.

Taken together, these results indicate that the formulations herein analyzed are suitable tools for brain targeted drug and contrast agent delivery. We suggest further development of mApoE and dApoE-NL entrapped with a drug payload for their employment as BBB endothelial cell or brain targeted drug delivery tools, respectively. We also selected PA-mApoE-NL and curcumin derivative3-TAT-NL as promising tools for their employment in combination for AD therapy and diagnosis. Further studies, based also on in vivo experiments, are needed to evaluate NL suitability for clinical exploitation.

Finally, we inquired the endocytic mechanisms that mediates the entry of NL in the endothelial cells of BBB. We employed RNA interference technique to down-regulate caveolin1 expression. Our preliminary data suggest that caveolin1 and the related caveolae-mediated endocytosis pathway may account for 40% of mApoE-NL cellular uptake. Future directions regard the down-regulation of other proteins specifically involved in different endocytic mechanisms, i.e. clathrin-mediated and adsoprptive endocytosis, in order to assess which endocytic mechanisms may account for ApoE and TAT-NL internalization.

1 - INTRODUCTION

The central nervous system (CNS) is the most critical and sensitive system in the human body. Proper neuronal function necessitates a highly regulated extracellular environment, wherein the concentrations of ions such as Na^+, K^+, and Ca^{2+} must be maintained within very narrow ranges. Furthermore, the metabolic demands of nervous tissue are considerable, with the CNS accounting for approximately 20% of oxygen consumption in humans. The CNS is also extremely sensitive to a wide range of chemicals; many of the substances we consume in our diet, although readily metabolized and excreted without harm to peripheral organ systems, are in fact quite neurotoxic. It is therefore essential that the interface between the CNS and the peripheral circulatory system functions as a dynamic regulator of ion balance, a facilitator of nutrient transport, and a barrier to potentially harmful molecules. This homeostatic aspect of the cerebral microcirculation, historically referred to as the “blood brain barrier” (BBB), performs all of these functions. (Hawkins B.T. and Thomas P.D., 2005)

The BBB has a total blood vessel length of about 600 km and an estimated surface area of $20m^2$, which is similar to the blood-cerebrospinal-fluid barrier (BCSFB). Because of the BCSFB faces the cerebral spinal fluid (CSF) and not the blood, the BBB, with its total blood flow and wide vascular bed, is considered the most important global influx barrier to the CNS (De Boer A.G. and Gaillard P.J., 2007).

1.1 - THE BLOOD BRAIN BARRIER

Due to its morphological and functional peculiarities, the blood-brain barrier (BBB) is the structure that prevalently controls the brain microenvironment. The BBB is localized at the endothelial cells constituting the brain capillaries (Engelhardt B. and Sorokin L., 2009).

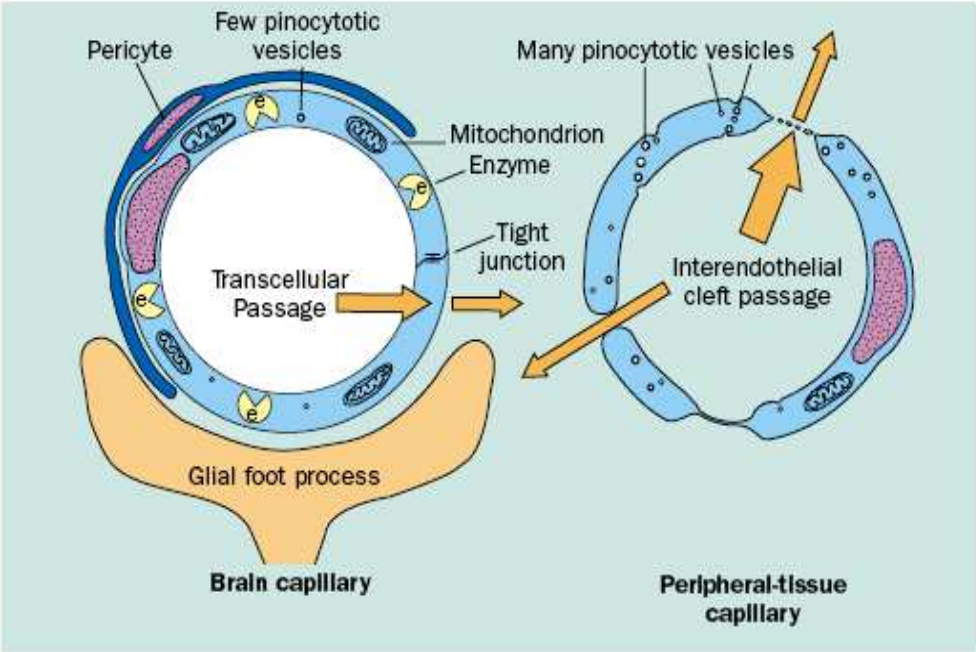

Fig. 1: Schematic representation of the main differences between brain capillaries and peripheral capillaries. *Cornford E.M. and Cornford M.E., 2002*

Compared to peripheral capillary endothelial cells, the BBB endothelial cells show higher number of mitochondria, associated to strong metabolic activity and the polarized expression of membrane receptors and transporters. The complex network of tight junctions interconnecting the cells prevents from free paracellular diffusion of hydrophilic molecules. The lack of fenestrations and the paucity of pinocytotic vesicles prevent from transcellular free passage of solutes (Engelhardt B. and Sorokin L., 2009; Weiss N. et al., 2009; Cornford E.M. and Cornford M.E., 2002).

The fully differentiated BBB consists of a complex unit comprising the endothelial cells with their basement membrane, the pericytes, perivascular antigen presenting cells and astrocytes endfeet with their associated parenchymal basement membrane (Engelhardt B. and Sorokin L., 2009).

The discovery of a barrier between the vascular system and the CNS dates back to 1880s, when Paul Erlich showed that if certain dyes were injected into the vascular system, they were rapidly taken up by the peripheral organs, with the exception of the brain and the spinal cord. These results were interpreted as a lack of CNS affinity for the dyes. A few years later, an Erlich's associate, Goldman, demonstrated that the same dyes, injected into the cerebrospinal fluid, were able to stain nervous tissue, but not peripheral organs. These results suggested that once within the CNS, the dyes were prevented to reach the vascular system. Other studies demonstrated that neurotoxic agents could be active on the CNS only when

directly injected into the brain, suggesting the existence of a barrier between blood and brain. It was the advancement of electron microscopy that led to the correlation of the barrier properties with the morphological features of the endothelial cells (Engelhardt B. and Sorokin L., 2009).

Some areas of the brain, which are located in the midline of the ventricular system, lack the BBB and constitute the circumventricular organs (CVOs). At these specific regions, brain capillaries are fenestrated and they allow communication between brain and blood through free diffusion of solutes and proteins, which is important for the proper function of these areas (Engelhardt B. and Sorokin L., 2009).

1.1.1 - Intercellular junction

The intercellular tight junctions (TJs) in CNS microvessels are the peculiar feature of BBB endothelial cells. They are a complex network of transmembrane (claudins, occludins and junctional adhesion molecules (JAM)-A, B and C) and cytoplasmic proteins (zonula occludens (ZO)-1, ZO-2, cingulin, junction-associated protein AF-6 and junction-associated antigen 7H6), linked to actin cytoskeleton (Engelhardt B. and Sorokin L., 2009).

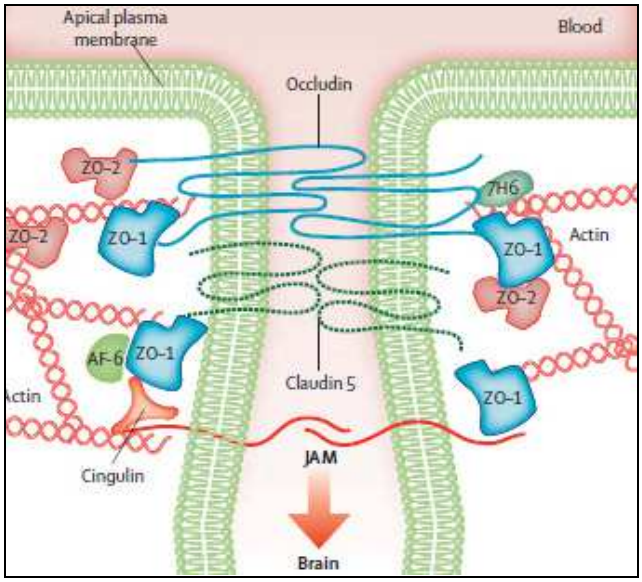

Fig. 2: Components of tight junctions (TJs). *Neuwelt E. et al., 2008*

Occludins present two extracellular loops, which provide the TJ “gate like” structure, four trans-membrane and three cytoplasmic domains. The last ones comprise one intracellular short turn, the N-terminal and the 150 amino-acid long C-terminus domain, which associates with ZO proteins and interacts with regulatory proteins (Redzic Z., 2011). Experiments of occludin deletion in mice resulted in multiple alterations throughout the organism without

apparent morphological and functional alterations at the TJs (Saitou M. et al., 2000). These studies suggested that occludins could be not essential for proper TJ establishment in vivo. However, other studies demonstrated that abnormal occludin lacking the N-terminal domain caused impaired TJ function in endothelial cell monolayers in vitro (Redzic Z., 2011). Occludins appear thus to be more related to TJ control and regulation than to TJ establishment (Wolburg H. et al., 2009). Occludin regulation at TJs has been demonstrated to depend on its phosphorylation and on its specific recycling mediated by two TJ associated proteins, Rab13, a member of the Rab family G-proteins and MICAL-L2, a Rab 13 binding protein (Terai T. et el, 2006; Wolburg H. et al., 2009).

Claudin protein family comprises 24 members, showing specific distribution in cells and tissues. The endothelial cell-specific claudin-5 but also claudin-3 and claudin-12 have been demonstrated to be localized at the CNS microvascular endothelial cells in mice and men (Engelhardt B. and Sorokin L., 2009; Wolburg H. et al, 2009). All the protein family members share the same structural pattern, which is characterized by four membrane-spanning regions, two extracellular loops and two intracellular domains, the short N-terminus and the long C-terminus sequences. The extracellular domains account for the TJ formation through protein-protein homophilic interactions and provide paracellular charge selectivity, so that each type of claudin regulates the diffusion of a specific range of solute size. The C-terminus sequence is responsible for binding to ZO-1, 2 and 3. Proper claudin interactions are essential for selective ion paracellular permeability (Redzic Z., 2011).

JAMs proteins A, B an C are integral membrane proteins which belong to the Ig superfamily. Their structure is characterized by an extracellular N-terminus domain, an extracellular domain, a membrane-spanning domain and a cytoplasmic C-terminus tail. At the extracellular side, they have different patterns of homophilic and heterophilic interactions with JAM molecules. Their intracellular C-terminus mediates interactions with ZO-1, cingulin, AF-6, 7H6 and scaffold proteins, and it exposes sites for phosphorylation, which could be substrates for PKC (Redzic Z., 2011).

The membrane associated guanylate kinase protein (MAGUK) family members ZO-1, 2 and 3, are localized at the peripheral cell cytoplasm, and link the integral membrane protein to actin cytoskeleton. They are also involved in the control of claudin spatial distribution (Redzic Z., 2011). The myosin-like protein cingulin exposes ZO protein binding sites at the globular head, and it can bind to other cingulin molecules at the tail. Known actin binding sites are localized on the ZO proteins and on the cingulins, and also on claudins and occludins (Redzic Z., 2011; Huber J.D. et al., 2001).

TJs in the CNS are dynamic structures that can go through modifications, following cell signalling pathways or as a consequence of protein-protein interactions. Alterations in TJ integrity and proper function have been clearly showed in diseases. Moreover, variations in occludin and claudin mRNA expression have been detected in cultured cells, compared to freshly isolated cells (Redzic Z., 2011).

Adherent junctions have been demonstrated to be important regulators of vessel permeability outside the CNS. At the BBB, adherent junctions do not directly regulate barrier permeability, but their proper establishment is required for the correct regulation of the TJ function. The primary component of BBB adherent junctions is vascular endothelial (VE)-cadherin, a Ca^{++}-regulated transmembrane protein which mediates cell-cell interaction through homophilic binding. Stabilization of the junctional complex is achieved by the linkage of VE-cadherin cytoplasmic tail to actin cytoskeleton mediated by β-catenin, α-actinin and vinculin (Engelhardt B. and Sorokin L., 2009). Recent studies demonstrated that adhesive interaction of VE-cadherin promotes claudin-5 expression at the transcriptional level, by inhibiting the transcription factor FoxO1 and preventing nuclear accumulation of β-catenin (Taddei A. et al., 2008). The adherent junction component β-catenin is strictly involved in TJ regulation and it is required for BBB maturation and function in vivo (Liebner S. et al., 2008).

1.1.2 - Astrocytes, leptomeningeal cells and pericytes

In the functional BBB unit, the vascular endothelium is ensheathed by a layer of astrocyte endfeet and associated leptomeningeal cells that coinvaginate with the endothelium during development and contribute to induce and maintain BBB permeability properties. Many studies on in vitro BBB models have demonstrated that astrocytes play an essential role in inducing BBB properties in endothelial cells. Due to BBB anatomical architecture, cell-cell communication is likely performed trough low molecular weight soluble factors (Engelhardt B. and Sorokin L., 2009), which could include glial-derived neurotrophic factor (GDNF), angiopoietin I and II (Weiss N. et al., 2009).

The 99% of the abluminal side of CNS microvessel basement membrane is covered by pericytes, but their role in BBB development or manteinance has not been clarified yet. The lack of investigations in this cell population biology is mainly due to the difficulty in isolating pericytes from the extra-cellular matrix (Engelhardt B. and Sorokin L., 2009).

Finally, neuronal innervation on brain capillary endothelial cells contributes in maintaining and modulating barrier properties (De Boer A.G. and Gaillard P.J., 2007).

1.1.3 - The basal membranes

In most tissues, two types of extracellular matrix (ECM) have been characterized: the basement membrane (BM) and the interstitial matrix. The former is a separation membrane and its function is to underlie polarized cells or ensheath myogenic tissues, nerves and adipocytes. It is a complex assembly of four major glycoprotein families, laminins, collagen type IV isoforms, heparan sulfate proteoglicans and nidogens. The latter is localized at the stroma of tissues and it interconnects cell layers. It is made up of fibrillar extracellular matrix proteins such as collagen types I, III, V and glycoproteins such as fibronectin or tenascins (Engelhardt B. and Sorokin L., 2009).

At the CNS, the interstitial matrix is little represented, due to the lack of tensile or elastic stress inside the CNS, and it contains low levels of fibrous proteins and of glycosaminoglycans. The major constituent of CNS extracellular matrix is thus the basement membrane (Engelhardt B. and Sorokin L., 2009). Two basement membranes can be distinguished at the CNS, the endothelial cell BM and the astroglial BM. The latter, with the addition of the leptomeningeal basement membrane, constitutes the parenchymal basement membrane. At CNS microvessels, where endothelial cell and parenchymal BM fuse, α4, α5 and α2 laminin chains but not α1 are expressed, and both perlecan and agrin heparan sulfate proteoglycans can be detected (Engelhardt B. and Sorokin L., 2009).

Although the basement membrane contribution to BBB properties has not been deeply studied yet, data showed that basement membrane components contribute to microvessel integrity and function (Engelhardt B. and Sorokin L., 2009).

1.1.4 - Transport of solutes

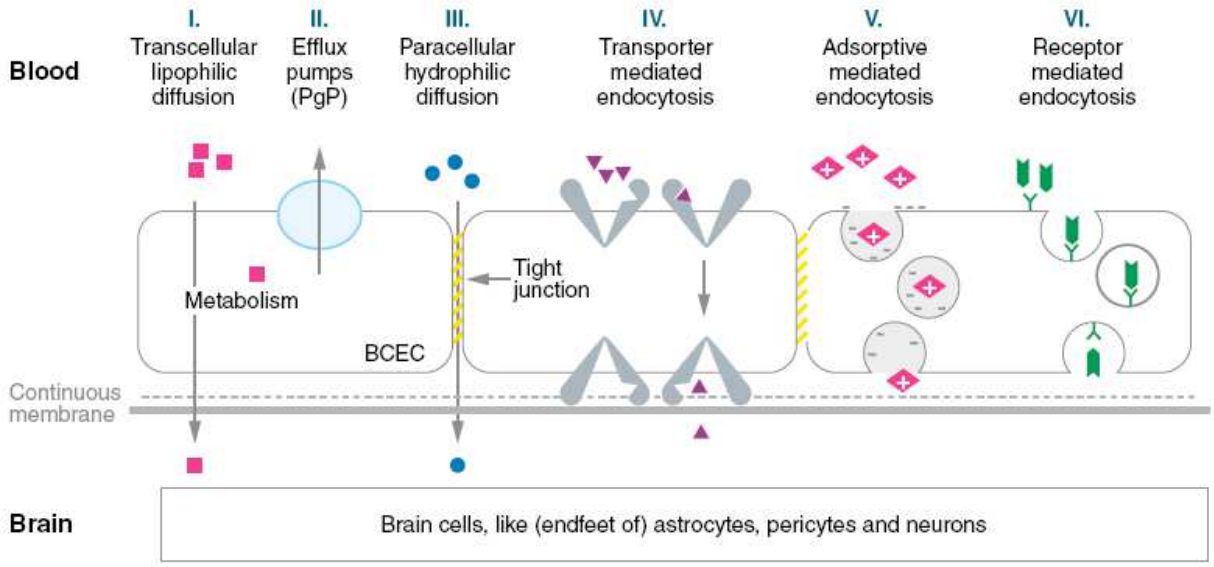

Fig. 3: Transport processes at the BBB. *A.G. De Boer and P.J. Gaillard, 2007*

Different transport mechanisms are represented at the BBB. Influx mechanisms can be divided into passive and active transports. Transcellular passive diffusion accounts for few small lipophilic molecules crossing the BBB. Paracellular diffusion of small hydrophilic compounds is instead strictly limited by TJs interconnecting endothelial cells and it is poorly represented. Active transport systems can be subdivided into adsorptive-, carrier-, and transporter-mediated transcytosis. Adsorptive-mediated trascytosis process is initiated by polycationic compound binding to cell membrane negative charges, followed by endocytosis and endosome formation. This process occurs with no involvement of receptors. Due to the low number of pinocytotic vescicles occurring at the BBB, this mechanism does not appear to be highly represented. Carrier-mediated transcytosis accounts for the delivery of nutrients, such as glucose and amino acids. It is highly substrate-specific and the transport rate strictly depends on the degree of the carrier occupation. Receptor-mediated transcytosis elicits larger molecules to enter the brain, and insulin receptor, transferring receptor, and the transporters for insulin like growth factor and for low density lipoproteins (LDL) have been involved in this process (Redzic Z., 2011; De Boer A.G. and Gaillard P.J., 2007). Despite their close apposition and their contact with physiological concentration of LDL, BBB endothelial cells up-regulate LDL receptor (LDLr) compared to peripheral endothelium. LDLr expression is modulated by astrocyte conditioning and it has been demonstrated to account for LDL

transcytosis in an *in vitro* model of BBB (Dehouck B. et al., 1997). Scavenger receptors SR-BI and SR-AI have also been detected at the BBB (De Boer A.G. and Gaillard P.J., 2007).

Efflux mechanisms are highly represented at the brain capillary endothelial cells, and they are mediated by transporters belonging to the ATP-binding cassette (ABC) protein superfamily. These transporters couple compound efflux against the concentration gradient to ATP-hydrolisis and they are the main responsible of drug and xenobiotics efflux from the brain (Redzic Z., 2011; De Boer A.G. and Gaillard P.J., 2007). Three transporter subfamilies belong to the ATP-binding cassette (ABC) transporter family: the multidrug-resistance proteins or P-glycoproteins (MRP, P-gp), the multidrug resistance-related proteins (MRPs) and the breast cancer-resistance protein (BCRP). These transporters show substrate specificity but overlapping features have also been detected (Redzic Z., 2011).

1.2 - DRUG DELIVERY TO CNS

The main obstacle in treating CNS disorders is to achieve a proper drug concentration inside the brain.

The net uptake of a drug by the brain through the BBB depends on the difference between the influx and efflux processes, which are controlled by several factors. The blood-brain concentration gradient is determined by the area under the blood-time curve and/or the maximal systemic concentration. Drug binding to plasma proteins or to blood cells defines the unbound drug fraction and may modulate drug uptake. Similar properties regulate drug efflux from the brain, except for the binding to the plasma proteins, which are not represented at the brain extracellular fluid (Scherrmann J.M., 2002).

Only some small molecules with proper lipophilicity, molecular weight and charge diffuse from blood to brain; it has been reported that approximately 98% of the small molecules and nearly all the large molecules cannot cross the BBB (Gabathuler R., 2009).

Different approaches have been developed to overcome the BBB and increase drug bioavailability at the CNS, invasive, pharmacological and physiological approaches.

1.2.1 - Invasive approaches

Intra-cerebro-ventricular infusion of drugs has been reported to lead to a very low drug diffusion in the cerebral parenchyma, only 1 to 2% of the injected drug being available at 1-2 mm from the injection site (Gabathuler R., 2009).

Convection-enhanced delivery is based upon the stereotactically guided insertion of a small-caliber catheter into the brain parenchyma, that allows drug injection and diffusion in the interstitial space. This technique has been shown to diffuse drug until 2 cm from the site of injection, however, some limitations occur, prevalently related to difficulty in reaching and infusing particular cerebral areas (Gabathuler R., 2009).

Intra-cerebral injection of a drug bolus or placement of biodegradable, chemotherapeutic impregnated devices into a tumor resection cavity rely on the diffusion principle to drive the drug into the brain. However, diffusion at the brain decreases exponentially with distance and a precise site of injection has to be determined (Gabathuler R., 2009).

Direct injection of recombinant adeno-associated virus (rAAV) or Lentiviruses (LV) expressing neurotrophins or carrying genetic material for gene therapy have been developed. However, this technique do not allow a global brain transduction, and a targeting efficiency. Moreover, it is associated with risks of raising immune response and of viral genome integration in host cells (Gabathuler R., 2009; De Boer A.G. and Gaillard P.J., 2007).

Disruption of BBB can be reached through osmotic solution injection, MRI-guided focused ultrasound and through application of bradykinin-analogue. The transient increase of BBB permeability allows drug penetration into the CNS (Gabathuler R., 2009). Opening the paracellular pathways is, of course, nonselective under the above circumstances, and albumin and excitatory neuro-transmitters and other potentially damaging substances may gain entry from blood to brain (Begley D. and Brightman M.W., 2003).

1.2.2 - Physiological and pharmacological approaches

Pharmacological approaches are prevalently based on chemical modification of the drug structure to increase its penetration across the BBB (Gabathuler R., 2009).

Evidence of increased drug permeability across the BBB following drug chemical modification or its association with lipid carriers has been provided (Gabathuler R., 2009). However, drug modification often results in the loss of therapeutic activity. Moreover, increasing molecule lipophilicity can also enhance its affinity for BBB efflux pumps (Gabathuler R., 2009).

Similar approaches have been developed using specific BBB receptors. Many studies were performed on Transferrin (Tf) and Insulin receptors, and drug conjugated with specific ligands, modified ligands or antibodies have been developed. The monoclonal antibody OX-26, which specifically binds Tf receptor at a different epitope from Tf, has been demonstrated to be a useful strategy to deliver drugs to the brain (Zhang Y. and Pardridge W.M., 2006). The

monoclonal antibody 83-14 against human Insulin Receptor has been created and it was shown to deliver conjugated drugs to CNS (Boado et al, 2007). Low density lipoprotein receptor related proteins 1 and 2 (LRP1, 2) which are expressed at the BBB, have been exploited to target drugs to CNS similarly to Tf and Insulin receptors. Recently, CRM197, a non toxic mutant of Diphteria Toxin has been developed as targeting vector to CNS. CRM197 goes through a well characterized and safe trancytotic process. This ability, along with its evolved intrinsic endosomal escape mechanism, makes CRM197 a promising tool for brain targeted drug delivery (De Boer A.G. and Gaillard P.J., 2007). However, its weak toxicity and the presence of antibodies in vaccinated people has limited its employment (Gabathuler R. et al., 2009). Adsorptive mediated endocytosis has been demonstrated at the BBB, and it is mediated by positively charged peptides interacting with negatively charged membrane regions. Drugs conjugated to cell penetrating peptides like TAT peptide have been utilized for increase the delivery to the brain and encouraging results were achieved (Gabathuler R., 2009).

Along with drug molecule modification, also drug encapsulation in delivery vectors based on nanoparticle systems are currently under development (Gabathuler R. et al., 2009).

1.3 - BBB IN CNS DISEASE

Many diseases affecting CNS, such as ischemic stroke, traumatic brain injuries, multiple sclerosis, infectious pathologies, primary or metastatic cancers and neurodegenerative diseases are associated to BBB failure, resulting in increased BBB permeability (Hawkins B.T. and Davis T.P., 2005; Weiss N. et al., 2009).

A common feature associated to CNS pathology and BBB increased permeability is the endothelium activation and the consequent expression of cytokines and adhesion molecules. This induces an increased movement of immune cells across the BBB, the secretion and transport of neuroimmune compounds by the cells that comprise the brain barriers, developmental changes in the BBB induced by perinatal inflammatory events and the traffic of pathogens across the BBB (Neuwelt E. et al., 2008).

Recently, BBB alterations have been associated to neurodegenerative diseases. Decreased number of mitochondria, increased amount of pinocytotic vesicles, collagen accumulation in basal membrane and necrosis at BBB endothelial cells in AD patient post-mortem brain biopsy had been already demonstrated (Weiss N. et al., 2009). More recently, functional BBB

alterations have been detected in AD patients compared to age-matched controls. Increased permeability has been detected using gadolinium-enhanced MRI or biochemical methods (Weiss N. et al., 2009). Recent studies correlate Aβ altered clearance at the BBB and its consequent accumulation at the CNS to both aberrant angiogenesis and endothelial cell senescence. Indeed, alterations at the endothelial cells are associated with low levels of Aβ clearance receptors and increased levels of its influx receptors (Zlokovic B.V., 2005). Moreover, increased expression of adhesion molecules at senile plaques suggest an inflammatory component involvement in the pathology progression (Weiss N. et al., 2009) and T lymphocyte cerebral infiltration has been detected in AD patients (Togo T. et al., 2002). In conclusion, research and clinical findings suggest that BBB dysfunctions could be involved in CNS pathology progression. Moreover, a better comprehension of BBB biology has led to delineate a putative role for BBB in the pathogenesis of neurodegenerative diseases, in particular following age-dependent alterations of its transport properties, as suggested by analysis performed on AD patients (Weiss N. et al., 2009).

Despite the presence of such broadly demonstrated alterations in CNS pathology, BBB has long been considered the major obstacle for drug delivery to CNS (Weiss N. et al., 2009).

1.4 - ALZHEIMER'S DISEASE

The problem of drug and also of contrast agent delivery across the BBB is still a challenge in treatment and diagnosis of Alzheimer's Disease (AD). Indeed, no therapies are available for this pathology, up to now, and certain diagnosis can be performed only after patient death. However, AD is becoming a world health problem. Indeed, AD is the most common form of dementia related to aging. It has been estimated that 24 million of people suffer for AD related dementia today, and this number is expected to double every 20 years, up to 42 million in 2020 and 81 million by 2040 (Ferri C.P. et al., 2005).

The first histopathological features associated to AD were extracellular amyloid plaques and intracellular neurofibrillary tangles, which up to now constitute the hallmarks of the pathology and the basis for post-mortem AD diagnosis. Synaptic degeneration, hippocamapal neuronal loss and aneuploidy are other features related to AD (Swerdlow R.H., 2007).

Amyloid plaques are accumulation of proteins in the form of β-pleated sheet fibrils, mainly composed of the 39-43 AA long peptide Amyloid β (Aβ), which is produced by Amiloyd

Precursor Protein (APP) proteolytic cleavage by secretases. APP is encoded by APP gene residing on chromosome 21. It is a type I transmembrane protein with a large extracellular domain, a membrane anchoring domain and a short intracellular C-terminus tail. Its physiological role has not been fully clarified, yet, and it appears to be involved in extracellular signal recognition, cell adhesion and apoptosis. In neurons, APP is involved in synaptogenesis, synaptic remodelling and neurite outgrowth. APP proteolytic cleavage can be performed through at least two different pathways; α-secretase or β-secretase cleavage generates a large secreted N-terminal peptide (sAPPα or sAPPβ respectively) and a C-terminal transmembrane peptide. This peptide is substrate for γ-secretase, which mediates an intramembrane proteolytic cleavage and generates p3 or Aβ peptides following α- or β-secretase activity, respectively. Along with these peptides, a 57-59 AA long APP-intracellular C-terminal peptide (AICP) is also released. The sequential β- and γ- secretase activity constitute the so-called amyloidogenic pathway (Buoso E. et al., 2010). Aβ degradation is mediated by enzymes, such as neprilysin and insulin degrading enzyme (IDE), which is down regulated in AD. APP proteolytic products are generated throughout the life, and increased Aβ production along with its reduced degradation could constitute the basis for its accumulation (Swerdlow R.H., 2007).

Neurofibrillary tangles are aggregates of abnormally configured, excessively phosphorylated tau proteins. Tau protein is usually associated to microtubule cytosckeleton and, opposing to undifferentiated cells, it is not phosphorylated in differentiated cells (Swerdlow R.H., 2007).

Characteristic features associated to cell cycle re-entry, such as increase in cyclin-dependent kinase (CDK) activity and DNA content, have been detected in AD patient brain, generating aneuploid neuronal nuclei with replicated chromosomes (Swerdlow R.H., 2007).

Sporadic AD accounts for the great majority of patients, and autosomal dominant inherited AD forms have been reported, which frequently show early onset. Except for the age of onset, no other differences in the neuropathological and clinical phenotype have been showed between the inherited and the sporadic variants of AD, thus suggesting shared pathological mechanisms. Mutations in APP gene or in presenilin 1 and 2 genes, which are part of the γ-secretases complex, have been related to inherited variants of AD. APOE gene, which encodes for apolipoproteinE show different variants (polymorphisms) which are distributed throughout the population. APOE4 variant has been related to younger age AD onset and with a related longer lifetime AD risk, compared to APOE2 and 3 variants (Swerdlow R.H., 2007; Selkoe D.J., 2001).

AD origin has not been fully understood, and different hypothesis rose to explain disease origin and evolution, the best known being the amyloid cascade hypothesis. According to this hypothesis, altered APP processing drives Aβ production and plaques formation. This leads to neurodegeneration, neuronal loss and consequential clinical dementia syndrome associated to AD (Swerdlow R.H., 2007).

AD therapeutic approaches aiming at reducing Aβ levels in the brain have been taken into consideration. Molecules with assessed properties of stabilizing soluble Aβ and of destabilizing its altered amyloidogenic conformer could be candidate drugs for AD therapy (Airoldi C.et al., 2011). Curcumin is a low molecular weight molecule derived from the perennial herb Curcuma Longa. Among its diverse biological effects, the ability of inhibiting amyloid polimerization has been demonstrated (Narlawar R. et al., 2008). However, its clinical exploitation has been hampered by its very poor hydrosolubility and stability in water solvents. Indeed, different studies have been performed, and none succeeded in achieving proper drug concentration at the brain tissue. This is likely related to difficulties in overcoming the BBB (Ray B. et al., 2011). Aβ has also been demonstrated to interact with specific components of cell membrane (Matsuzaki A., 2007). Therefore, anionic phospholipids, such as phosphatidic acid and cardiolipin have been showed to interact with amyloid β peptide (Gobbi M. et al., 2010).

Nanoparticles (NPs) are promising tools for increasing drug delivery to AD brain. Indeed, they can be multiple functionalized to achieve concurrent BBB crossing and amyloid β peptide binding (Gobbi M. et al., 2010)

1.5 - NANOTECHOLOGY AND NANOMEDICINE IN DRUG DELIVERY

Nanotechnology is a scientific area involved in the manipulation of atoms and molecules leading to the production of structures in the nanometer scale range (Moghimi S.M. et al, 2005).

Nanomedicine is the application of nanotechnology to healthcare and holds great promise for revolutionising several medical treatments and therapies such as diagnosis, drug delivery and tissue regeneration (Sanvicens N. and Pilar Marco M., 2008). It is based on nanoparticles constituted by different kinds of materials, which dimensions range between one and few hundreads nanometers. The physical and chemical properties of the materials can

dramatically change when scaled down to nanometer size and the new acquired properties dominate the nanoparticle physics and chemistry (Moghimi S.M. et al, 2005).

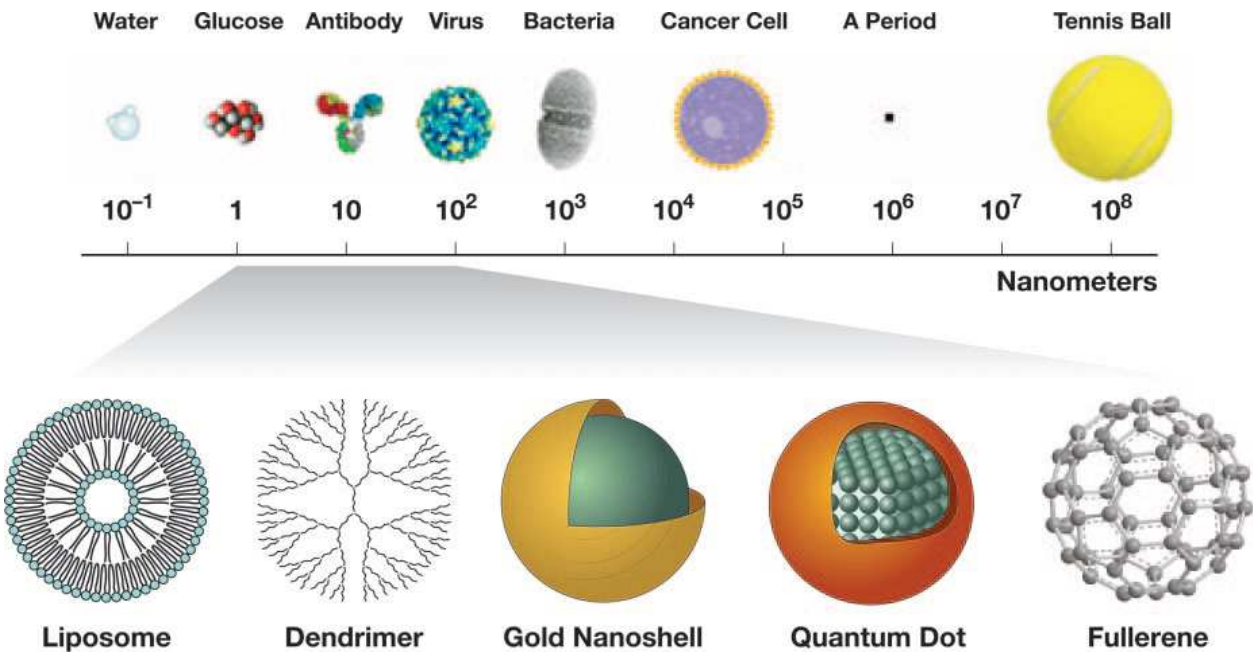

Fig. 4: Nanosized structures. *McNeill et al., 2005*

Three generations of nanovectors have already been developed. The early ones belonging to the first generation are constituted of the simple colloids and lead to passive delivery; they can be modified on their surface to avoid immune system recognition and degradation. The second generation nanovectors are engineered to allow targeted delivery of the payload through ligand-receptor binding. The third generation nanoparticles aim at crossing biological barrier and at organizing time sequential vector functions (Sanvinces N. and Pilar Marco M., 2008).

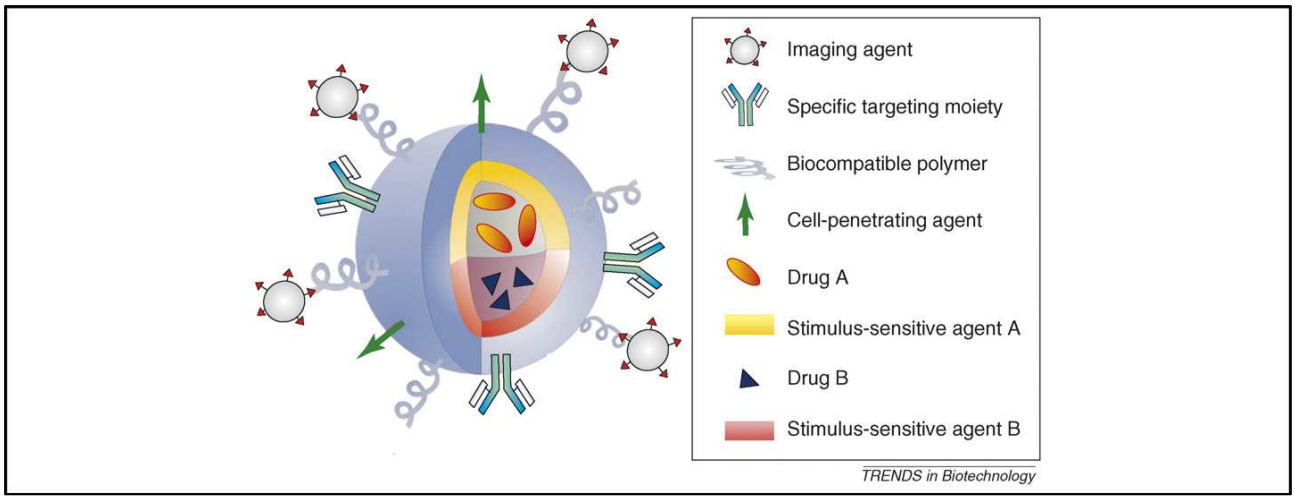

Fig. 5: Schematic view of multifunctional nanoparticles for drug delivery.

Sanvinces N. and Pilar Marco M., 2008

Nanoparticle (NP) employment in drug delivery shows many advantages compared to traditional therapeutic approaches. Biocompatibility and biodegradability are important features when considering a new drug delivery vector. Lipid-based and polymer-based nanoparticles, which fulfil these requirements, have been developed. Nanoparticle size, which usually does not exceed 200nm, is critical for avoiding filtration and clearance systems. Renal filtration and rapid elimination is usually responsible for clearance of particles below 10 nm diameter, and reticulo-endothelial, along with liver and spleen filtration accounts for the clearance of particles larger than 200 nm. Nanoparticles, ranging between 10 and 200 nm, show proper dimensional features to escape rapid elimination and also to accumulate at tumors, due to specific peculiarities of tumor associated blood vessels (Enhanced Permeability and Retention effect). Nanoparticle surface modification plays an important role in vector clearance, once injected in the blood flow. PEGylated nanoparticles ("stealth" nanoparticles) show higher stability and retention in the blood circulation compared to non PEGylated ones. Nanoparticle increased surface area per volume allow their encapsulation with relatively large amount of contrast agents and drugs, which can greatly enhance detection sensitivity in diagnostic and drug transport in drug delivery. Drug encapsulation prevents from drug degradation in the blood circulation and, along with nanoparticle surface functionalization, elicits targeted delivery and controlled released of intact drugs (Beija M et al., 2012; Caruthers S.D. et al., 2007; Moghimi S.M. et al., 2005).

Nanoparticles ranging from 1 to 20 nm, such as colloidal gold, ironoxyde crystals and quantum dots (QDs) semiconductor nanocrystals already have diagnostic application in biology and medicine. Moreover, heterogeneous nanobased systems, such as polymeric

micelles, dendrimers, poliplexes and liposomes have been developed and different drugs and contrast agents have been encapsulated, covalently attached or adsorbed onto their surface (Moghimi S.M. et al, 2005).

Liposomes are phospholipid vesicles made up of one or more phospholipid bilayers containing an aqueous core (Hillaireau H. and Couvreur P., 2009). Due to their amphiphilic nature, they can be loaded with both hydrophilic drugs, entrapped in their aqueous core and lipophilic drugs dissolved in the lipid bilayer (Sanvinces N. and Pilar Marco M., 2008). Liposomes have documented advantages compared to other drug delivery systems developed up to now. They showed increased drug loading capacity, and versatile structural features that elicits easy surface decoration, biodegradability, biocompatibility and minimum toxicity (Markoutsa E. et al., 2010).

Cancer therapy is one of the most promising field of nanoparticle application, due to the increasing need of targeted drug delivey at the specific site of action, and of reduced side effect on healthy tissues. Some nanoparticle based anticancer drugs are already on the market, and along with their equal or higher efficacy compared with free drug formulations, reduced side effects were detected (Beija M et al., 2012).

Even though nanoparticle employment in drug and contrast agent targeted delivery appears a promising strategy, toxicological feature associated to nanoparticle have to be considered. Following treatments with polymeric nanoparticles, alterated gene expression and cell death due to apoptosis or necrosis pathways have been detected in few studies (Moghimi S.M. et al., 2005).

Future perspective of nanomedicine is to improve targeted drug delivery, with drug accumulation at the site of action without side effects, and the development of theragnostic vectos, for combined diagnosis and therapy of diseases (Beija M. et al., 2012).

The development of nanoparticles for combined therapy and diagnosis of AD is one of the aims of the NAD project, a large scale European Project supported by the European Community's Seventh Framework Programme. The present study is part of the this project. NP functionalized for both BBB targeting and amyloid β peptide binding, developed within the NAD project, were herein tested.

As already described above, within BBB almost only specifically regulated transcellular passage can occur, mainly by receptor mediated transcytosis. Thus, new strategies for brain targeted drug delivery exploit BBB endogenously expressed receptors to elicit drug and carrier passage across the BBB. LDLr expression has been detected at BBB

endothelial cells, and LDLr mediated- transcytosis of low density lipoproteins has been demonstrated (Dehouck B. et al., 1997). Indeed ApolipoproteinE-associated nanoparticles have been demonstrated to overcome the BBB and to reach brain parenchyma (Zensi A. et al., 2009), and ApolipoproteinE interaction with LDLr has been characterized. The specific domain involved in LDLr binding has been localized between the amino acids 140 and 150, and the tandem linear repeat sequence corresponding to amino acid residues 141-150 has been demonstrated to retain receptor binding ability. Monomeric sequences corresponding to amino acid residues 141-150 and to residues 141-155 did not show receptor binding properties (Dyer C.A. et al., 1995).

Adsorptive-mediated endocytosis has been documented at BBB endothelial cells. This mechanism has been demonstrated to be receptor independent, and to be mediated by positively charged molecule adsorption onto negatively charged regions on plasma membrane (De Boer A.G. and Gaillard P.J., 2007).

Human Immunodeficency Virus type 1 (HIV-1) transactivator of transcription (TAT) is a 101 amino-acid protein. Its entry appears to be prevalently mediated by heparan sulphate proteoglycans (HSPG), the major source of macromolecular polyanions at the cell surface. Even though this mechanism is the broadly accepted endocytosis pathway, recent studies have demonstrated that also sterycal hindrance, and not only charge, can influence TAT endocytosis pathway. Moreover, other endocytic mechanism have been suggested to account for TAT internalization (Li G. et al., 2012).

Within the NAD project, the sequence corresponding to amino acid residues 141-150 (ApoE monomer), its tandem dimer (ApoE dimer) $(141\text{-}150)_2$ and TAT petide were selected as BBB targeting peptides. Chemically stabilized curcumine derivatives and anionic phospholipids (phosphatidic acid and cardiolipin) were exploited as Aβ peptide binding compounds for NL functionalization.

1.6 - *IN VITRO* BBB MODELS

The unique features characterizing BBB endothelial cells are induced and maintained through the interactions among the constituents of the neurovascular unit. Along with in vivo studies, which take into account its complexity, reliable *in vitro* BBB models are strictly required to study transport mechanisms and dynamic functions in both physiological and pathological conditions in simplified settings (Cecchelli R. et al., 2007).

Choosing the best BBB modelling approach is usually a compromise among capacity, cost, time and how closely the model is required to resemble in vivo features. An ideal *in vitro* BBB model is required to fulfil certain criteria, such as reproducible permeability of reference compounds, restrictive paracellular permeability, good screening capacities, a preserved physiological cell architecture, the formation of proper TJs, adequate expression of BBB specific transporters and a stable phenotype along with cell doublings (Cecchelli R. et al., 2007; Gumbleton M. and Audus K.L., 2001).

1.6.1 - Isolated brain capillaries

The main advantage of using isolated brain capillaries as BBB models is their close affinity to in vivo conditions, and this allowed researchers to gain important insights into BBB endothelial cell biology. Nevertheless, co-incubation experiments of isolated capillaries and the tested compounds allow to inquire only the transport from the abluminal to the luminal side of the BBB, lacking important information in the develop of a new CNS targeted drug (Cecchelli R. et al, 2007).

1.6.2 - Primary or low passage brain capillary endothelial cell culture

Primary endothelial cells are generally derived from bovine or porcine tissue, mainly because of their brain size and availability. Human cells are not considered a feasible option prevalently for ethical reasons and for the consequent lack of material. The number of cells that can be obtained from a rat brain is low, but rat based cell models are particularly useful if they are combined with in vivo experiments in the same species. Moreover, the growing number of mouse models of diseases increased the interest in developing in vitro BBB models based on murine cells (Cecchelli R. et al., 2007).

Several protocols for cell extraction from brain tissue have been developed, prevalently based on enzymatic digestion or on homogenization followed by filtration steps. These cells can be used soon after their isolation or can be stored and used at low culture passages (generally comprised between 3 and 7) (Cecchelli R. et al., 2007).

The main advantage of these models is their ability to maintain many morphological and biochemical features of the endothelial cells in vivo, including endothelial specific markers, expression of polarized enzymes, transporters, receptors and complex TJs (Cecchelli R. et al., 2007; Gumbleton M. and Kenneth L.A., 2001).

As it is known that glial cells modulate BBB expression properties, different approaches have been developed to establish more reliable models. Co-cultures of endothelial

cells and primary astrocytes have been settled, either seeding the two cell types in close opposition at the two sides of a porous membrane, or seeding the astrocytes at the bottom of a well in which the membrane with the endothelial cells is inserted. Other approaches were developed based on astrocyte-conditioned medium to modulate BBB properties expression at the endothelial cells. Finally, primary endothelial cell treatment with other factors such as cAMP or glucocoticoids to modulate BBB expression properties have received much attention (Cecchelli R. et al., 2007).

These more complex models of course allow a better comprehension of BBB biology and pathology compared to the simple ones, based on the endothelial cells alone. However, the introduction of new variables in the model should be considered during data analysis. The choice of the best model for each kind of study has to be evaluated accurately (Cecchelli R. et al., 2007).

Beside the close resemblance with the in vivo situation of this model, the lack of quantification of intra-batch or inter-batch reproducibility in the isolated cell phenotypic properties should be taken into account, when using these kinds of models (Gumbleton M. and Audus K.L., 2001; Cestelli A. et al., 2001).

1.6.3 - Immortalized brain endothelial cells

Several immortalized cell lines, derived from bovine, porcine, mouse, rat and human cells, have been developed in the recent years. Conditionally immortalized cell lines have also been generated from transgenic rats and mice and these cells show better retention of in vivo function compared with traditionally immortalized cell lines (Terasaki T. et al., 2003). Up to now, none of the immortalized cell lines shows the necessary restrictive paracellular barrier properties that are essential for their use in conventional transendothelial permeability drug screenings. However, genetically engineered brain endothelial cell lines are easy to culture. They also provide a homogeneous and phenotypically stable population of cells and their use improves the reproducibility of results. In addition, they provide large numbers of clonally identical cells for master cell banking, and they are readily traceable for future genetic manipulation (Uyttendaele H. et al., 2000; Gumbleton M. and Audus K.L., 2001). Thus, they can represent the best compromise for high-throughput screening of engineered nanoparticles (Roux F. and Couraud P.O., 2005).

1.6.3a - RBE4 cell line

RBE4 cell line is the most characterized among the different immortalized cell lines. It was generated in 1994 by Roux and colleagues by transfection with the plasmid pE1A/neo carrying the E1A region of Adenovirus 2 (Roux F. and Couraud P.O., 2005). Successive selection was based upon the cell exhibition of a non transformed phenotype, their expression of endothelial cell markers and of BBB specific properties (Roux F. and Couraud P.O., 2005).

RBE4 cells show an cobblestone morphology (Uyttendaele H. et al., 2000), without foci formation, indicating a non transformed phenotype. Expression of Factor VIII-related antigen and adhesion molecules such as ICAM-1 and E-cadherin, along with nitric oxide release following cytokine induction clearly demonstrate their endothelial origin (Roux F. and Couraud P.O., 2005). RBE4 cells express the 55KDa BBB specific GLUT1 transporter, although at significant lower levels, compared to in vivo situation. GLUT1 transporter affinity for glucose is conserved in the immortalized cell line, but its down regulation is accompanied by GLUT3 up-regulation, which is not specific for BBB (Roux F. and Couraud P.O., 2005; Regina A. et al., 2000). LAT1, a BBB specific transporter for large neutral amino acids is expressed at RBE4 cells, and its Km is similar to in vivo measurements (Roux F. and Couraud P.O., 2005). RBE4 cells have been shown responsive to astroglial conditioning. It has been demonstrated that co-culturing with astrocytes induced a reduction in paracellular permeability to hydrophilic markers, and that astrocyte conditioned medium induced increased enzymatic activity and increased expression of E-cadherins. Neuronal induction of occludin synthesis and localization to cell periphery has been also documented in RBE4 cells (Roux F. and Couraud P.O., 2005). As mentioned for GLUT1 transporter, reduction of other specific transporters or enzymatic activities have been documented in RBE4 cells. γ-glutamyl-transpeptidase and alkaline phosphatase activity was reduced when compared to isolated brain capillary measurements (Roux F. and Couraud P.O., 2005). mdr1a P-gp gene was significantly down-regulated in RBE4 cells, along with an up-regulation of the non specific mdr1b P-gp gene (Regina A. et al, 1998).

As already mentioned, RBE4 cells have been shown not to generate the restricted paracellular barrier properties required for their use in transendothelial free drug passage screenings (Roux F. and Couraud P.O., 2005).

Nevertheless, RBE4 cells or other immortalized cell lines can be used as reliable in vitro BBB models for the study of drug uptake or efflux mediated by specific transporters, when they show conserved properties. Moreover, they constitute suitable tools for screening

engineered nanoparticles, and for studying immune cell adhesion and infiltration at the CNS (Roux F. and Couraud P.O., 2005).

1.6.3b - hCMEC/D3 cell line

hCMEC/D3 is a new cell line developed by Weksler and colleagues in 2005 by sequential lentiviral transduction of hTERT and SV40 large T antigen into primary culture human adult brain endothelial cells. hCMEC/D3 cells showed a non transformed phenotype over more that 100 population doublings without any sign of senescence or dedifferentiation. hCMEC/D3 cells express endothelial cell markers, such as PECAM-1, VE-cadherins, β- and γ-catenins, in their proper junctional domains, and cytoplasmic granules of von Willebrand factor, which clearly demonstrate their endothelial origin. BBB specific features were also tested in hCMEC/D3 cells. ZO-1, JAM-A and claudin-5 expression was detected at cell-cell contacts, while claudin-3 and occludin expression was detected but not localized at junctional sites. Adhesion molecule expression was revealed by FACS analysis and hCMEC/D3 cells were demonstrated to up-regulate these molecules in response to inflammatory cytochines. Chemokine receptor, which are localized at the BBB endothelial cells in vivo, were detected at hCMEC/D3 cells (Weksler B.B. et al., 2005).

Along with the evaluation of endothelial and BBB marker expression, permeability studies were performed to inquire hCMEC/D3 cell functional BBB properties. Higher permeability to small paracellular hydrophilic markers, such as sucrose, were registered, compared to the reference BBB models. Low levels of TEER (~ 40 Ohm*cm^2) were obtained and no increase in TEER values were registered after cAMP or astrocyte medium conditioning. Nevertheless, experiments of in vitro-in vivo correlation using hCMEC/D3 cells and adult rat or mouse brain perfusion were performed with several compounds with different physico-chemical properties and increasing hydrophobicity. A good correlation score was obtained between in vitro and in vivo BBB permeability (Weksler B.B. et al., 2005).

The expression of functional P-gp, MRP1 and 5 and BCRP transporters and of transferrin (Tf) receptor was demonstrated in hCMEC/D3 cells (Weksler B.B. et al., 2005; Poller B. et al., 2008). LDL receptor was detected in hCMEC/D3 cells and its expression was increased after treatment with statins (Pinzon-Daza M.L. et al., 2012). hCMEC/D3 cells were deeply characterized for both morphological and functional BBB expression properties and no alterations in the assessed phenotype were detected during cell doubling (Weksler B.B. et al., 2005).

Although no significant response to astroglial conditioning was detected, hCMEC/D3 cells appear to be a useful BBB model mimicking brain restricted permeability for several compounds, except for small hydrophilic molecules (Weksler B.B. et al., 2005).

Due to the expression of adhesion molecules and chemokine receptors, hCMEC/D3 cells can be also considered a useful BBB model to study immune system cell interaction with brain endothelial cells (Weksler B.B. et al., 2005).

1.7 - ENDOCYTIC MECHANISMS

Endocytosis consists of the ex novo production of intracellular membranes from the plasma membrane, leading to internalization of membrane lipids, receptors, integral membrane proteins and extracellular fluids. Through endocytosis and exocytosis the plasma membrane regulates cell interaction with external environment, but also cell internal dynamics, such as mitosis, antigen presentation, migration and intracellular signalling cascades (Doherty G.J. and McMahon H.T., 2009). Several endocytosis pathways have been described so far, but the specific mechanisms underlying each of them have not been fully clarified, yet.

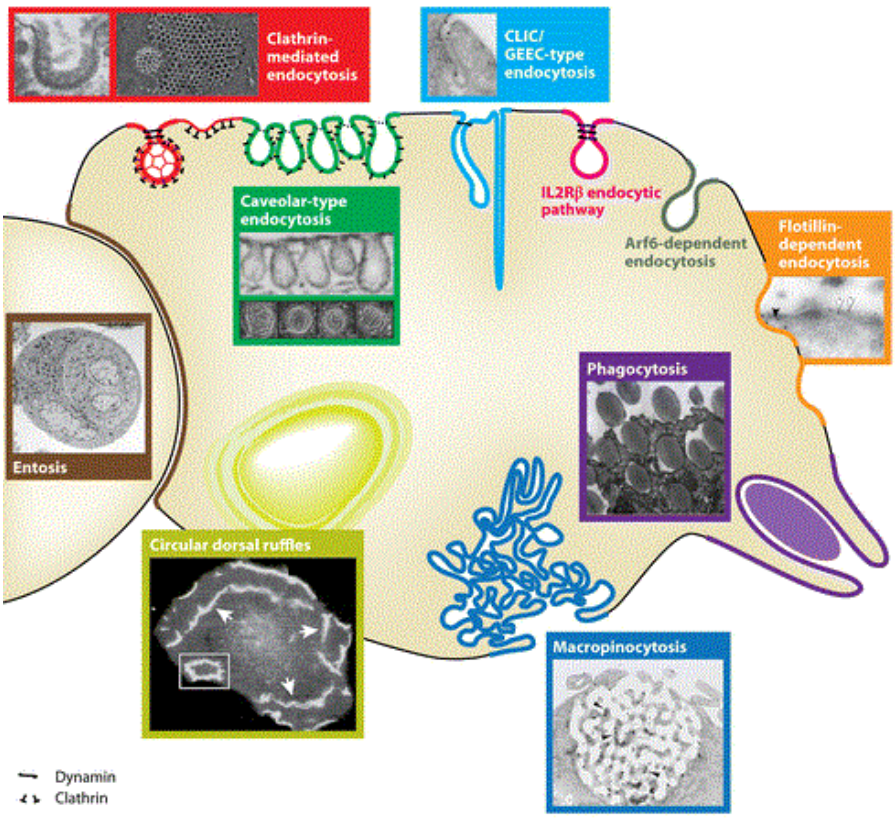

Fig. 6: Endocytosis mechanisms. *Doherty G.J. and McMahon H.T., 2009*

1.7.1 - Clathrin mediated endocytosis

Clathrin mediated endocyosis (CME) is the most deeply characterized among the endocytic mechanisms and accounts for the internalization of myriad of cargos. After cargo-receptor interaction, clathrin coated pits and vesicles (CCPs and CCVs respectively) can bud from plasma membrane. CCP/CCV budding is a complex process originated by cargo and accessory proteins accumulating at the cell membrane, which coordinate clathrin nucleation and polimerization into curved lattices. This process induces membrane curvature and stabilization; clathrin polimerization, along with the action of accessory proteins, drives the vesicle formation and brings the membranes surrounding the vescicle neck into close apposition. Vesicle fission from the membrane is mediated by the GTPase dynamin, through GTP hydrolysis. Different accessory proteins are involved in CME endocytosis, such as AP2 adaptor and the epsin protein family, which link cargo to clathrin and bind directly to inositol lipids helping in driving membrane curvature. Epsin proteins have been demonstrated to induce membrane curvature through the insertion of the $\alpha 0$ helix in the outer leaflet of the bilayer, and their role appears essential for clathrin mediated endocytosis (Vanden Broeck D. and De Wolf M.J.S., 2006; Ford M.G. et al., 2002). The Epsin N-terminal homology (ENTH) domain, which mediates membrane curvature, has been demonstrated to be highly conserved and unique for clathrin mediated endocytosis at the plasma membrane (Vanden Broeck D. and De Wolf M.J.S., 2006). Epsin proteins contain binding sites for both clathrin and AP2 proteins. At the C-terminus, three repeats of the EH domain binding consensus NPF (asparagine-proline-phenylalanine) mediate epsin binding with Eps15 (Rosenthal J.A. et al., 1999). Adaptor and accessory proteins show shared and overlapping functions that account for the flexibility of this mechanism (Doherty G.J. and McMahon H.T., 2009).

Even though many efforts were done to unravel the mechanisms leading to CCP/CCV vesicle budding and cargo sorting, the complete sequence of events have not been completely clarified, yet. Moreover, the regulation of the vesicle size is still a debated issue. Different CCP/CCV sorting to different endosomes and to proper intracellular destination likely depends on the cargo protein itself. Thus, differential receptor affinity for specific adaptor protein could be responsible for this mechanism. However, CCPs/CCVs carrying more than one kind of cargo molecule and adaptor proteins have been identified. The consequent composition of these CCPs/CCVs would depend on a wide variety of different factors (Doherty G.J. and McMahon H.T., 2009).

Endocytic/recycling pathway following CCP/CCV membrane budding has been deeply studied with the employment of transferrin as clathrin mediated endocytosis marker.

The small GTPases Rab4, Rab5 and Rab11 have been demonstrated to be important regulators of this pathway. Rab5 is localized on both CCP/CCV and on the early endosomes. These structures constitute the first “station” after cargo/receptor complex internalization, where also EEA1, a Rab5 effector protein, can be detected. Here, most cargoes dissociate from their receptors and are delivered to late endosomes and lysosomes for degradation, but also recycling can occur. Receptor are often recycled to the cell surface. Rab4 and Rab11 localize on endosomal membranes in distinct domains from Rab5 and appear to be involved in different stages of recycling process (Soennichsen B. et al., 2000).

1.7.2 - Caveolin-1 and flotilin associated endocytosis

Caveolae are flask-shaped membrane invaginations which size is generally between 50 and 80 nm. They are lined by caveolin proteins and enriched with cholesterol and sphingolipids, and they are highly represented in endothelial and smooth muscle cells and in fibroblasts (Hillaireau H. And Couvreur P., 2009).

Caveolin3 is the isoform specifically expressed in muscle cells, while caveolin1 and 2 are ubiquitous. While the role of caveolin2 has not been fully clarified yet, caveolin1 appears to be essential and sufficient for caveolae formation. Indeed, cells that do not express caveolin1 are devoid of morphologically evident caveolae, and overexpression of caveolin1 in caveolae-deficient cells, is sufficient to induce the formation of flask shape invaginations, resembling caveolae (Doherty G.J. and McMahon H.T., 2009). Caveolae appear to undergo formation in the Golgi complex, where they acquire detergent insolubility and cholesterol enrichment, along with partial Caveolin-1 oligomerization (Doherty G.J. and McMahon H.T., 2009). Caveolin1 is palmytoilated and binds the fatty acid tails of the glycosphingolipid GM1. At cellular membranes it can co-localize with both GM1 and Gb3, which are enriched at lipid rafts. Caveolin1 has intracellular N- and C- termini and it forms an hairpin structure embedded in the plasma membrane, which appears to reach through into the outer monolayer of the plasma membrane. It is able to form oligomers of 14-16 monomers, which are stabilized by cholesterol and fatty acids (Doherty G.J. and McMahon H.T., 2009).

Despite these structural findings, the precise role of caveolin1, the specific lipid composition of caveolae and the role of other caveolae-associated protein have to be clarified. Due to their abundance in many cell types, a role for caveolae in cell trafficking is certain. Several markers have been shown to undergo internalization through this mechanism, like SV40 virions and Cholera Toxin B (CTxB) (Kirkham M. And Parton R.G., 2005; Parton R.G. and Simons K., 2007), even though this is still debated. Currently, the most convincing role in

cell trafficking associated to caveolae appears to be transcytosis in endothelial cells (Doherty G.J. and McMahon H.T., 2009). Caveolin1 positive vesicles show a wide variance in their structure, life cycle and ability to fuse with each other or with other organelles. Both caveolae and caveolae-aggreagates have been shown to undergo cell membrane budding, but some of them have also been shown to be linked to plasma membrane. After internalization, caveolae have been demonstrated to fuse with both classical early endosomes and caveosomes. However, in any membrane of the endocytic pathway through which they traffic, they constitute structurally stable microdomains. Caveolin1 scaffolding function is responsible for caveolae segregation, and likely also for their sorting (Pelkmans L. et al., 2004; Parton R.G. and Simons K., 2007).

Recent studies show that caveolae-mediated pathway could be more connected to other endocytosis pathways than expected, and partial overlapping has emerged. Caveolin1 has also been postulated to be strongly related to regulatory function along with its role in caveolae-mediated endocytosis pathway. It has been demonstrated to specifically bind GDP-bound cdc42, and caveolin1 depletion results in activated cdc42 increase at the cell membrane, at least in specialized pancreatic β-cells (Nevins A.K. and Thurmond D.C., 2006). This suggests that relationships may exist between caveolae-mediated endocytosis and CLIC/GEEC pathway (clathrin independent carrier/GPI-anchored protein-enriched early endosomal compartment, see below). Caveolin1 null mice show defects in vascular tone regulation and in transcytosis, even though they do not show reduced life span. Overexpression of caveolin1 can deeply inhibit lipid microdomain associated endocytosis, and caveolin1 phosphorilation/dephosphorilation can interfere with lipid microdomain formation at plasma membrane. Moreover, a new role for caveolae have been suggested in anterograde trafficking, surface protein protection from internalization and competition with other pathways for particular essential lipids. Caveolae are also likely involved in cell signalling. Indeed, several signalling proteins are associated to these structures. Little is known about other proteins involved in caveolae mediated endocytosis. Recently, PTRF (cavin) was shown to associate with caveolae and to be required for their formation, suggesting that caveolin1 is not sufficient for caveolar formation (Hill M.M. et al, 2008; Doherty G.J. and McMahon H.T., 2009).

Flotilin proteins 1 and 2 have been shown to cluster in membrane microdomains and to form structures resembling caveolae. Nevertheless, when transfected in caveolin1 null cells, lacking caveolae, they are not able to drive the formation of caveolae-like invagination. Flotilin 1 and 2 have thus been associated to the uptake of cell surface proteoglycans through

a clathrin and caveolin1 indipendent endocytic mechanism, that could be mediated by CLIC/GEEC pathways (Doherty G.J. and McMahon H.T., 2009).

1.7.3 - Clathrin and caveolin independent endocytosis

Different endocytic mechanisms have been demonstrated to be clathrin and caveolin independent, cholesterol dependent and to require different lipid microdomains. Several molecules rely on these endocytic pathways for being internalized, such as viruses, toxins, GPI-linked proteins, receptors (Doherty G.J. and McMahon H.T., 2009).

CLIC/GEEC pathway shows a prevalent tubular or ring-like morphology at EM analysis and it seems to be regulated by the small G protein cdc42. Vesicle formation likely depends on membrane curvature mediated by the membrane constituents enriched in the microdomains. This process recruit other cellular proteins, which drive the further membrane curvature. This originate tubular/vescicular structures that are delivered into GEEC and determines vesicle scission from the plasma membrane. Several GPI-anchored proteins, such as the folate receptor, have been demonstrated to exploit this mechanism for being internalized. Following uptake, the cargo intracellular fate bypass conventional rab-5 positive endocytic compartments, and likely differ among cell types. Despite these findings, the physiological functions of these mechanism has still to be assessed (Doherty G.J. and McMahon H.T., 2009).

A rhoA, rac1, PAK1 and 2 dependent endocytosis pathway has been described, accounting for the interleukin 2 receptor β (IL2Rβ) internalization. This pathway is likely distinct from the CLIC/GEEC pathway and appears to be dynamin dependent. The internalized membranes appear to communicate at some extent with the intracellular compartments related to clathrin-mediated endocytosis (Doherty G.J. and McMahon H.T., 2009). Recent studies unravelled an essential role of PAK1 in this mechanism. PAK1-mediated phosphorilation of cortactin serine residues 405 and 418 is essential for its interaction with N-WASP, the enhancer of actin polimerization, and IL2Rβ endocytosis (Grassart A. et al., 2008; 2010).

A dynamin independent, Arf-6 dependent pathway has been demonstrated to account for the internalization of GPI-linked protein CD59, the major histocompatibility complex (MHC) class I proteins and the K^+ channel kir3.4. Arf-6 endosomes appear to be different from CLIC/GEEC endocytic structure, but they can likely communicate with both transferrine-positive compartments and with the Arf-6 dependent recycling pathway (Doherty G.J. and McMahon H.T., 2009).

1.7.4 - Macropinocytosis

Macropinocytosis is a clathrin and caveolin independent, rac1, actin, PAK1 and cholesterol dependent endocytic mechanism. Compared to the previously described pathways, macropinocytosis is a larger-scale process. It is characterized by the formation of membrane protrusions that subsequently fuse with themselves, or back with the plasma membrane, resulting in the internalization of extracellular components entrapped in this structure (Doherty G.J. and McMahon H.T., 2009).

Cholesterol is required for activated rac1 recruitment and rac1 mediated PAK1 recruitment and activation. PAK1 is a serine/threonine kinase and it has been demonstrated to be specifically involved in clathrin and caveolin independent endocytosis pathways (Grassart A. Et al., 2010) and to be necessary and sufficient to induce macropinocytosis (Dharmawardhane S. Et al., 2000). In macropinocytosis, PAK1 has been shown to be involved in the formation of membrane ruffles and the macropinocytic cup, through actin polimerization stimulation mediated by the LIMK1-cofilin pathway. Recent studies unravelled a new role for PAK1 in mediating CtBP1/BARS phosphorilation, which is essential for the macropinosome fission from plasma membrane (Liberali P. Et al., 2008). Other proteins have been demonstrated to promote macropinocytosis, such as phosphatidylinositol-3-kinase (PI3K), ras, src, and, more recently, also HDAC6 and hsp90, but their role is still unclear. Rab5 and its effector rabanchyrin5, which are associated to conventional endocytic compartments in clathrin mediated endocytosis, have been demonstrated to be involved in ruffle formation and macropinocytosis. This process is generally induced by cell stimulation with growth factors and it leads to endocytosis of the growth factor receptors. This suggests that macropinocytosis could by involved in cell desensitization, but this has not been fully clarified, yet. The formation of the so-called circular dorsal ruffles (CDRs) is cortactin and dynamin dependent, and other several kinases and adhesion molecules are involved in this process, along with the membrane specific lipid composition and receptor activation (Doherty G.J. and McMahon H.T., 2009).

1.7.5 - Other endocytic mechanisms

Podosomes and invadosomes are different kinds of membrane ruffles, which can be distinguished from CDRs prevalently because of their ventral localization. Podosomes are endogenously produced by macrophages and osteoclasts and are actin-rich and actin dependent membrane protrusions involved in the early steps of cell-matrix adhesion process. They contain focal adhesion components, the src tyrosine kinase, Arp2/3 complex, and other

actin regulatory proteins; dynamin, cortactin and the BAR domain-containing protein endophilin-2 are also required at these sites. Podosomes have a well established function in cell adhesion. It is still to be clarified if they could also be involved in endocytosis processes (Doherty G.J. and McMahon H.T., 2009).

Invadosomes are membrane ruffles produced by tumor invading cells, and they are able of endocytosing and degrading extracellular matrix components, contributing to tumor cell invasion. Invadopodia are actin-rich structures that resemble podosomes for their protein content and requirement (Doherty G.J. and McMahon H.T., 2009).

Phagocytosis is a clathrin independent, small G proteins dependent internalization mechanism of opsonised particles, performed by professional phagocytic cells. Following antibody-opsonised particle interaction with membrane Fc receptor, filpodial protrusions are formed in a cdc42 dependent manner. Internalization occurs and it has been demonstrated to be rac1 dependent. Actin polimerization and IQGAP1 interaction with formin Dia1 are required for phagocytosis. Actin regulatory proteins, such as N-WASP and Arp2/3 complex are recruited to the phagocytic membrane. Phagocytosis of particle opsonised with the complement effector fragment C3b occurs in response to the ligation of the modified integrin CR3. Despite its similarities with the cdc42 dependent mechanism, this pathway occurs in a rhoA dependent manner. It does not depend on the formation of membrane protrusions, despite the recruitment of Arp2/3 complex. Adhesion molecules, such as vinculin and paxilin, are also required, suggesting a role of local adhesive structures in this process (Doherty G.J. and McMahon H.T., 2009).

Recent studies have demonstrated that after cell detachment from matrix, that generally induces cell death, a still living cell can be internalized into another. This process is dependent upon rhoA and actin and the internalized cell can undergo degradation or release from the host cell. Much work is needed to understand this process (Doherty G.J. and McMahon H.T., 2009).

1.8 - RNA INTERFERENCE

RNA interference is a physiological mechanism regulating genes and genomes at different levels of genome function. It is driven by small non coding RNA sequences, which generally have an inhibitory effect (Carthew R.W. and Sontheimer E.J., 2009).
Based upon their origins, structures, associated effector proteins and biological roles, three main small interfering RNA classes have been recognised: short interfering RNAs (siRNAs), microRNAs (miRNA) and the piwi-interacting RNAs (piRNAs) (Carthew R.W. and Sontheimer E.J., 2009).

Once clarified their mechanisms of action, short interfering RNAs have unravelled interesting features for their employment as research tools. Indeed, their specificity of action allowed targeting and suppressing the expression of specific genes. siRNA-based techniques has thus been employed in the last few years for the study of gene function and regulation (Wadhwa R. et al., 2004).
Gene suppression with siRNA technique shows relevant advantages compared to other approaches for studying gene and protein function, like gene knock-down and over-expression of mutated proteins. Opposing to knock-down technique, RNAi can be regulated using different vectors and do not require gene function elimination at the embryo stage, so that it can be adopted to study genes essential for cell viability (Wadhwa R. et al., 2004). Compared to over-expression of dominant negative mutated proteins, siRNA technology is a much more efficient protein down-regulation system, considering the translation efficiency, which is approximately 5000 protein copies/mRNA molecule for a typical mRNA. Moreover, it does not result in a high intracellular content of mutated proteins, which could rise secondary unkown effect (Vanden Broeck D. and De Wolf M.J.S., 2006).
RNAi driven by siRNA in mammalian cells can be performed with transient transfection of chemically sintetized or in vitro transcribed siRNA, or with transfection of vector based siRNA, which provides stable target gene inhibition. The number of genes specifically inhibited by siRNA is increasing along with the cell types in which this technology has been shown to lead to a 60-80% reduction of the target gene expression (Wadhwa R. et al., 2004).

In the recent past mammalian genes involved in DNA damage response, membrane trafficking, DNA methylation, signalling and cell metabolism have been characterized using siRNA technique (Wadhwa R. et al., 2004). In the last few years, RNAi has become a new tool for the study of the endocytic mechanisms, and it has been shown to have higher

specificity and lower toxicity compared to the conventional drug based strategy (Broeck V.D. and De Wolf M.J.S., 2006).

1.8.1 - Short interfering RNAs (siRNAs)

Short interfering RNAs (siRNAs) were originally related to genome defence activity, they were thought to be of exogenous origin and to act as transgene- and virus-induced silencer. In the recent years, endogenous sources of siRNAs were discovered, ranging from repetitive sequences like transposons to trans-acting siRNAs, which are diced from specific genomic transcripts and that regulate discrete sets of target genes (Carthew R.W. and Sontheimer E.J., 2009; Lippman and Martienssen, 2004; Vazquez et al., 2004).

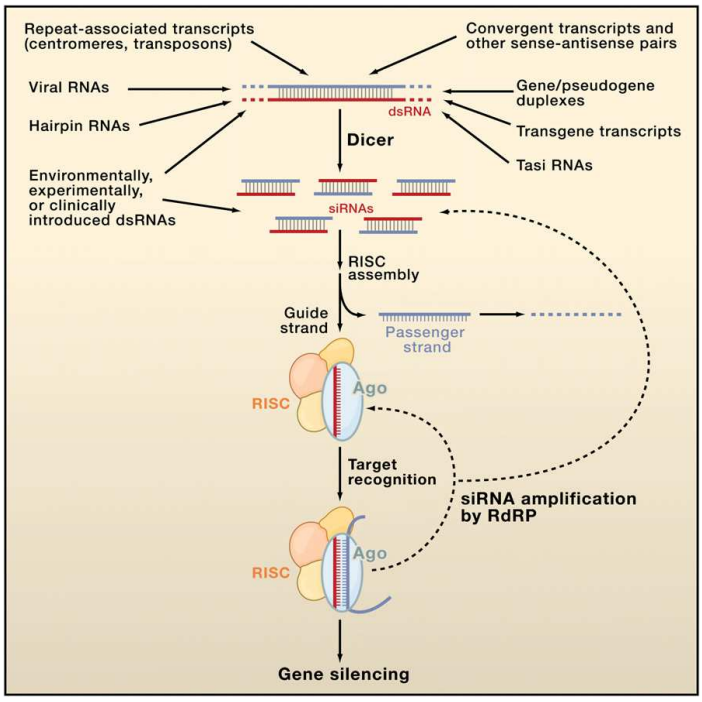

Fig. 7: siRNA sources and mechanism of action. *Carthew R.W. and Sontheimer E.J., 2009*

siRNAs originate from long, linear, perfectly base-paired, dsRNA precursors, which are processed by Dicer, enter the RISC complex and drive mRNA target recognition by Watson-Crick base pairing leading to target degradation (Carthew R.W. and Sontheimer E.J., 2009).

Dicer belongs to a class of large RNase III enzymes, dsRNA-specific nucleases, which are characterized by several domains in a specific order from the amino-to-carboxy terminus: a DEXD/H ATPase domain, a DUF283 domain, a PAZ domain, two tandem RNase III domains and a dsRNA-binding domain (dsRBD). Some members of this family show slight differences from this model, for instance in the apparent absence of a functional ATPase domain or PAZ

domain, or in the presence of a variable number of dsRBD from two to zero at the C-terminus. Different numbers of Dicer orthologues can be found in different species. Mammals have only a single Dicer which is involved in the biogenesis of both siRNAs and miRNAs, while Drosophila have two distinct Dicers, which show functional specialization (Carthew R.W. and Sontheimer E.J., 2009).

According to the model developed from biochemical, genetic and structural studies, the long dsRNA molecule bind with one end the Dicer PAZ domain and extend along the surface of the protein until it reaches a processing centre. This is made up of the two RNase III domains, each of which cuts one of the molecule strands. The reaction leaves a molecule with ~ 2nt 3' overhangs and a 5' monophosphate, which is required for later stages of the process (Carthew R.W. and Sontheimer E.J., 2009).

RISC assembly pathway for the production of a single stranded siRNA (siRISC) has been well characterized in both Drosophila and in humans. RISC assembly in humans starts from the formation of the RISC-loading complex by the proteins Dicer, TRBP and Ago-2, a member of the Argonaute protein family. This complex can be assembled even in the absence of dsRNA trigger. RISC-loading complex can bind dsRNA, dice it into siRNA, load siRNA into the Ago-2 protein and discard the passenger strand to generate functional RISC (Carthew R.W. and Sontheimer E.J., 2009).

The mechanism leading to strand selection in still unclear in mammals. In vitro and in vivo experiments showed that selection is driven by the relative thermodynamic stabilities of the two duplex ends. The strand having its 5' terminus at the less stably base-paired end is thus favoured as the guide strand. However, no rules have been discovered for duplexes with equal base-pairing stabilities at their ends, and they will incorporate either strand into RISC with approximately the same frequency (Carthew R.W. and Sontheimer E.J., 2009).

siRNA canonical silencing mechanism is characterized by perfect sequence matching with target mRNA. The guide strand drives RISC complex to the target which is degraded by the PIWI domain of the Ago protein. The endonucleolytic activity is directed to the phosphodiester linkage between the target nucleotides that are base paired to siRNA residues 10 and 11 (counting from 5'), and the cleavage product is then substrate for degrading processes. Free RISC is then available for further silencing activity. Effector phases of siRNA silencing seem to be localized in the cytoplasm, into subcellular foci called P-bodies, which are enriched in mRNA degradation factors. However, RNA silencing activity has been detected also in the nucleus (Carthew R.W. and Sontheimer E.J., 2009).

Other pathways involving siRNA activity have been documented, and they show differences compared to the canonical one. When mismatches are present near the centre of the siRNA/target duplex or the Ago proteins lack endonucleolytic activity, post-transcriptional silencing can be performed in a “miRNA-like” manner. In the last ten years, siRNA driven silencing has been shown to act not only at a post-transcriptional level but also through chromatine remodelling (Carthew R.W. and Sontheimer E.J., 2009).

2 - AIM OF THE WORK

The aim of this work is to establish and develop reliable *in vitro* models of blood brain barrier (BBB), in order to test nanoliposomes (NL) as brain targeted drug and contrast agent vectors for joint therapy and diagnosis of Alzheimer's Disease (AD). This study is part of a large-scale, fiver-year project, the NAD Project (Nanoparticles for Therapy and Diagnosis of Alzheimer Disease), supported by the European Community's Seventh Framework Programme (FP7/2007-2013) under grant agreement n° 212043.

Firstly, we settled two in vitro BBB models, based on immortalized cell lines of human and rat origin (hCMEC/D3 and RBE4 cells, respectively), characterized by different features, allowing an integrated evaluation of barrier permeability. Indeed, genetically engineered brain endothelial cell lines are easy to culture and they also provide a homogeneous and phenotypically stable population of cells. These two characteristics make these cells easy to use for high-throughput assays and improve the reproducibility of the results. In addition, immortalized cell lines provide large numbers of clonally identical cells for master cell banking, and they are readily traceable for future genetic manipulation (Uyttendaele H. et al., 2000).

Subsequently, we analysed the interaction of NL with these *in vitro* BBB models. In particular, we tested NL, which have been mono-functionalized for BBB targeting or double-functionalized for BBB targeting and amyloid β peptide binding. We investigated cellular internalization and intracellular fate of the two subsets of NL, and we assessed NL permeability across cell monolayer.

Finally, we inquired the endocytic mechanisms that mediate cellular uptake of NL mono-functionalized for BBB targeting. To this aim, we employed RNA interference technique to down-regulate caveolin1, which has been associated to caveolae-mediated endocytosis (Doherty G.J. and McMahon M.T., 2009). We evaluated the uptake of NL differentially functionalized for BBB targeting, in order to assess caveolin1 involvement in their uptake pathways.

3 - MATERIALS AND METHODS

3.1 - CELL CULTURES

Human brain endothelial cells (hCMEC/D3) were provided by Institut National de la Santè et de la Recherche Médicale (INSERM, Paris, France). hCMEC/D3 cells cultured between passages 25 and 35 were used. For culturing, the cells were seeded at a concentration of 27000cells/cm^2 and grown in tissue culture flasks coated with 0.1mg/ml rat tail collagen type I (Invitrogen, Italy), in the following medium: EBM-2 medium (Lonza, Basel, Switzerland) supplemented with 5% foetal bovine serum (FBS) (M-Medical, Italy), 1% Penicillin-Streptomycin, 1.4µM hydrocortisone (Sigma, Milan, Italy), 5µg/ml ascorbic acid (Sigma, Milan, Italy), 1/100 chemically defined lipid concentrate (Invitrogen), 10mM HEPES (M-Medical) and 1ng/ml basic FGF (bFGF) (Sigma, Milan, Italy). The cells were cultured at 37°C, 5% CO_2/saturated humidity. Cell culture medium was changed every 2-3 days.

Rat brain endothelial cell line (RBE4) was provided as a gift by Dr. M. Aschner (Department of Pediatrics, Vanderbilt Kennedy Centre, Nashville, Tennessee, USA). Cells at passages 15-60 were grown on tissue culture flasks coated with 0.1mg/ml rat tail collagen type I, in the following medium: Ham's F10 Nutrient Mix:αMEM (1:1 v/v) supplemented with 10% foetal bovine serum (FBS), 1% Penicillin-Streptomycin, 1% L-glutamine and 300µg/ml Geneticin (Invitrogen). RBE4 cells were seeded at a density of 13000cells/cm^2 and let to grow at 37°C, 5% CO_2/saturated humidity until confluence.

3.2 - NANOLIPOSOMES (NL)

3.2.1 - NL functionalized with human ApoE- derived and TAT-1 peptides

Nanoliposomes (NL) were composed of Sphingomyelin (Sm) and Cholesterol (Chol) at 1:1 molar ratio, mixed with 2.5 molar % of 1,2-stearoyl-*sn*-glycero-3-phosphoethanolamine-N-[maleimide(poly(ethylene glycol)-2000)] (mal-PEG-PE) .

Double functionalized NL were provided after 5 molar % addition of dimyristoylphosphatidic acid (PA) or cardiolipin (CL).

The sequence [CWG-(LRKLRKRLLR)-NH2 (M=1698.18 g/mol)] corresponding to amino-acid residues 141-150 of the human ApoE protein it will be referred as to monomer ApoE (mApoE). Its tandem dimer $(141\text{-}150)_2$ [CWG-(LRKLRKRLLR)- (LRKLRKRLLR)-NH2 (M=3030.94 g/mol)] it will be referred as to dimer ApoE (dApoE). The sequence

[(GRKKRRQRRRPPQ)-GWC (M=2068 g/mol)] it was referred as to TAT-1 sequence. mApoE, dApoE or TAT-1 peptide was added to the NL at a final peptide : mal-PEG-PE ratio 1:5 (low density, LD) or 1.2:1 (high density, HD). When dealing with multiple BBB ligands functionalization, equal molar amount of both TAT-1 and dApoE peptides have been located at high densitiy (peptide : mal-PEG-PE ratio 1.2:1) at NL surface.

NL for FACS analysis and CLSM experiments were fluorescently labelled using 0.5% N (4,4-difluoro-5,7-dimethyl-4bora-3a,4a-diaza-s-indacene-3-dodecanoyl) sphingosyl phosphocholine, fluorescently labelled Sphingomyelin (BODIPY-Sm). NL for radioactivity assays were radioactively labelled with less than 0.0001% of the total lipids of [^{3}H]-DPPC or [^{3}H]-Sphingomyelin ([^{3}H]-Sm).

[^{3}H]curcumin-4 loaded NL were provided after incorporation of [^{3}H]curcumin-4 in the initial phase of NL preparation.

3.2.2 - NL functionalized with TAT-1 peptide and with curcumine derivative3

Nanoliposomes (NL) were composed of Sphingomyelin (Sm) and Cholesterol (Chol) at 1:1 molar ratio, mixed with 2.5 molar % of mal-PEG-PE and 10 molar % of a PEGylated lipid containing an azido terminus (3-deoxy-1,2-dipalmitoyl-3-(4'-methyl(O-(2-azidoethyl)-heptaethylenglycol-2-yl)-ethylcarbamoylmethoxy ethylcarbamoyl-1H-1',2',3'-triazol-1'-yl)-*sn*-glycerol) (azido-PEG-lipid), synthesized according to previous publication (Mourtas S. et al., 2011).

A curcumin derivative with a terminal alkyne group (*N*-propargyl 2-(3',5'-di(4-hydroxy-3-metoxystyryl)-1H-pyrazol-1'-yl)-acetamide) (curcumin derivative3) was synthesized as previously described (Airoldi C. et al., 2011), and linked to NL by a click chemistry reaction involving its alkyne triple bond and the azido terminus on azido-PEG-lipid. The amount of curcumin derivative3 (curcumine derivative3-PEG-lipid) associated to NL was about 5% of total lipids, as quantified by mass spectrometry.

TAT-1 peptide was linked to NL by a thiol-maleimide reaction and was present on liposome surface as 1.8-2.1 molar % of total lipid content.

NL for CLSM experiments were fluorescently labelled using 0.5% BODIPY-Sm. NL for radioactivity assays were radioactively labelled with less than 0.001% of the total lipids of [^{3}H]-Sm.

3.3 - UPTAKE EXPERIMENTS

hCMEC/D3 cells were seeded at a density of 40000cell/cm^2 in collagen-coated glass coverslips (diameter 22mm, VWR International, Leuven, Belgium) positioned in 35mm Petri dishes (Scientific Plastic Labware) for confocal microscopy experiments and in collagen-coated 12-well plates (Corning, USA) for FACS analysis and radioactivity assays. RBE4 cells were seeded at a density of 25000cells/cm^2. All the experiments were performed on confluent monolayers, at DIV 2.

Cells were rinsed with PBS and incubated with nanoliposomes at the final lipid concentration of 0.1mM. All the incubations were performed in serum free medium (SFM). Incubations were performed for 30, 60, 180 and 300 minutes for time course experiments, and they were performed for 3 hours or over night for NL uptake and NL intracellular fate investigations.

For experiments with ^{3}[H]-curcumin4, RBE4 cells were incubated with NL containing 20000dpm/ml ^{3}[H]-curcumin4 at the final lipid concentration of 0.1mM, or with comparable radioactivity amount of free ^{3}[H]-curcumin4.

Cells were then processed for FACS analysis, radioactivity assays or immunofluorescence and confocal laser scanning microscopy (CLSM) experiments.

3.4 - FACS ANALYSIS

After incubation, cells were rinsed three times with PBS to remove NL which were not associated to cells. Cells were detached with trypsin, they were centrifuged at 130g for 5 minutes and the pellet was resuspended in PBS supplemented with 10% FBS. Data corresponding to 20000 events in a user-determined area were acquired for every experimental condition with FACSCanto cytofluorimeter (Becton Dickinson, San Josè, California, USA). The analysis was performed using DIVA software on a FACSCantoI (Becton Dickinson, San Josè, California, USA).

3.5 - RADIOACTIVITY ASSAYS

After incubation, cells were rinsed with PBS and treated with 0.1% trypsin to remove NL cell surface adsorbed radioactivity. Cells were detached with trypsin and collected. The cell suspension was mixed with 5 ml scintillation cocktail (Ultima Gold, Perkin Elmer) and

the cell associated radioactivity was measured with a Tri-Carb 2200 CA Liquid Scintillation Analyzer (Packard) (Perkin Elmer).

3.6 - IMMUNOFLUORESCENCE

After incubation, cells were rinsed three times with PBS and were fixed with 10% formalin solution (Sigma-Aldrich, Milan, Italy) for 20 minutes at room temperature. Cells were rinsed sequentially in High Salts (HS)-PBS (20mM phosphate buffer, 500mM NaCl) and Low Salts (LS)-PBS (10mM phosphate buffer, 150mM NaCl) and permeabilized for 30 minutes in Gelatin Dilution Buffer (GDB) (0.4% gelatine, 0.6% Tryton X-100, 40mM phosphate buffer, 900mM NaCl). Cells were incubated with primary antibody diluted in GDB or in 1% BSA for 4 hours at room temperature in a humid chamber. Following three washes with HS-PBS, cells were incubated with fluorophore conjugated-secondary antibody diluted in GDB for 1 hour at room temperature in a humid chamber. After subsequent washes with HS-PBS LS-PBS and PBS, cells were incubated with fluorophore-conjugated phalloidin, diluted 1:100 in PBS, for 1 hour at room temperature, in a humid chamber and with 20µM DAPI (Invitrogen) diluted in PBS. After three washes with PBS the samples were mounted using ProLong Gold Antifade Reagent mounting medium (Invitrogen).

Primary antibodies:

- Mouse anti-EEA1 (BD Biosciences) 1:250 in GDB
- Rabbit anti-Lamp1 (Abcam, UK) 1:200 in 1% BSA

Secondary antibodies:

- AlexaFluor561 nm-conjugated Goat anti-mouse IgG (Invitrogen) 1:100
- AlexaFluor561 nm-conjugated Goat anti-rabbit IgG (Invitrogen) 1:100

Fluorophore –conjugated Phalloidins:

- Texas Red-conjugated Phalloidin (Invitrgen)
- AlexaFluor633 nm-conjugated Phalloidin (Invitrogen)

3.7 - CONFOCAL MICROSCOPY

Images were acquired with a LSM710 inverted confocal laser scanning microscope equipped with a Plan –Neofluar 63x/1.4 oil objective (Carl Zeiss, Oberkochen, Germany). Excitation was performed using an Ar-laser 25mW for Bodipy (λ = 488 nm), a DPSS 15mW

for Rhodamine (λ = 561 nm), a diode 30mW for DAPI (λ = 405 nm) and an He-Ne laser 5mW for AlexaFluor 633nm (λ = 633 nm). Acquisition parameters were unvaried through all the samples we analyzed.

3.8 - PERMEABILITY ASSAYS

RBE4 cells were seeded in 12-well Transwell® inserts (Corning, USA) coated with rat tail collagen type I 0.1mg/ml at a concentration of 200000cells/cm^2 in a final volume of 0.5ml per insert. hCMEC/D3 cells were seeded at a final concentration of 60000cells/cm^2 in a final volume of 0.5ml per insert. The filters (donor chambers) were inserted in the acceptor chambers containing 1ml of cell culture medium.

TEER was monitored in the days following cell seeding starting from day 3, using an EVOM Endohm chamber (World Precision Instruments, Sarasota, FL, USA). All the experiments were performed with confluent monolayer showing TEER values higher than 40Ohm*cm^2, tipically after 6-7 DIV for RBE4 cells and 11-14 DIV for hCMEC/D3 cells.

Nanoliposomes labelled with radioactive probes were added to the donor chamber at a final lipid concentration of 100µM in serum free medium (SFM).

For ^{3}[H]-curcumin4 experiments, nanoliposomes containing 20000dpm/ml ^{3}[H]-curcumin4 at the final concentration of 100µM, or comparable radioactivity amount of free ^{3}[H]-curcumin4 were added to the donor compartment in serum free medium (SFM).

In the acceptor compartment, serum reduced medium (1%) for RBE4 cells, and complete medium for hCMEC/D3 cells were used. At 0, 60 and 180 minutes, radioactivity content was measured in the acceptor chamber through liquid scintillation counting.

Experiments with [^{14}C]-sucrose, a hydrophilic paracellular passage marker, were performed to monitor the cell monolayer tightness.

Transendothelial permeability coefficient (PE) was calculated according to the Eq (1) (Bickel U., 2005):

$$\frac{1}{P_E} = \frac{1}{P_T} - \frac{1}{P_B}$$

with PT the Total Permeability coefficient corresponding to the porous membrane, the collagen coating and the cell monolayer and PB the Blank Permeability coefficient corresponding to the porous membrane and the collagen coating, which are calculated according to the Eq (2)

$$P_T \text{ or } P_B = \frac{V_R}{A}\frac{\Delta C_R}{C_D \Delta t},$$

with VR the medium volume in the acceptor chamber; CR the compound concentration in the acceptor chamber; A the porous membrane area; CD the compound concentration in the donor chamber.

3.9 - CELL VIABILITY

Cell viability was evaluated with MTT assay. MTT [3-(4,5-Dimethylthiazol-2-yl)-2,5-diphenyltetrazolium bromide] is uptaken by cells and transformed into formazan by mitochondrial succinate dehydrogenase. Accumulation of formazan directly reflects the activity of mitochondria, an indirect measurement of cell viability. Cells were incubated with nanoliposomes at the final lipid concentration of 100µM in culture medium for up to 48 hours, corresponding to twice the cell doubling time, and MTT stock solution (5 mg/mL) was added to each culture at a final concentration of 1.2 mM. After removing MTT solution, cells were permeabilized with ethanol and centrifuged at 800g for 10 minutes. The absorbance was measured with a spectrophotometer at wavelength of 560 nm and at reference wavelength of 690 nm. The percentage of cell vitality was calculated according to the Eq (3)

[(OD 560nm – OD 690nm) sample / (OD 560nm – OD 690nm) control]*100

To monitor cell monolayer tightness following nanoliposome incubation, we performed co-incubation with un-labelled nanoliposomes and [^{14}C]-sucrose in Transwell® systems. At 0, 60, 180 min [^{14}C]-sucrose related radioactivity was measured in the acceptor chamber and PE was calculated as described above.

3.10 - PLASMID AMPLIFICATION AND PURIFICATION

JM109 competent cells (Promega, USA) were transformed with SureSilencing shRNA vectors (Qiagen, USA), according to the manifacturer's instructions, with little modifications. Briefly, five aliquots of JM109 cells were thawed on ice and 2µl of each plasmid was added to the aliquots. After 10 minutes on ice, thermal shock was performed at 42°C for 45 seconds, followed by 2 minutes on ice. 250µl of ice-cold SOC medium was added to the cell

suspension and they were let to grow for 1hour at 37°C with shaking. Then cells were seeded on LB AGAR plates (LB standard broth (10g NaCl, 10g Tryptone, 5g yeast extract in 1L at pH 7), supplemented with 20g AGAR/L) supplemented with 50µg/ml ampicillin at 37°C over night.

Three isolated colonies for each plate were picked and inoculated into 2.5ml of fresh LB broth supplemented with 50µg/ml ampicillin, and let to grow at 37°C over night with shaking.

DNA was extracted and purified using QIAfilter Plasmid Mini kit (Qiagen, USA), according to the manifacturer's instructions. A PstI restriction enzyme (New England Biolabs, NEB, USA) digestion was performed as follows to verify that purified plasmids contained shRNA inserts:

H_2O	38.5 µl
Buffer (10X)	5 µl
PstI	20 U (1 µl)
BSA (100X)	0.5 µl
DNA	5 µl

After 80 minutes incubation at 37°C, and 20 minutes enzyme inactivation at 80°C, digestion products were separated on a 0.8% agarose gel in TBE buffer (Tris Borate 90mM, EDTA 20mM) supplemented with 0.5 µg/ml Ethidium Bromide.

For each plasmid, one small culture, which contained the insert, was used to inoculate 250ml LB broth supplemented with 50µg/ml ampicillin and incubation with shaking was performed at 37°C over night. Plasmid DNA was extracted with EndoFree Plasmid Maxi kit (Qiagen, USA), according to the manifacturer's instruction and quantified with NANODROP (Thermoscientific).

PstI restriction enzyme digestion was performed as described above on the purified DNA to verify the shRNA insert presence.

3.11 - hCMEC/D3 CELL TRANSFECTION

hCMEC/D3 cells were seeded at the concentration of 42000cells/cm^2 on a rat tail collagen type I coated 6-well plate and left to grow untill 70% confluent, tipically for 24 hours.

Cells were transfected with purified SureSilencing shRNA vectors targeting caveolin1 using Lipofectine (Invitrogen) as transfection reagent (1:4 DNA:Lipofectine), according to the manifacturer's instructions.

All the plasmids carrying targeting sequences (clones 1 to 4) were transfected, and the plasmid carrying the scramble sequence (C-) was used as a negative control. After 24 hours cells were detached with trypsin and seeded in cell culture medium supplemented with G418 (Invitrogen) at the final concentration of 800µg/ml for selection. This process was continued until enough cells were available for generating frozen stocks. Successively, G418 concentration was reduced to 400µg/ml.

3.12 - WESTERN BLOT

Transfected cells were collected from 100mm Petri dishes and centrifuged at 4500g at 4°C for 5 minutes. The pellet was mechanically resuspended in PBS supplemented with protease inhibitors (Leupeptin 1µM and PMSF 75 Units/ml in isopropanol) and sonicated. The protein total content was measured by BCA assay (Sigma-Aldrich, Milan, Italy), according to the manifacturer's instructions and equal amount of proteins (20µg) were loaded. Samples were resuspended in LAEMMLI buffer and boiled for 5 minutes. Proteins were separated by SDS-gel electrophoresis on a 12% polyacrilamide gel and transferred to a nitrocellulose membrane (GE Healthcare). The membrane was saturated with 5% milk in PBS supplemented with 0.2% Tween20 (blocking solution). Primary antibodies and horseradish peroxidise-conjugated secondary antibody were diluted in blocking solution and the signal was detected by chemiluminescence (ECL) (Pierce, USA). Images were acquired with Kodak dS Image Station 2000R and signal quantification was performed with Kodak Image Station 2000. The amount of caveolin1 protein was calculated after normalization on actin protein content for each sample.

Primary antibodies:

- Rabbit anti-caveolin1 (BD Biosciences, USA) 1:2000
- Rabbit anti-β actin (Sigma-Aldrich, Milan, Italy) 1:1500

Secondary antibody:

- Horseradish peroxidise conjugated-Goat anti-rabbit (Pierce, USA) 1:5000

3.13 - INVESTIGATION OF NL CELL UPTAKE MECHANISMS

hCMEC/D3 cells (hCMEC/D3 WT) and transfected hCMEC/D3 cells (hCMEC/D3 shRNA) at the same culture passage were seeded at the concentration of 65000cells/cm^2 on rat tail collagen type I coated 12-well plates for FACS analysis and on collagen coated glass coverslips (diameter 22mm) positioned in 35mm Petri dishes for CLSM experiments.

Cells were rinsed with PBS, pre-treated with PBS for 30 minutes and incubated with mApoE-NL, dApoE-NL or TAT-NL in serum free medium (SFM). hCMEC/D3 WT cells pre-treated and incubated in presence of filipin 3µM were used as a control.

For FACS analysis, cells were processed as described above. For CLSM experiments, cells were fixed with 10% formalin solution for 20 minutes, and permeabilized using 0.2% Tryton X-100 in PBS. Actin cytoskeleton was stained with Texas Red-conjugated Phalloidin (Invitrogen) and nuclei were counterstained with 20µM DAPI. Samples were mounted using ProLong Gold antifade reagent (Invitrogen) and images were acquired as described above.

hCMEC/D3 WT cells were also co-incubated with mApoE-NL and AlexaFluor 594 nm-conjugated Cholera Toxin B subunit 0.2µg/ml (Invitrogen) in serum free medium (SFM) for 3 hours at 37°C. Cells were fixed with 10% formalin solution and nuclei were counterstained with 20µM DAPI. Samples were mounted using using ProLong Gold antifade reagent (Invitrogen) and images were acquired as described above.

3.14 - STATISTICAL ANALYSIS

Each experiment was performed at least in triplicate. The differences were evaluated for statistical significance using Student's t-test.

4 - RESULTS

4.1 - EVALUATION OF CELL MONOLAYER PROPERTIES

Trans-epithelial/endothelial electrical resistance (TEER) is a measurement of the ion passage across the cell monolayer, and TEER has been assumed as an indirect marker of cell monolayer tightness related to BBB expression properties. TEER increased in the days following cell seeding on Transwell® systems and reached a plateau after 6-7 DIV for RBE4 cells (tipically 45.1 ± 3.8 $\Omega*cm^2$) and after 11-14 DIV for hCMEC/D3 cells (tipically 47.1 ± 4.2 $\Omega*cm^2$). We performed all the permeability experiments at the time points corresponding to the maximum TEER values for both cell lines.

Permeability to small hydrophilic molecules is another parameter indicating cell monolayer tightness and BBB expression properties. We used [^{14}C]-sucrose as paracellular passage marker and we registered PE values of $7.71*10E^{-4}$±$8.54*10^{-5}$ cm/min for RBE4 cells and $1.68*10E^{-3}$±$2.6*10^{-5}$ cm/min for hCMEC/D3 cells, in accordance to data reported in literature (Gumbleton M. and Audus K.L., 2001; Weksler B.B. et al, 2005; Poller B. et al., 2008).

4.2 - CELL VIABILITY

All the liposomes were tested for cell toxicity with MTT assays. We incubated hCMEC/D3 and RBE4 cells with NLs for 3h, and for up to 48h, corresponding to twice the cell doubling time. At these time points all the preparations we used were non-toxic, at least at the concentrations herein utilized (data not shown).

In order to check if nanoliposomes might induce alteration in cell monolayer paracellular permeability, hCMEC/D3 and RBE4 cells were seeded on Transwell® systems and incubated with un-labelled nanoliposomes in presence of [^{14}C]-sucrose for 3 hours, which is the maximum time point we considered within permeability experiments. [^{14}C]-sucrose associated radioactivity was measured at 0, 60, 180 min in the acceptor chamber and PE was calculated as described above. PE of sucrose alone or after co-incubation with mApoE-HD-NL, dApoE-HD-NL and TAT-HD-NL of RBE4 cells are reported in Table 1. Variations in PE for [^{14}C]-sucrose were not detected in RBE4 cells nor in hCMEC/D3 cells (data not shown),

thus indicating no alteration of the monolayer tightness during liposome incubation, at least at the concentration herein utilized. NL double functionalized were also tested and no alterations in the cell monolayer tightness were detected (data not shown).

	PE
SUCROSE	$7.84*10E^{-4} \pm 5.44*10E^{-5}$
SUCROSE + mApoE-HD-NL	$8.67*10E^{-4} \pm 4.45*10E^{-5}$
SUCROSE + dApoE-HD-NL	$7.25*10E^{-4} \pm 3.23*10E^{-5}$
SUCROSE + TAT-HD-NL	$8.55*10E^{-4} \pm 2.12*10E^{-5}$

Tab. 1: PE of sucrose co-incubated with mApoE-HD-NL, dApoE-HD-NL and TAT-HD-NL, compared to PE of sucrose alone in RBE4 cells. *mApoE: ApoE monomer; dApoE: ApoE dimer; HD: high density*

4.3 - NL FUNCTIONALIZED FOR BBB TARGETING

4.3.1 - Uptake of BBB targeted NL

We investigated cellular uptake of fluorescently labelled (Bodipy-Sm) NL without functionalization and functionalized with ApoE monomer (aa 141-150), its tandem dimer $(141\text{-}150)_2$ and with TAT peptide in RBE4 cells by means of FACS and CLSM techniques.

RBE4 cells were incubated with NLs for 30, 60, 180 or 300 min, then detached with trypsin and collected for FACS analysis. NL internalization increased over time, without reaching *plateau*, at least until the last time point we considered (Fig. 8 and 9). NL without functionalization showed the lowest cell association and uptake (Fig. 8). Functionalization with ApoE monomer or tandem dimer enhanced NL uptake, depending on the peptide density located on the liposome surface. At any peptide density, the ApoE monomer (mApoE) performed higher uptake compared to ApoE dimer (dApoE) (Fig. 8).

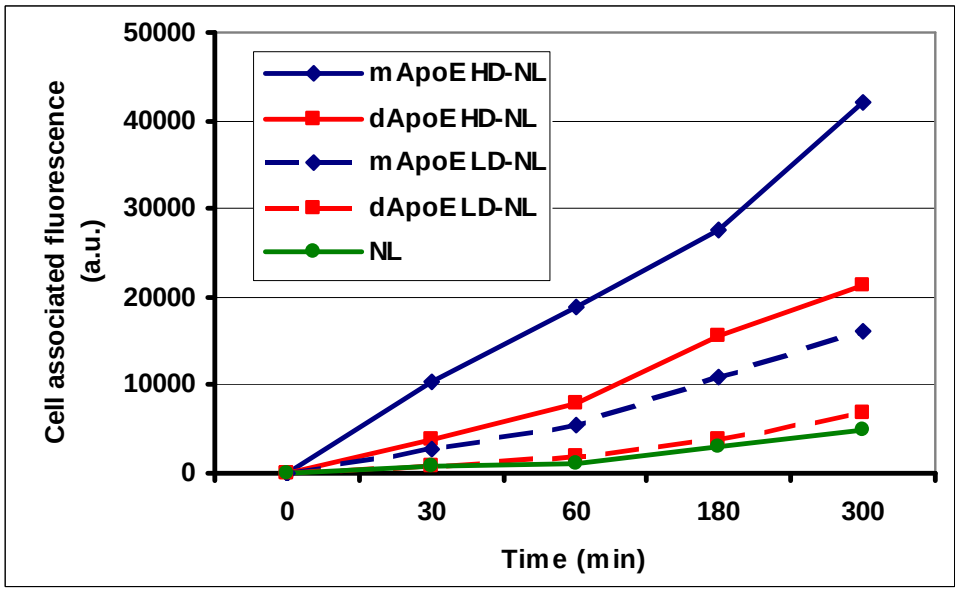

Fig. 8: Time dependent uptake of Bodipy-SM labelled unfunctionalized (NL) and differentially functionalized NL by RBE4 cells.

Cells were incubated with NL, dApoE-LD-NL, mApoE-LD-NL, dApoE-HD-NL and mApoE-HD-NLs for 30, 60, 180 and 300 minutes and collected for FACS analysis. Cell associated fluorescence signal increased over time without reaching *plateau*, until the last time point we considered. NL without functionalization showed slightly detectable cell associated fluorescence signal (green line). mApoE-NL showed the highest cellular uptake when high density monomer ApoE were located on NL surface (straight blue line). Lower cellular uptake was achieved when dApoE at high density (straight red line), mApoE at low density (dotted blue line) and dApoE at low density (dotted red line) were located on NL surface. *mApoE: ApoE monomer; dApoE: ApoE dimer; LD: low density; HD: high density*

Functionalization with TAT peptide increased NL cellular uptake at higher extent compared to both ApoE monomer and tandem dimer at high surface-peptide density (Fig. 9).

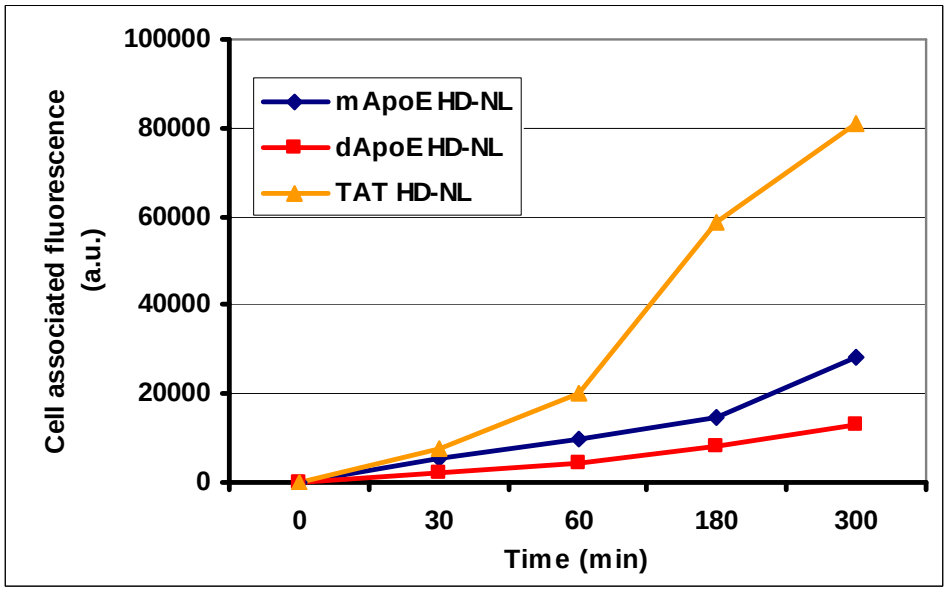

Fig. 9: Time dependent uptake of Bodipy-SM labelled ApoE-HD-NL and TAT-HD-NL by RBE4 cells. Cells were incubated with dApoE-HD-NL, mApoE-HD-NL and TAT-NL for 30, 60, 180 and 300 minutes and then collected for FACS analysis. Cell associated fluorescence signal increased over time without reaching *plateau*, until the last time point we considered. As we already demonstrated, mApoE-HD-NL (blue line) showed higher uptake compared to dApoE-HD-NL (red line). TAT functionalization further enhanced NL cellular uptake (yellow line).

We then analyzed NL internalization and intracellular localization with CLSM studies. RBE4 cells were incubated with fluorescently labelled (Bodipy-Sm) NL for 180 minutes and fixed with formalin solution. Again, NL without surface functionalization showed extremely low membrane association and cellular uptake (Fig. 10A). Functionalization with ApoE monomer or tandem dimer increased NL internalization depending on peptide density on liposome surface. Again mApoE-NL promoted higher internalization compared to dimer at any peptide density we tested (Fig. 3B, C, D, E). At 3h of incubation, NL functionalized with ApoE monomer at high density were internalized in endothelial cells and NL associated fluorescence signal is clearly detectable below the plasma membrane and in the perinuclear region (Fig. 10E and G, arrowhead). Liposomes functionalized with ApoE tandem dimer displayed lower cellular accumulation with NL associated fluorescence signal being prevalently localized beneath the membrane (Fig. 10D and F, arrows), while accumulation in the perinuclear region was much lower compared to ApoE monomer functionalization.

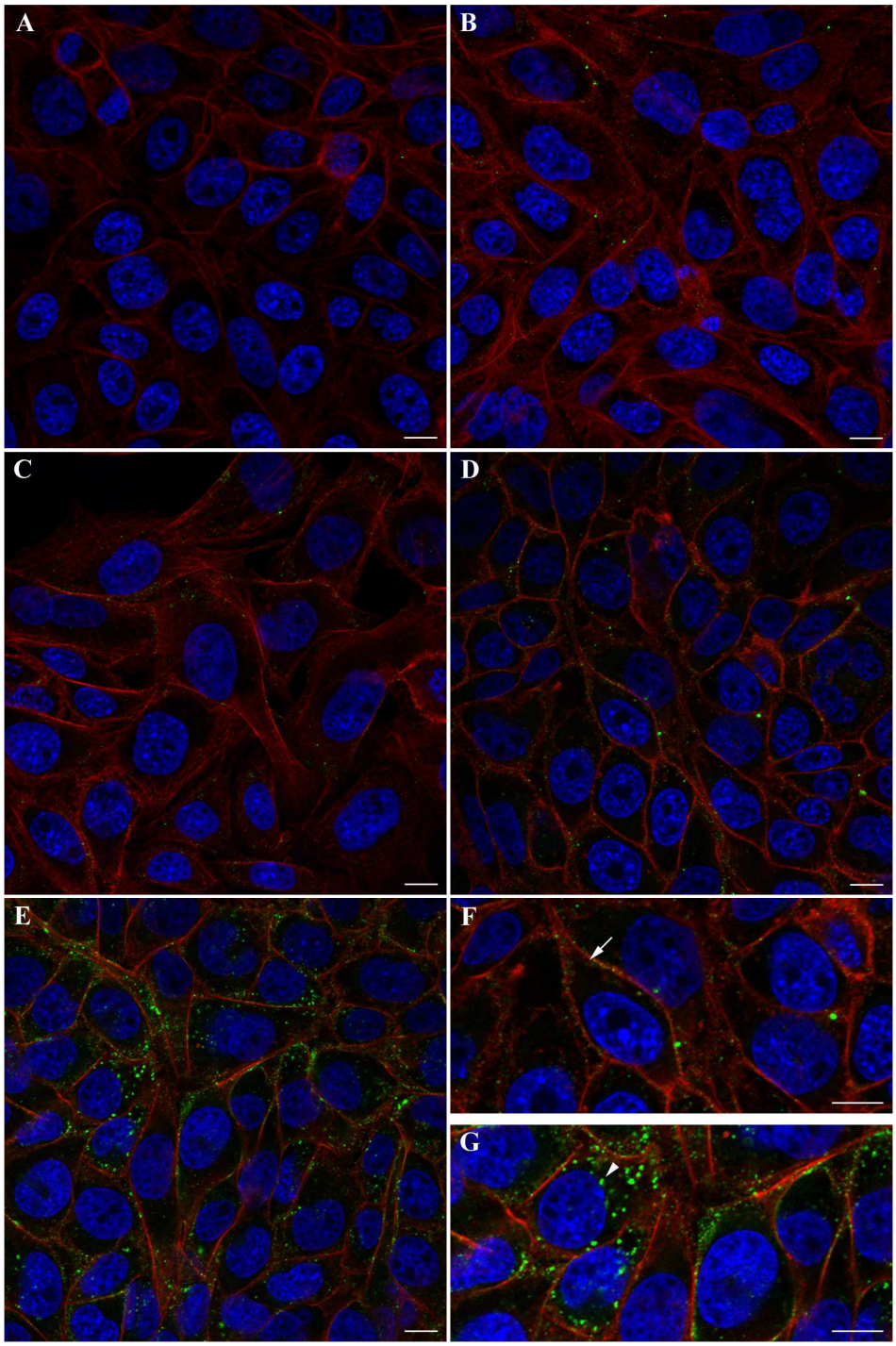

Fig. 10: CLSM of RBE4 cells incubated with ApoE functionalized NL

RBE4 cells were incubated for 3 hours with unfunctionalized NL (A), dApoE-LD-NL (B), mApoE-LD-NL (C), dApoE-HD-NL (D), mApoE-HD-NL (E). No cellular uptake nor membrane association was detectable with unfunctionalized NL (A), and fluorescence signal was slightly visible with dApoE and mApoE-LD-NL (B, C). dApoE-HD and mApoE-HD-NL clearly showed cellular accumulation (D, E), with distinct staining patterns. NL associated fluorescence signal (green) is localized below the plasma membrane and in the perinuclear region (G, arrowheads) when using mApoE-HD-NL, while it remains located below the plasma membrane when incubating with dApoE-HD-NL (F, arrows). Actin cytoskeleton is stained with Texas red conjugated-phalloidin (red) and nuclei are counterstained with DAPI (blue). Bars: 10µm.

TAT functionalization increased cellular uptake at higher extent compared to dApoE-HD and mApoE-HD functionalizations (Fig. 11). Similarly to mApoE-NL, at 3 hours of incubation TAT-NL associated fluorescence signal is clearly localized below the plasma membrane and in the cell perinuclear region (Fig. 11B, C arrowheads).

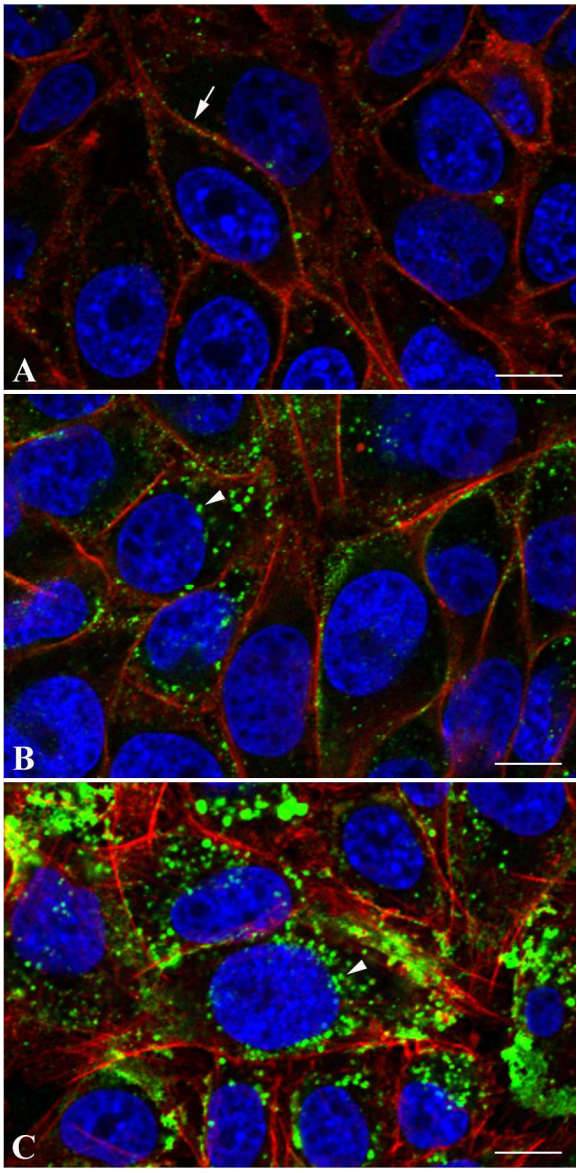

Fig. 11: CLSM of RBE4 cells incubated for 3 hours with fluorescently labelled (Bodipy-Sm) dApoE-HD-NL, mApoE-HD-NL and TAT-HD-NL

RBE4 cells were incubated for 3 hours with Bodipy-Sm dApoE-HD-NL (A), mApoE-HD-NL (B) and TAT-HD-NL (C) (green), fixed with formalin solution and mounted for CLSM. TAT functionalization (C) further increased cellular uptake compared to dApoE-HD and mApoE-HD functionalizations (A, B). As already showed, dApoE-HD-NL associated fluorescence signal is localized below the plasma membrane (A, arrow). Similar staining patterns are clearly detectable in cells incubated with mApoE-HD-NL and TAT-HD-NL, with NL associated fluorescence signal localized below the plasma membrane and enriched in the pericnuclear region (B, C arrowheads). Actin cytoskeleton is stained with Texas red conjugated-phalloidin (red) and nuclei were counternstained with DAPI (blue). Bars: 10µm.

We then investigated the uptake within RBE4 cells of NL, labelled with ^{3}H-Sm and double-functionalized with both dApoE and TAT peptides. Cells were incubated for 3 hours with NL, then detached with trypsin and collected for radioactivity assays. According with our previous CLSM results, TAT-NL again displayed significant higher uptake compared to dApoE-NL (respectively 11.1±0.77% and 6.5±0.37% of the administered dose, $p<0.01$). Concurrent functionalization with TAT and dApoE peptides enhanced cellular uptake up to 14.6±0.4% of the administered radioactivity, further increasing cellular uptake compared with single TAT functionalization ($p<0.05$) (Fig. 12). Similar results were achieved with hCMEC/D3 cells (data not shown).

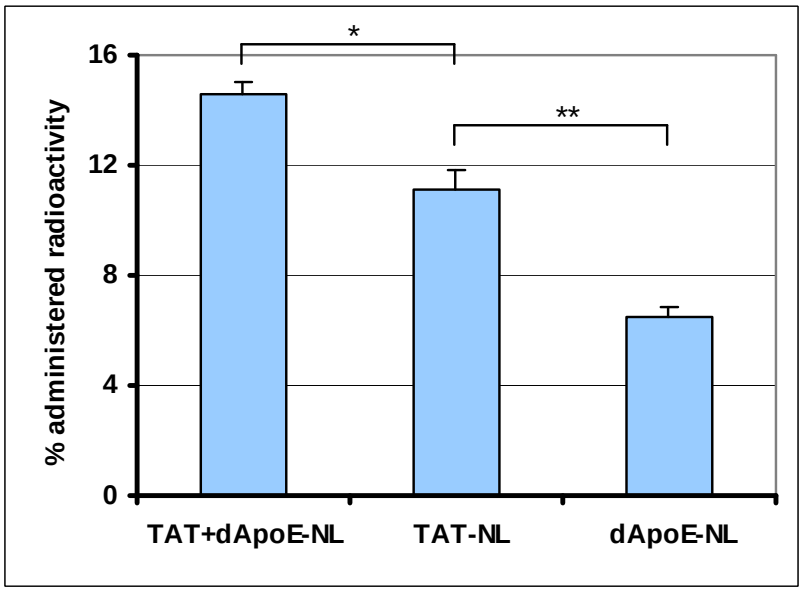

Fig. 12: RBE4 uptake of ^{3}H-Sm labelled NL functionalized with both TAT and dApoE peptides, TAT peptide or dApoE peptide.

RBE4 cells were incubated for 3 hours with ^{3}H-DPPC labelled TAT+dApoE-NL, TAT-NL and dApoE-NL and cell associated radioactivity was counted. Significative enhancement of cellular uptake was achieved with TAT-NL compared to dApoE-NL (respectively 11.1±0.77% and 6.5±0.37% of the administered dose). NL uptake by RBE4 cells was further increased when both TAT and dApoE peptides were located at the NL surface compared to single functionalized TAT-NL (respectively 14.6±0.4% and 11.1±0.77% of the administered dose) *$p<0.05$; **$p<0.01$

4.3.2 - Permeability of BBB targeting NL

As already described, BBB is a tight structure, where only specifically regulated transcellular passage is allowed to occur. Cell internalization can thus be considered the first

step for transcytosis process. We thus considered ApoE and TAT functionalized NL, which showed cellular uptake, but not NL without functionalization, for further permeability experiments.

We investigated the permeability, across the RBE4 cell monolayer, of ^{3}H-DPPC labelled NL, functionalized at the surface with the ApoE monomer or its tandem dimer at different peptide densities.

RBE4 cells were seeded on porous membrane of Transwell® systems and NL suspension was added in the donor chamber. Radioactivity was measured in the acceptor chamber after 0, 60 and 180 min of incubation and the endothelial monolayer permeability coefficient (PE) was calculated as described above. When RBE4 cells were incubated with dApoE-NL no enhancement of PE value was achieved increasing peptide density on liposome surface (Fig. 6). On the contrary, incubation with mApoE-HD-NL induced 2.5-fold increase of NL PE across RBE4 cell monolayer compared to mApoE-LD-NL (Fig. 13). Similar results were achieved with hCMEC/D3 cells (data not shown).

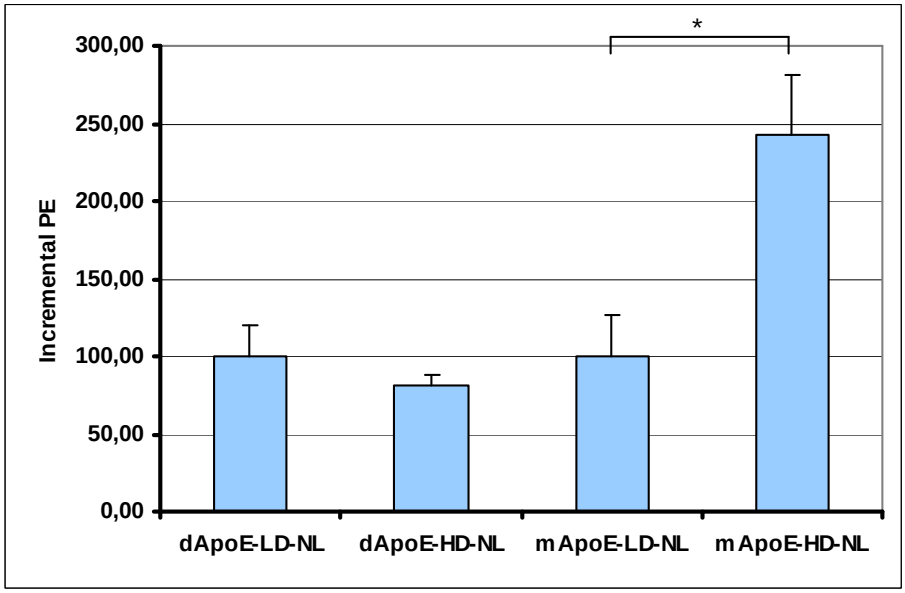

Fig. 13: PE of ^{3}H-DPPC labelled ApoE-NL across RBE4 cell monolayer

RBE4 cells were incubated with ApoE-NL for 3 hours on Transwell® systems and radioactivity in the acceptor chamber was measured at 0, 60, 180min. PE was calculated and expressed as the increment of LD-NL-PE. No permeability increase was detected when using dApoE-HD-NL compared to dApoE-LD-NL. Enhancement of 2.5–fold was achieved when cells were incubated with mApoE-HD-NL, compared to dApoE-LD-NL. *$p<0.05$.

We then investigated the permeability of ^{3}H-Sm labelled NL functionalized with TAT peptide, dApoE peptide or both TAT and dApoE peptides across RBE4 cell monolayer with radioactivity assays.

RBE4 cells were seeded on porous membrane on Transwell® systems and NL suspension was added in the donor chamber. Radioactivity was measured in the acceptor chamber after 0, 60 and 180 min of incubation and PE was calculated. Despite significant increase in NL cellular uptake when using TAT-NL compared to dApoE-NL, no differences in PE were detected ($4.13*10^{-4}\pm1.98*10^{-4}$ and $3.64*10^{-4}\pm4.03*10^{-5}$ respectively) and no increase was achieved after double functionalization with both peptides ($4.07*10^{-4}\pm3.58*10^{-5}$). These results were confirmed in hCMEC/D3 cells (data not shown).

4.4 - UPTAKE AND PERMEABILITY STUDIES OF [^{3}H]-curcumin4 INCORPORATED INTO mApoE AND dApoE-NL

Once assessed the internalization and permeability features of functionalized NL, we examined the cellular uptake and PE of a drug payload entrapped in functionalized vectors. We tested NL functionalized for BBB targeting with ApoE peptides (monomer and tandem dimer) and loaded with a tritiated curcumin derivative ([^{3}H]-curcumin4) for Aβ peptide binding.

[^{3}H]-curcumin4 was added to the donor chambers of the Transwell® system as free drug or after its entrapment into mApoE-HD-NL, mApoE-LD-NL, dApoE-HD-NL, or dApoE-LD-NL, (2000dpm [^{3}H]-curcumin4/0.1μmoles of lipids). At 0, 60, 180 min radioactivity was measured in the acceptor chambers and PE was calculated. At the end of incubation, cells were collected for measuring cell associated radioactivity.

A small amount of radioactivity was found associated to cells when incubated with free [^{3}H]-curcumin4 (<2% of the radioactivity administered), while drug uptake was increased after its entrapment in dApo-LD, mApoE-LD and dApoE-HD-NL (10.9±0.6%, 11.1±0.99%, 8.68±0,36%, respectively, $p<0.05$). The highest increase was achieved when drug was entrapped in mApoE-HD-NL (13.74±0,53%, $p<0.01$) (Fig. 14).

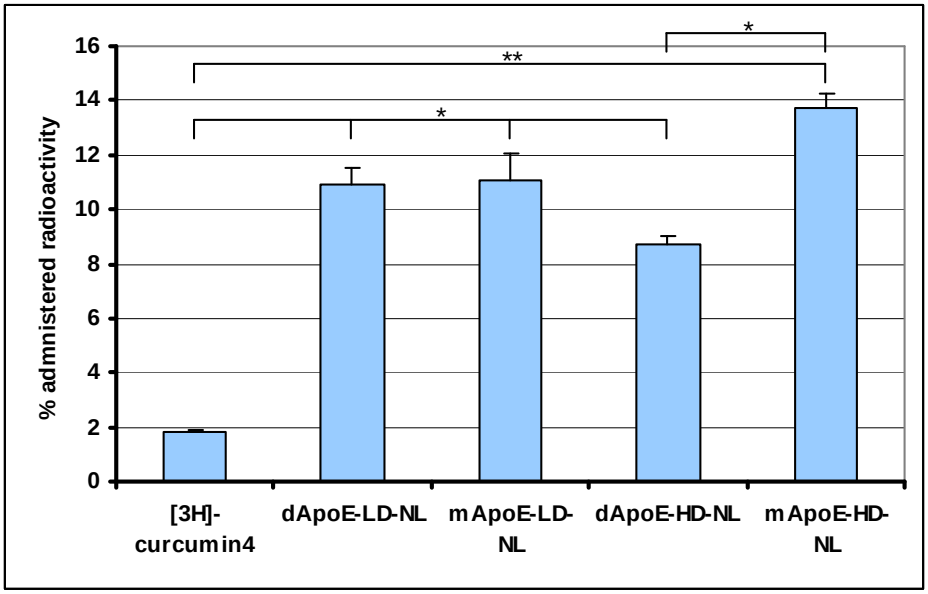

Fig. 14: Cellular uptake of [^{3}H]-curcumin4 by RBE4 cells

RBE4 cells were seeded on Transwell systems and incubated for 3 hours with equal amounts of [^{3}H]-curcumin4 alone or entrapped into dApoE-LD-NL, mApoE-LD-NL, dApoE-HD-NL and mApoE-HD-NL and cell associated radioactivity was measured. Less than 2% of the administered radioactivity was detected associated to cells when they were incubated with [^{3}H]-curcumin4 alone. Higher uptake was achieved when RBE4 cells were incubated with [^{3}H]-curcumin4-loaded dApoE-LD, mApoE-LD and dApoE-HD-NL (11.1±0.99%, 10.9±0.6% and 8.7±0.36% respectively), and the highest internalization was detected with mApoE-HD-NL (13.7±0.53%). *p<0.05; **p<0.01. *mApoE: ApoE monomer; dApoE: ApoE tandem dimer; HD: high density; LD: low density*

Permeability studies showed a slight increase in drug PE when it was entrapped in mApoE-LD and dApoE-LD-liposomes (+16.8% and +27.3%, respectively) and a higher increase when it was entrapped in mApoE-HD-liposomes (+38.3%, $p<0.05$). Surprisingly, the highest enhancement was achieved with drug entrapment in dApoE-HD-liposomes (+83.1%, $p<0.01$) (Fig. 15).

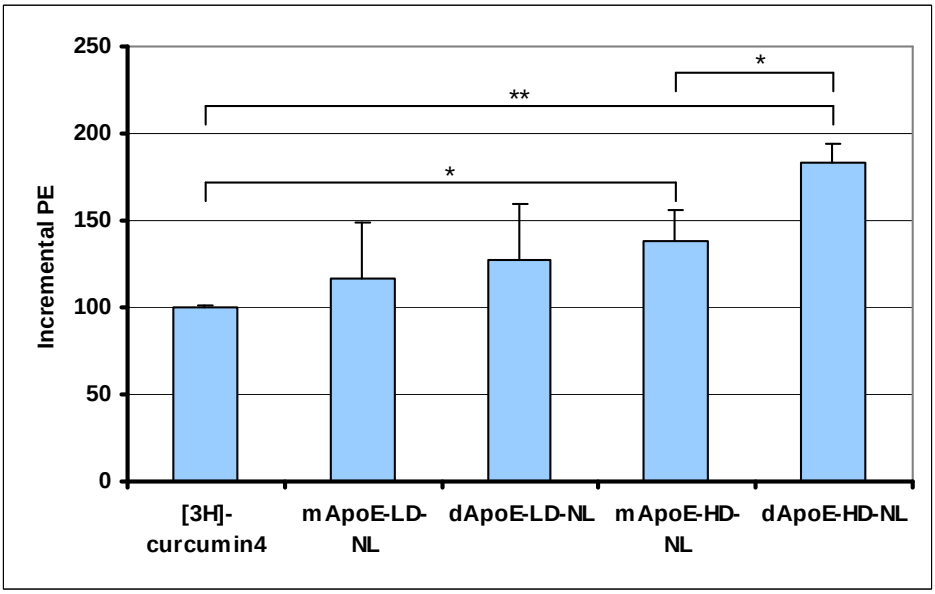

Fig. 15: PE of [^{3}H]-curcumin4 across RBE4 cell monolayer

RBE4 cells were seeded on Transwell® system and incubated for 3 hours with equal amounts of [^{3}H]-curcumin4 alone or entrapped into mApoE-LD-NL, dApoE-LD-NL, mApoE-HD-NL and dApoE-HD-NL. Radioactivity was measured at 0, 60, 180 min in the acceptor chamber and PE was calculated and expressed as incremental values compared to [^{3}H]-curcumin4 alone. Slight increase was achieved when [^{3}H]-curcumin4 was entrapped into mApoE-LD and dApoE-LD-NL (16.8% and 27.3% respectively). Higher increased was achieved with loading into mApoE-HD-NL (38.3%) and the highest increase was achieved with dApoE-HD-NL (83.1%). *$p<0.05$; **$p<0.01$.

4.5 - NL DOUBLE FUNCTIONALIZED FOR BBB TARGETING AND Aβ BINDING

4.5.1 - Uptake of double functionalized NL

Once assessed the internalization and permeability features of NL functionalized for BBB targeting, we then investigated cellular uptake of NL functionalized for BBB targeting with ApoE peptides or TAT peptide at high density, and exposing Aβ targeting ligands on the outer leaflet or anchored to NL surface.

We tested NL double functionalized with phosphatidic acid (PA) or cardiolipin (CL), for Aβ peptide binding, and with ApoE peptides, for BBB targeting, on hCMEC/D3 cells, with CLSM studies and radioactivity assays.

hCMEC/D3 cells were incubated for 3h with fluorescently labelled (Bodipy-Sm) PA/CL-NL, PA/CL-mApoE-NL or PA/CL-dApoE-NL, fixed with formalin solution and mounted for CLS microscopy. PA/CL-NL without BBB targeting functionalization showed no cellular association nor uptake (Fig. 16A, B), and higher uptake was achieved with PA/CL-ApoE-NL (Fig. 16C, D, E, F). The highest internalization was achieved with PA-mApoE-NL (Fig. 16E). Progressively lower uptake was detected with CL-mApoE (Fig. 16F), PA-dApoE (Fig. 16C) and CL-dApoE-NL (Fig. 16D). NL associated fluorescence was prevalently localized below the plasma membrane and in the perinuclear region when cells were incubated with PA-mApoE-NL (Fig. 16E). The amount of the green spots localized around the nucleus decreased with PA-dApoE-NL, being the NL staining prevalently localized beneath the cell membrane (Fig. 16C).

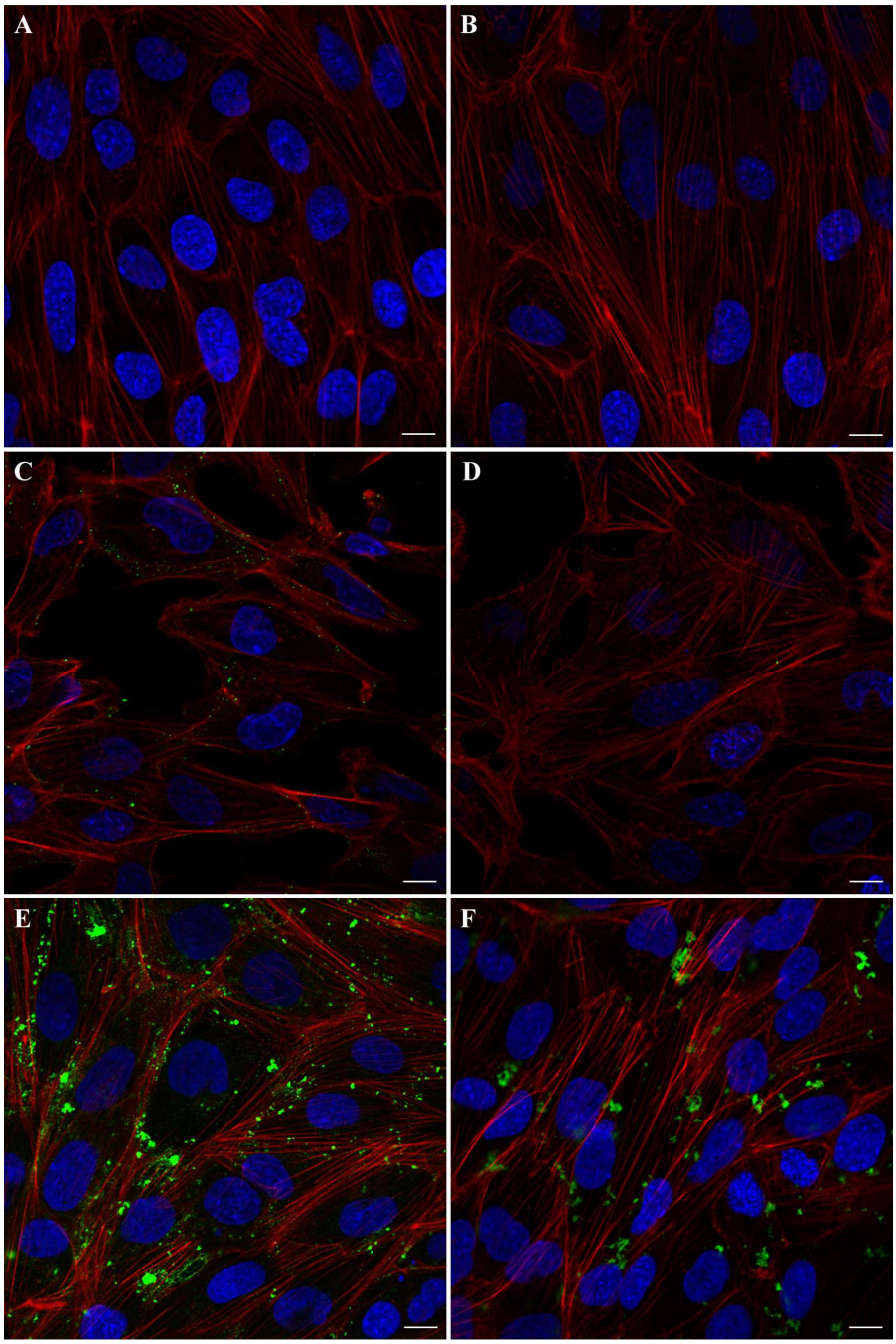

Fig. 16: CLSM of hCMEC/D3 cells incubated with Bodipy-Sm labelled PA/CL- NL PA/CL-mApoE-NL and PA/CL-dApoE-NL

hCMEC/D3 cells were incubated for 3 hours with PA/CL-NL, mApoE-PA/CL-NL and dApoE-PA/CL-NL, fixed with formalin solution and mounted for CLSM. PA/CL-NL without BBB functionalization showed no cellular uptake nor membrane association (A, B), and ApoE functionalization enhanced cellular internalization (C, D, E, F). mApoE-NL showed higher cellular uptake compared to dApoE-NL when NL were functionalized with PA (E, C, respectively) as well as with CL (F, D, respectively). NL associated fluorescence signal (green) is clearly localized below the plasma membrane and in the perinuclear region when cells were incubated with PA-mApoE-NL. When cells were incubated with PA-dApoE-NL, NL associated fluorescence signal was clearly detectable beneath the plasma membrane but not in the perinuclear region. Actin cytoskeleton was stained with Texas red conjugated-phallodin (red) and nuclei were counterstained with DAPI (blue). Bars: 10µm. *PA: phosphatidic acid; CL: cardiolipin*

Radioactivity assays were performed to confirm and quantify CLSM results. hCMEC/D3 cells were incubated for 3 hours with ^{3}H-DPPC-labelled PA/CL-NL or PA/CL-mApoE-NL, which displayed higher uptake. Cell associated radioactivity was measured after NL removal and mild trypsin treatment to remove membrane surface-adsorbed radioactivity. Only 5% of the administered radioactivity was found associated to cells incubated with PA/CL-NL, while an increase of 60% of cell associated radioactivity was achieved when hCMEC/D3 cells were incubated with PA-mApoE-NL ($p<0.05$). A mild increase (5%) was obtained with CL-mApoE-NL (Fig. 17). Similar results were achieved with RBE4 cells (data not shown).

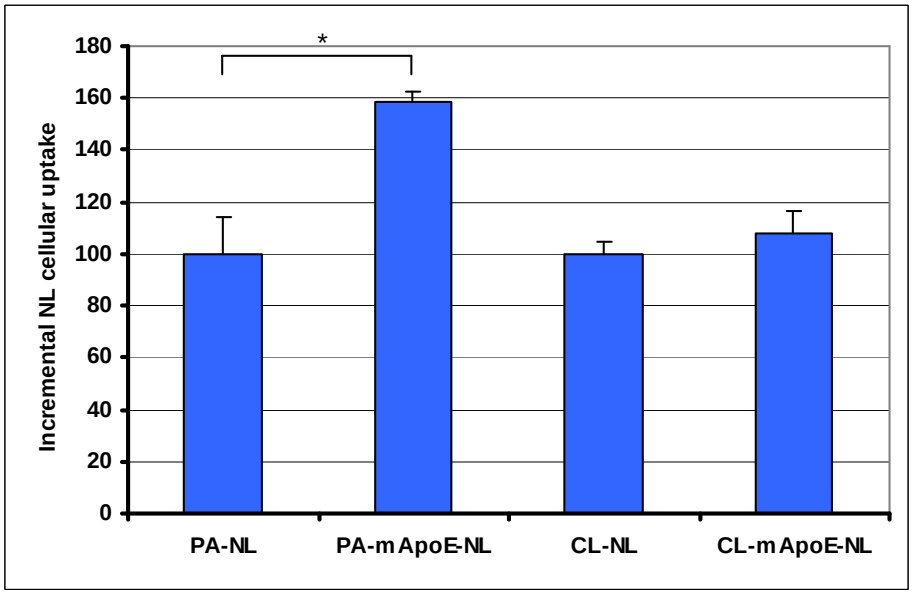

Fig. 17: Cellular uptake of ^{3}H-DPPC labelled PA/CL-NL and PA/CL-mApoE-NL

hCMEC/D3 cells were incubated for 3 hours with PA-NL, CL-NL, PA-mApoE-NL and CL-mApoE-NL and cell associated radioactivity was measured. Cellular uptake was expressed as the increment of cell associated radioactivity after further introduction of mApoE functionalization compared to PA or CL-NL. A statistically significant increase in cellular uptake was detected when cells were incubated with PA-mApoE-NL compared to PA-NL (+60%). Only slight enhancement of cellular uptake was reached with CL-mApoE-NL compared to CL-NL (+5%). *$p<0.05$

We tested NL double functionalized with curcumin derivative3 (Airoldi C. et al., 2011) to target Aβ peptide and with TAT peptide to target BBB. hCMEC/D3 cells were incubated for 3 hours with fluorescently labelled (Bodipy-Sm) curcumin derivative3-NL and curcumin derivative3-TAT-NL. No fluorescence was detectable with curcumin derivative3-NL (Fig. 18A), and TAT functionalization enhanced NL cellular uptake (Fig. 18B). NL associated fluorescence is clearly detectable in the cell cytoplasm and in the perinuclear region (Fig. 18B).

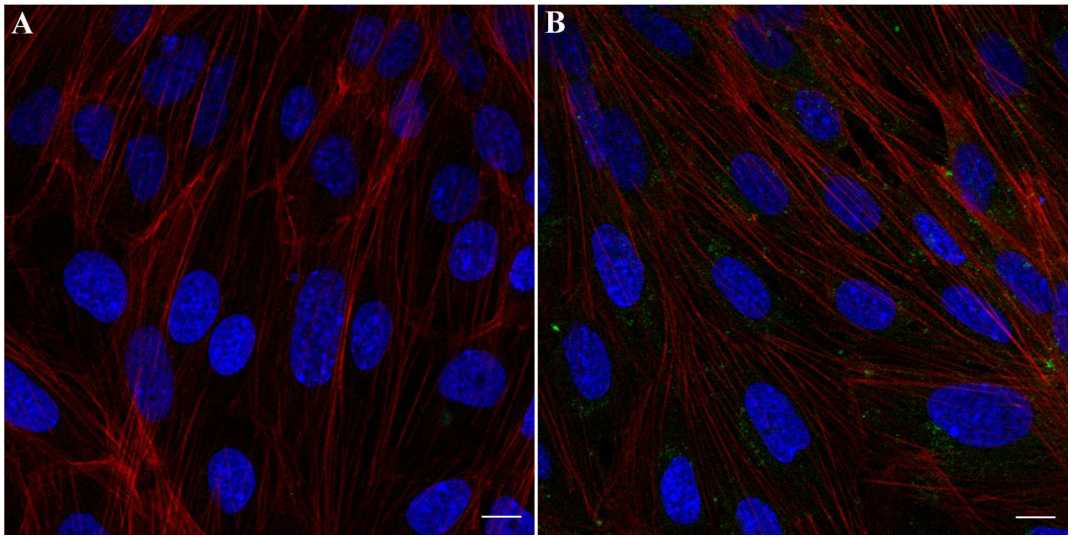

Fig. 18: CLSM of hCMEC/D3 cells incubated for 3 hours with Bodipy-Sm labelled curcumin derivative3-NL and curcumin derivative3-TAT-NL

hCMEC/D3 cells were incubated with Bodipy-Sm labelled (green) curcumin derivative3-NL (A) and curcumin derivative3-TAT-NL (B) for 3 hours, fixed with formalin solution and mounted for CLSM studies. No cellular uptake nor membrane association was detectable with curcumin derivative3-NL (A), and enhanced cellular uptake was clearly visible after further TAT functionalization (B). NL associated fluorescence signal is localized in the cytoplasm and in the perinuclear region. Actin cytoskeleton was stained with Texas red conjugated-phalloidin (red) and nuclei were counterstained with DAPI (blue). Bars: 10µm

Radioactivity assays were performed to quantitatively confirm CLSM studies. hCMEC/D3 cells were incubated for 3 hours with ^{3}H-Sm-labelled curcumin derivative3-NL or curcumin derivative3-TAT-NL and collected for cell associated radioactivity measurements. Only 0.52 ± 0.08 % of the administered radioactivity was found associated to cells incubated with curcumin derivative3-NL. TAT functionalization increased the amount of cell associated radioactivity up to 1.39 ± 0.27 % of the administered dose ($p<0.05$) (Fig. 19).

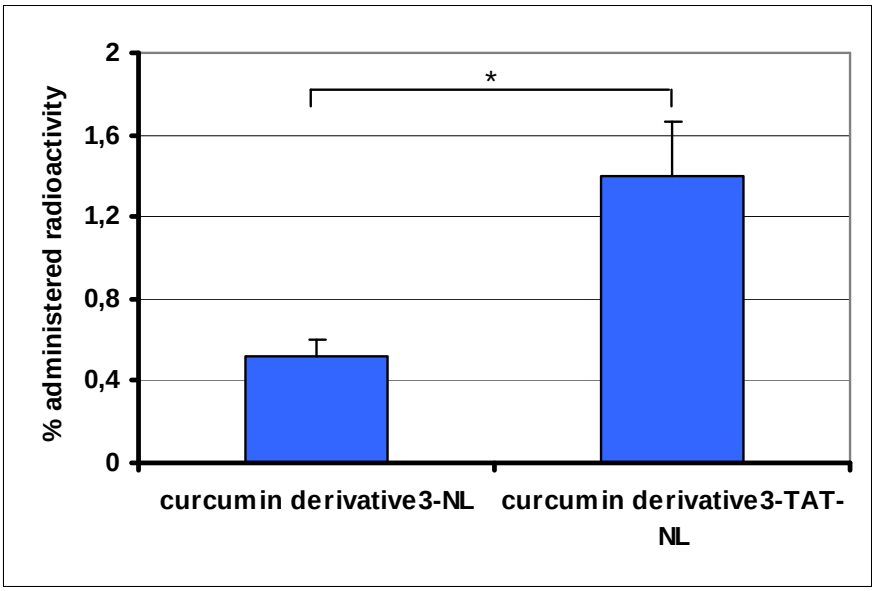

Fig. 19: Cellular uptake of 3H-Sm labelled curcumin derivative3-NL and curcumin derivative3-TAT-NL by hCMEC/D3 cells.

hCMEC/D3 cells were incubated for 3 hours with ^{3}H-Sm labelled curcumin derivative3-NL and curcumin derivative3-TAT-NL, and collected for cell associated radioactivity measurements. Further functionalization with TAT peptide induced about 2.5–fold increase in curcumin derivative3-NL cellular uptake. * $p<0.05$

4.5.2 - Intracellular fate of double functionalized NL

Once assessed cellular internalization, we investigated by CLSM the intracellular fate within hCMEC/D3 cells of NL double functionalized for both BBB targeting and Aβ peptide binding.

We incubated hCMEC/D3 cells for 3 hours or overnight (data not shown) with fluorescently labelled (Bodipy-Sm) PA-dApoE-NL, PA-mApoE-NL, CL-dApoE-NL and CL-mApoE-NL and we performed an immunostaining against the late endosomes and early lysosomes marker LAMP1. In agreement with our previous results, mApoE functionalization increased cellular uptake at higher extent compared to dApoE functionalization of PA-NL (Fig. 20C, A, respectively) as well as of CL-NL (Fig. 20D, B, respectively). No co-localization was detected between fluorescence associated to NL and LAMP1, at any incubation time we considered (Fig. 20).

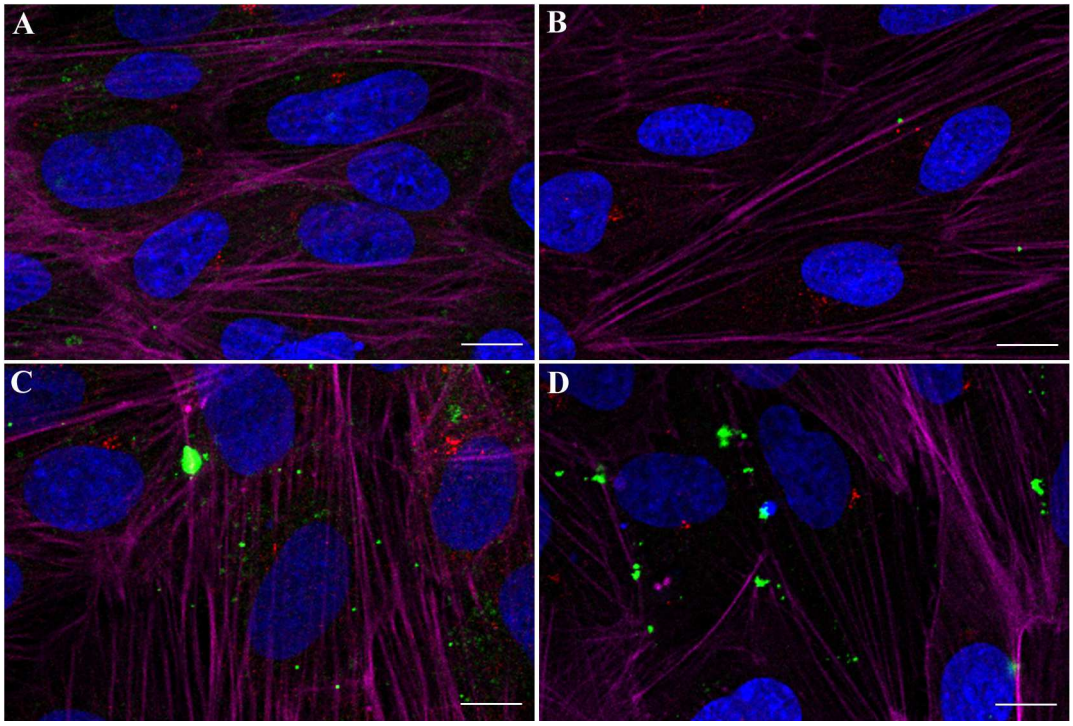

Fig. 20: CLSM of hCMEC/D3 cells incubated for 3 hours with fluorescently labelled (Bodipy-Sm) PA-dApoE, PA-mApoE, CL-dApoE and CL-mApoE-NL and immunostained for late endosome and lysosome marker LAMP1

hCMEC/D3 cells were incubated for 3 hours with fluorescently labelled (Bodipy-Sm) (green) PA-dApoE, PA-mApoE, CL-dApoE and CL-mApoE-NL, immunostained with LAMP1 (red) for detection of late endosomes and lysosomes and mounted for CLSM. As previously demonstrated, PA-dApoE (A) and CL-dApoE-NL (B) showed lower cellular uptake compared to PA-mApoE (C) and CL-mApoE-NL (D) respectively, with PA-mApoE-NL showing highest cellular accumulation. No-colocalization of NL and LAMP1 associated fluorescence was detected in any sample we analyzed and at any incubation time we considered (A, B, C, D). Actin cytoskeleton was stained with AlexaFluor 633nm conjugated-phalloidin (magenta) and nuclei were counterstained with DAPI. Bars: 10µm.

We then incubated hCMEC/D3 cells for 3 hours and overnight (not shown) with fluorescently labelled (Bodipy-Sm) curcumin derivative3-TAT-NL, and we performed an immunostaining against the early endosome marker EEA1 or against LAMP1. NL did not co-localized with the early endosome marker EEA1 nor with the late endosome and early lysosome marker LAMP1 (Fig. 21A, B).

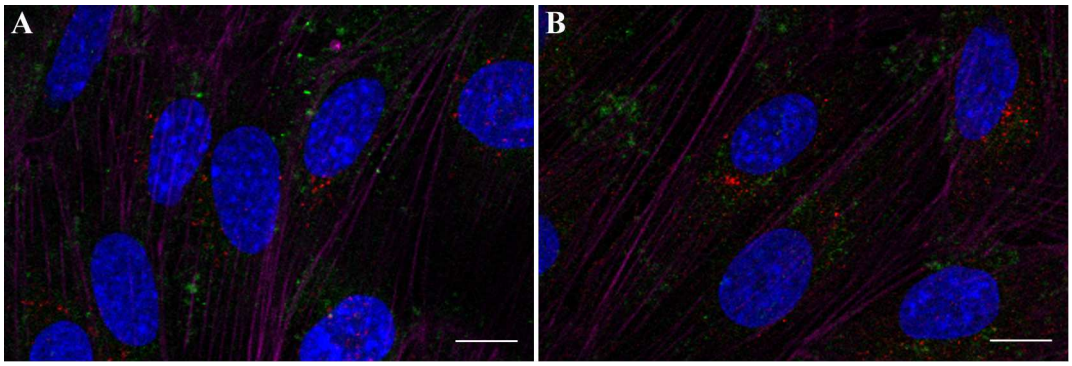

Fig. 21: CLSM of hCMEC/D3 cells incubated for 3 hours with (Bodipy-Sm) curcumine derivative3-TAT-NL and immunostained for early endosome and late endosome and early lysosome markers

hCMEC/D3 cells were incubated for 3 hours with fluorescently labelled (Bodipy-Sm) (green) curcumin derivative3-TAT-NL, immunostained against EEA1 (A) (red) or LAMP1 (B) (red) for detection of early endosomes or late endosomes and early lysosomes, respectively, and mounted for CLSM. No-colocalization was detected with the intracellular compartments we considered (A, B). Actin cytoskeleton was stained with AlexaFluor 633nm conjugated-phalloidin (magenta) and nuclei were counterstained with DAPI (blu). Bars: 10µm.

4.5.3 - Permeability of double functionalized NL across endothelial cell monolayer

We demonstrated that mApoE and TAT functionalizations increased cellular uptake of PA/CL-NL, and curcumin derivative3-NL respectively, without interfering with NL ability of binding Aβ peptide (Re F. et al., 2011). Moreover, increased NL uptake did not induce co-localization with the acidic cellular compartments. We thus investigated double functionalized NL permeability across the endothelial cell monolayer.

We studied PA/CL-NL and PA/CL-mApoE-NL permeability across the RBE4 cell monolayer, by means of radioactivity assays.

^{3}H-DPPC labelled NL were added to the donor chamber of Transwell® system at the final concentration of 0.1mM as total lipids and radioactivity was measured in the acceptor chamber at 0, 60, 180 min. PA-mApoE-NL PE was 3-fold increased compared to PA-NL. Only slight enhancement was detected when CL-NL were further functionalized with mApoE (+2%) (Fig. 22).

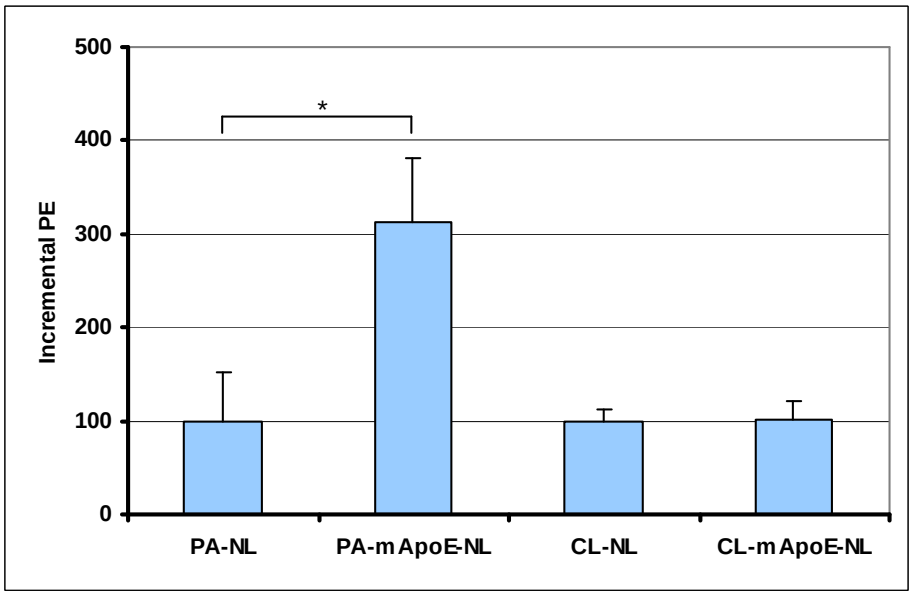

Fig. 22: ^{3}H-DPPC labelled PA/CL-NL and PA/CL-mApoE-NL endothelial permeability across RBE4 cell monolayer (incremental PE).

RBE4 were seeded on Transwell® systems and incubated with ^{3}H-DPPC labelled PA/CL-NL and PA/CL-mApoE-NL for 3 hours. Radioactivity in the acceptor compartment was measured at 0, 60, 180 min. mApoE functionalization induced 3-fold increase in PA-NL PE. No significative differences were detected when CL-NLs were further functionalized with mApoE peptide (+2%). * $p<0.05$

We studied curcumin derivative3-NL and curcumin derivative3-TAT-NL permeability across hCMEC/D3 cell monolayer, with readioactivity assays.

^{3}H-Sm-labelled curcumin derivative3-NL or curcumin derivative3-TAT-NL were added to the donor chamber of Transwell® systems at a final concentration of 0.1mM, for 3h. After 0, 60 and 180 min of incubation radioactivity was measured in the acceptor chamber and PE was calculated. The PE of curcumin derivative3-NL was increased with further TAT functionalization (+75%, $p<0.05$) (Fig. 23).

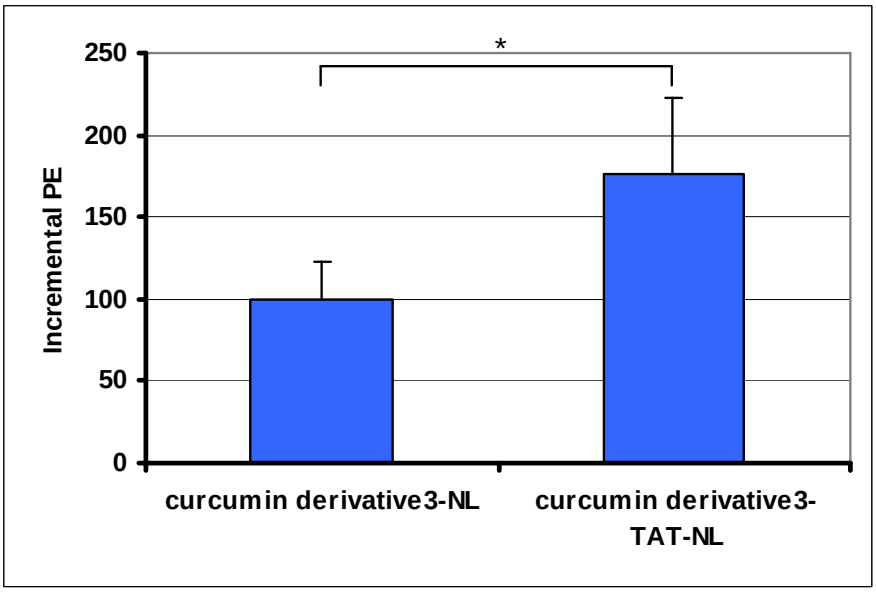

Fig 23: ^{3}H-Sm labelled curcumin derivative3-NL and curcumin derivative3-TAT-NL endothelial permeability across hCMEC/D3 cell monolayer (incremental PE)

hCMEC/D3 cells were seeded on Transwell systems and incubated for 3 hours with 3H-Sm labelled curcumin derivative3-NL and curcumin derivative3-TAT-NL. Radioactivity was measured after 0, 60, 180 min and PE was calculated. 75% increase in curcumin derivative3-NL PE was achieved after further TAT functionalization. *$p<0.05$

4.6 - UPTAKE MECHANISMS OF NL BY hCMEC/D3 CELLS

Once assessed NL cellular uptake, intracellular fate and PE, we inquired NL endocytic mechanism to entry endothelial cells, employing siRNA technique to stably down-regulate caveolin1 expression in hCMEC/D3 cells. NL internalization in down-regulated and WT cells was evaluated with FACS analysis and CLS microscopy studies, and the involvement of caveolin1 and its related endocytic mechanism was assessed. We performed all these experiments with NL mono-functionalized for BBB targeting with ApoE and TAT peptides located at low density on NL surface.

4.6.1 - Amplification and purification of SureSilencing shRNA Plasmids

We considered four shRNA plasmids targeting Caveolin1 (clones 1, 2, 3, 4), according to manifacturer's instructions. A plasmid containing a non targeting sequence was provided as negative control. An E. Coli JM109 strand was transformed with SureSilencing shRNA Plasmids, using thermal shock technique. DNA was extracted, amplified and purified using EndoFree Plasmid Maxi kit. After quantification, DNA was digested with PstI restriction enzyme and the digestion products were controlled on agarose gel. The two diagnostic bands indicating the presence of the shRNA insert were detected in all the digestion products we analyzed (data not shown). The tested plasmids were then utilized for further transfection experiments.

4.6.2 - hCMEC/D3 cells transfection and Western Blot

hCMEC/D3 cells were seeded and left to grow until they reached 70% confluence, typically after 1 DIV. Transfection with SureSilencing shRNA targeted to caveolin1 was performed using Lipofectin as transfection reagent. All the four plasmids containing targeting sequences and the negative control (C-) were used. After 24h from transfection, cells were trypsinized and seeded in selection medium. During selection process, cell morphology was monitored and no alterations were detectable in all the transfected cells compared to negative control and un-transfected cells (data not shown).

Cells transfected with all the clones were seeded and collected for western blot analysis to quantify caveolin1 protein. Clone 2 and clone 4 registered a slight reduction of the protein levels (18%), compared to negative control, while a greater reduction was detected in clone 1 (42%) and clone 3 (43%), which was used for all the further experiments (Fig. 24).

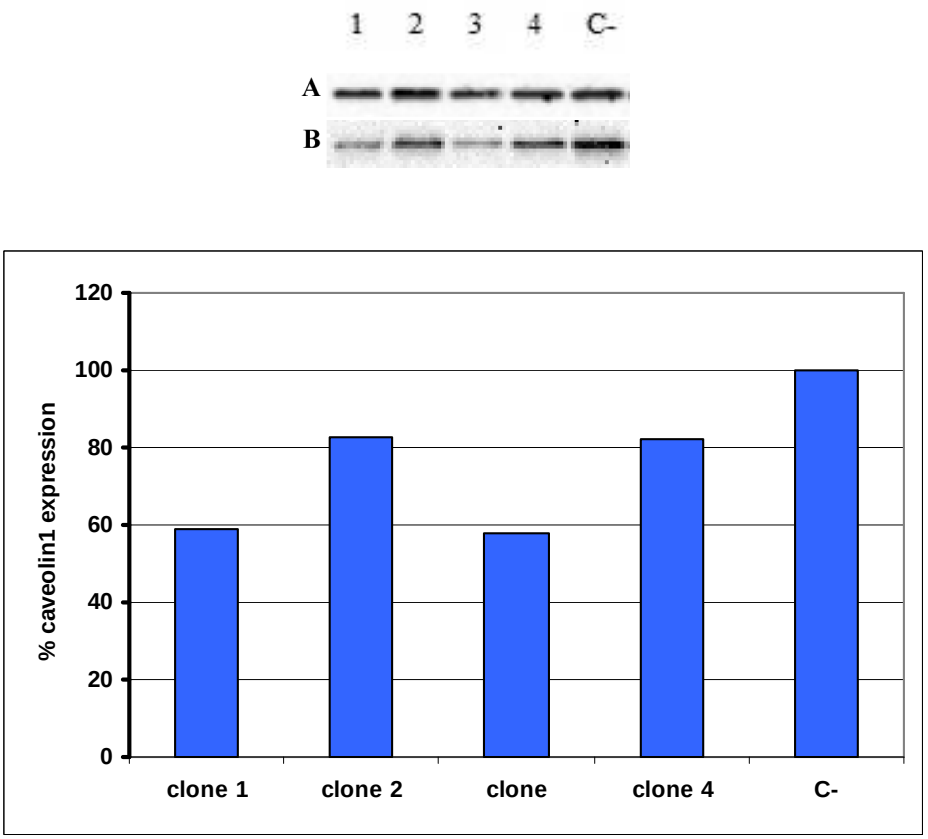

Fig. 24: Western Blot analysis and quantification of residual caveolin1 expression in hCMEC/D3 cells transfected with shRNA vector

hCMEC/D3 cells were collected and analyzed by western blot assay to evaluate residual expression of caveolin1 (B). Residual amount of caveolin1 was calculated after normalization on actin protein content for each sample (A). Reduction ranging from 20% (clone 2 and 4) to 42% (clone 1) and 43% (clone 3) was detected compared to negative control, and the clone expressing the lowest amount of caveolin1 (clone 3) was selected for further experiments. *C-: negative control*

4.6.3 - Assessment of caveolin1 involvement in NL uptake by FACS

NL uptake was investigated in hCMEC/D3 clone 3, stably transfected with shRNA targeting caveolin1 (hCMEC/D3 shRNA) and in un-transfected cells (Wild Type, hCMEC/D3 WT).

hCMEC/D3 shRNA and WT were incubated with fluorescently labelled (Bodipy-Sm) mApoE-NL, dApoE-NL and TAT-NL for 3h and collected for FACS analysis. The same experiments were performed on hCMEC/D3 WT cells treated with filipin 3µM (hCMEC/D3 Fil), a drug known to interfere with caveolae-mediated endocytosis. Preliminary results showed that the internalization of mApoE-NL was significantly reduced in hCMEC/D3 shRNA cells, while it was not affected in hCMEC/D3 Fil cells (Fig. 25). dApoE and TAT-NL

internalization was not affected in hCMEC/D3 shRNA cells nor in hCMEC/D3 Fil cells, compared to hCMEC/D3 WT cells (Fig. 25).

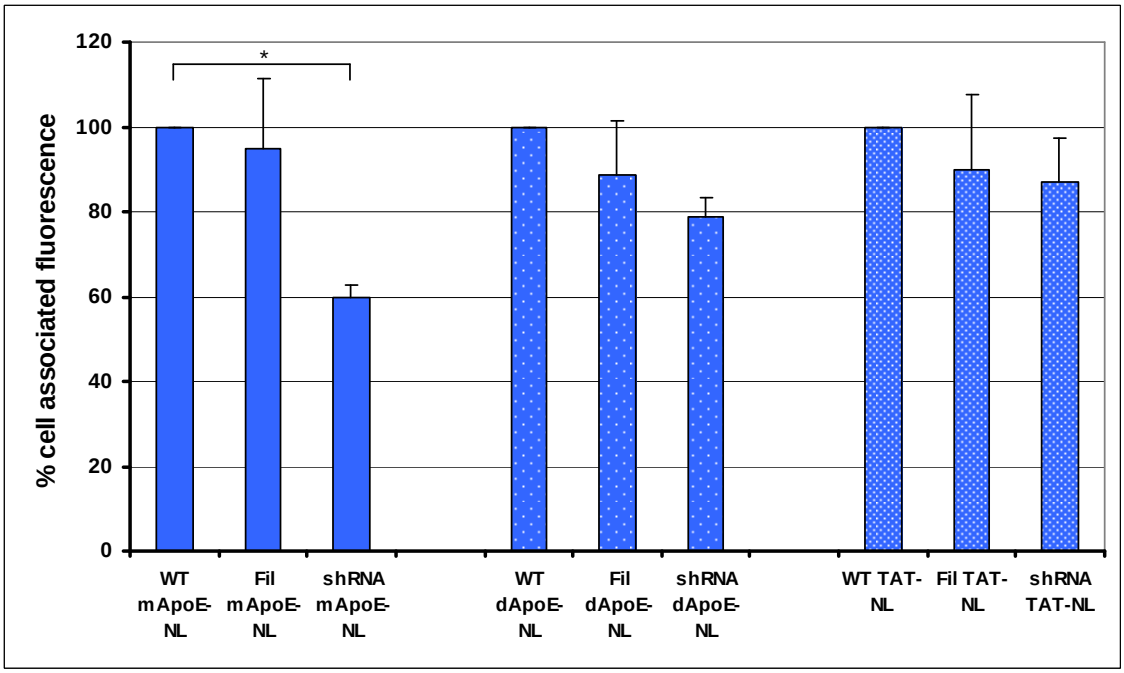

Fig. 25: Uptake of mApoE, dApoE and TAT-NL by untransfected hCMEC/D3 cells (WT), hCMEC/D3 cells treated with Filipin 3µM (Fil), or hCMEC/D3 cells stably transfected with shRNA targeting caveolin1 (shRNA).

hCMEC/D3 WT and hCMEC/D3 shRNA cells were incubated for 3 hours with mApoE, dApoE or TAT-NL and collected for FACS analysis. Cells treated with filipin 3µM were used as control. Significant reduction of mApoE-NL cell associated fluorescence was detected in hCMEC/D3 cells down-regulated for the expression of caveolin1 (-40%). No significative reduction was achieved with cells treated with filipin 3µM compared to WT cells. dApoE and TAT-NL internalization was not affected by caveolin1 down-regulation nor by filipin treatment. * $p<0.05$. *WT: hCMEC/D3 untransfected cells; Fil: hCMEC/D3 cells treated with Filipin; shRNA: hCMEC/D3 cells stably down-regulated for caveolin1 expression*

4.6.4 - Assessment of caveolin1 involvement in NL uptake by CLSM

CLSM was employed to support FACS analysis and to further disclose the mechanism of mApoE-NL endocytosis. hCMEC/D3 shRNA, WT and Fil cells were incubated with fluorescent (Bodipy-Sm) mApoE-NL for 3h, fixed with formalin solution and mounted for CLSM.

mApoE-NL were clearly internalized by hCMEC/D3 WT cells, as previously demonstrated, and NL associated fluorescence was clearly visible in the cell perinuclear region (Fig. 26A). In hCMEC/D3 shRNA cells NL associated fluorescence signal was reduced (Fig. 26C), while

in Fil cells no modification in NL internalization could be detected compared to WT cells (Fig. 26B).

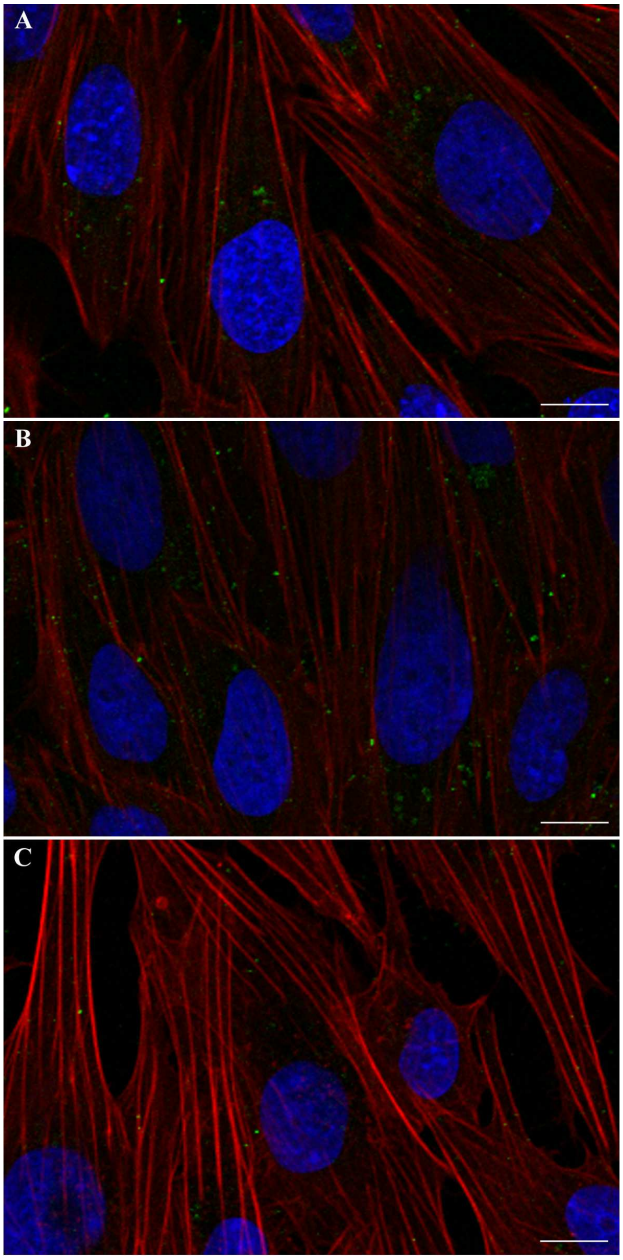

Fig. 26: Uptake of mApoE-NL by hCMEC/D3 WT cells, hCMEC/D3 WT cells treated with filipin 3µM and hCMEC/D3 cells stably transfected with shRNA targeting caveolin1

hCMEC/D3 WT, Fil and shRNA cells were incubated for 3 hours with fluorescently labelled (Bodipy-Sm) mApoE-NL (green), fixed with formalin solution and mounted for CLSM. As we already demonstrated previously, mApoE-NL are internalized by hCMEC/D3 WT cells and NL associated fluorescence signal is clearly detectable in the cytoplasm, below the plasma membrane and in the perinuclear region (A). Treatment with filipin 3µM showed no alteration in cell morphology and did not decrease mApoE-NL cellular uptake (B). A clear reduction of mApoE-NL associated fluorescence is detectable in the perinuclear region of hCMEC/D3 shRNA cells, down-regulated for caveolin1 (C). Actin cytoskeleton was stained with Texas red conjugated-phalloidin (red) and nuclei were counterstained with DAPI (blu). Bars: 10µm.

hCMEC/D3 WT cells were then co-incubated for 3h with both mApoE-NL and Cholera Toxin B (CTB), a marker for caveolae-mediated endocytosis, fixed with formalin solution and mounted for CLSM.

CTB associated staining was detected in the cell perinuclear region, as expected (Schnitzer J.E. et al., 1996; Kirkham M. et al., 2005), (Fig. 27A) and NL associated fluorescence was prevalently localized in the cell perinuclear region, as already shown. Partial co-localization of NL and CTB positive vesicles was detected (Fig. 27B).

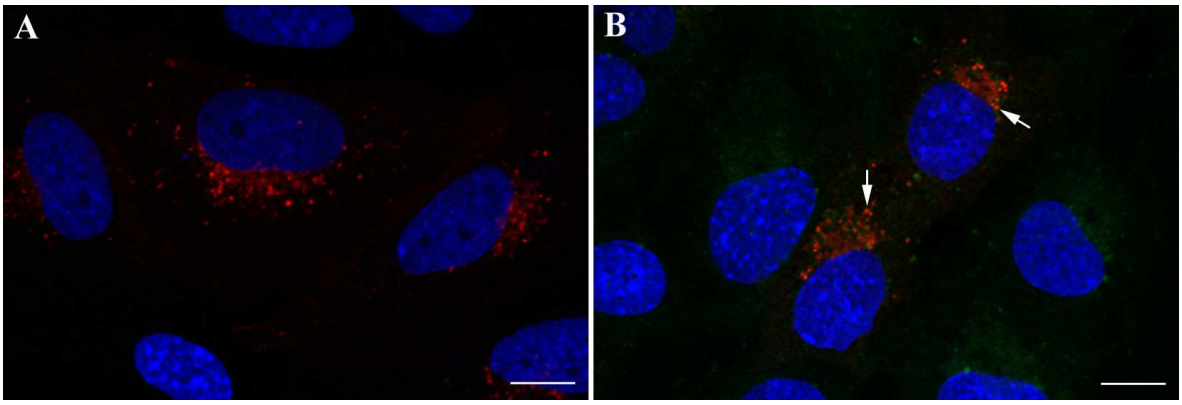

Fig. 27: CLSM of hCMEC/D3 WT cells co-incubated for 3 hours with AlexaFluor 594nm conjugated-Cholera Toxin B and Bodipy-Sm labelled mApoE-NL

hCMEC/D3 WT cells were co-incubated for 3 hours with AlexaFluor 594nm conjugated-Cholera Toxin B (CTB) (red) and Bodipy-Sm labelled mApoE-NL (green), fixed with formalin solution and mounted for CLSM. CTB staining is localized in the cell perinuclear/Golgi-like region, as already demonstrated (A) and show partial co-loalization (B, arrows) with mApoE-NL associated signal, thus indicating a likely partial share of a common endocytosis pathway. Nuclei were counterstained with DAPI. Bars: 10µm.

5 - DISCUSSION

Alzheimer's Disease (AD) is the most common form of age related dementia and it is predicted to affect 1 in 85 people globally by 2050. Up to now no therapies are available for AD and certain diagnosis is performed only after patient death. Thus, new diagnostic tools and therapies are needed for early detection and treatment of AD (Dartigues J.F., 2009). Sporadic AD is the most common form, accounting for 95% of AD patients, and its origin has not been clarified yet. Among the different theories that have been formulated, the amyloidogenic cascade hypothesis has acquired large consensus over the past two decades. According to it, the increased Aβ production and its decreased clearance from the brain lead to Aβ accumulation and its aggregation within the senile plaques, the main hallmarks of AD (Swerdlow R.H., 2007). In the late stage of disease, brain Aβ is in equilibrium with the circulating Aβ. Strategies to remove Aβ from the blood, thus favouring its clearance ("sink effect") are under developing (Wang Y.J. et al., 2006). Moreover, tools to overcome the blood brain barrier and to reach the brain Aβ and limiting its aggregation are needed.

To this aim, within nanoparticles, nanoliposomes (NL) are promising tools since they are biocompatible and biodegradable, they can be designed to avoid degradation, and they can be functionalized to overcome the BBB and bind Aβ (Beija M et al., 2012; Caruthers S.D. et al., 2007; Moghimi S.M. et al., 2005).

5.1 - CHARACTERIZATION OF IN VITRO BBB MODELS

In this study we settled in vitro BBB models based on immortalized cell lines, to assess nanoliposomes (NL) as potential tools to overcome the BBB and to deliver drugs and contrast agents within the brain, for joint AD therapy and diagnosis. Many efforts were made in the past years to develop reliable in vitro BBB models. However, no models perfectly resembling in vivo features have been developed yet. Immortalized cell lines usually do not have the required permeability restriction properties for studying free drug passage across the BBB. However, they have been demonstrated to maintain their characteristics along with cell doublings, allowing comparison among different experiments (Cecchelli R. et al., 2007; Gumbleton M. and Kenneth L.A., 2001). Up to now, in vitro BBB models based on immortalized cell lines seem to be a good choice for dealing with engineered nanoparticles high throughput screenings (Roux F. and Couraud P.O., 2005).

First of all, we tested our models for barrier expression features through TEER measurements and evaluation of endothelial permeability (PE) of sucrose, a well-known hydrophilic marker of the paracellular transport. The sucrose PE and TEER measurements were in agreement with data previously reported (Gumbleton M. and Audus K.L., 2001; 2011; Weksler B.B. et al, 2005; Poller B. et al., 2008). We investigated the NL internalization and permeability on both hCMEC/D3 and RBE4 cell based in vitro BBB models. Despite their different features, the two in vitro BBB models showed a significant reproducibility concerning NL cellular uptake or permeability. This clearly indicates that our models can be suitable tools for achieving an integrated evaluation of NL cell uptake and permeability.

5.2 - NL MONO-FUNCTIONALIZED FOR BBB TARGETING

At the BBB, almost only specifically regulated transcellular passage can occur, prevalently by receptor mediated transcytosis. Thus, new approaches for drug delivery to the brain exploit BBB endogenous transporters to achieve drug and carrier passage. The low density lipoprotein receptor (LDLr) is expressed at the BBB and accounts for LDL transcytosis (Dehouck B. et al., 1997). Indeed, the region localized between the amino acids 140 and 150 of the ApolipoproteinE is required for receptor binding. The tandem linear repeat sequence corresponding to amino acid residues 141-150 has been shown to retain receptor binding ability, while monomeric sequence corresponding to amino acid residues 141-150 has not (Dyer C.A. et al., 1995). Moreover, adsorptive-mediated endocytosis has been documented at BBB endothelial cells (De Boer A.G. and Gaillard P.J., 2007), and it is likely involved in the uptake of TAT peptide.

Taken into accounts these considerations, we screened NL functionalized to target the BBB with human ApoE-derived peptides, the ApoE monomer (mApoE), (amino-acids 141-150) and its tandem dimer $(141\text{-}150)_2$ (dApoE); subsequently, we considered NL functionalized with TAT derived peptide. TAT cationic charges facilitate interaction with the normally negatively charged BBB, triggering permeabilization of the cell membrane via a receptor/transporter independent pathway (Derossi, D., et al., 1996). We demonstrated that NL without BBB targeting functionalization did show neither cell membrane association nor uptake. In particular, ApoE and TAT peptides increased cellular uptake. TAT peptide showed the highest cellular internalization, and mApoE enhanced cellular uptake at higher extent compared to dApoE, both at low and at high peptide surface density. Time course

experiments and FACS analysis revealed that each functionalization increased NL cellular uptake over time, without reaching *the steady state* after up to 5 hours of incubation.

No clear evidences of receptor-mediated uptake emerge from these results, since receptor-mediated endocytosis requires the presence of free and available receptor and it generally undergoes saturation. In accordance with our data, mApoE peptide sequence has been reported to contain many positively charged amino acids. An endocytic mechanism, mediated by unspecific adsorption onto cellular membrane heparan sulphate proteoglycans, has thus been proposed for mApoE as well as for TAT peptide (Sauer I. et al., 2005). Previous studies showed that dApoE sequence retains receptor-binding ability, even though it displays 1000-time reduced binding affinity as compared to natural ligand. According to our results, receptor-mediated uptake accounts only in part for dApoE-NL cellular internalization. Our data can be explained by the lack of amino acid residues involved in stabilizing and aligning the receptor-binding region, which have been localized between amino acid residues 170 and 180 (Sauer I. et al., 2005).

CLSM studies are in agreement with FACS results, and they showed differences in staining patterns related to specific NL functionalization. dApoE peptide NL functionalization originated a punctuate staining pattern prevalently localized just below the plasma membrane. mApoE and TAT functionalized NL localized in the peripheral region of cell cytoplasm below the plasma membrane, and a clear staining was also detectable within the perinuclear region. Punctuate staining and the perinuclear localization of both mApoE and TAT functionalized NL suggest that an endocytic mechanism may be responsible for NL uptake, leading to the formation of endocytotic vesicles. The absence of internalization with un-functionalized NL and the evinced direct relationship between cellular uptake and the peptides density located on liposome surface demonstrate that endocytosis process clearly depends on the peptides presence. Distinctions in the total amount of fluorescence signal and in the intracellular localization of NL suggest that different uptake mechanisms may account for specific functionalized NL. Further support to this hypothesis was achieved through concurrent functionalization with dApoE and TAT peptides. dApoE-NL cellular uptake was significantly increased after further TAT functionalization. This demonstrates that NL cellular interaction is driven by both peptides located at the NL surface.

We then investigated permeability across endothelial cell monolayer of BBB targeted functionalized NL. Un-functionalized NL were not considered within these experiments, due to their extremely low interaction with cerebral microvascular endothelial cells. Due to BBB permeability restriction properties, 100-200nm sized objects cannnot freely diffuse through

paracellular passage. Their interaction with endothelial cells is thus required for further transport across the BBB, likely the first step of a transcytosis process.

We demonstrated that only mApoE functionalization at high density increased NL PE compared to low density. On the contrary, dApoE functionalization did not show significant enhancement of NL PE when the peptide density on liposome surface increased. TAT peptide functionalization, alone or in combination with dApoE peptide, did not increase NL PE compared to dApoE NL single functionalization, despite significant increase in cellular uptake. We can hypothesize that TAT-NL and TAT-dApoE-NL could be retained for long time into cell cytoplasm, thus limiting their transcellular flow rate. Longer incubation time during permeability experiments would be required to assess this issue. We cannot exclude that a fraction of the administered TAT-NL and TAT-dApoE-NL could be stably entrapped into cell cytoplasm and metabolized.

Moreover, toxicity features were evaluated at both single cell and cell monolayer level, through MTT assays and measurements of sucrose PE, respectively. Our results indicated that neither toxicity nor alteration of monolayer tightness were associated to NL interaction with brain microvascular endothelial cells (hCMEC/D3 and RBE4). Our data thus indicate that transcellular passage may have to occur to achieve NL crossing of the BBB, since the paracellular passage is strongly inhibited by preserved endothelial monolayer tightness.

Finally, we detected specificities in the relationship between NL uptake and PE when different functionalizations were employed. Distinct internalization mechanisms and related specific intracellular fate and metabolism could explain our results, and our experiments were aimed at investigating these issues.

Taken together, our results demonstrated that, in our *in vitro* experimental conditions, TAT-NL show the best cellular uptake, when dealing with mono-functionalized NL. However, mApoE functionalization at high density is the best performing when considering combined internalization and PE across in vitro BBB model.

5.3 - NL DOUBLE FUNCTIONALIZED FOR BBB TARGETING AND AMYLOID β PEPTIDE BINDING

Once assessed the dynamics of BBB targeted NL within BBB endothelial cells, we moved towards double functionalized NL, carrying BBB targeting peptides and Aβ targeting ligands in order to investigate possible tools for joint AD therapy and diagnosis. In one set of

experiments, NL were loaded with a tritiated curcumine derivative, [^{3}H]-curcumine4, whereas in another set of experiments NL were designed to expose Aβ targeting ligands on the NL outer surface.

Curcumin is a low molecular weight molecule derived from the perennial herb Curcuma Longa and it has been reported to have several biological effects, such as anti-inflammatory and anti-oxidant properties (Airoldi C. et al., 2011). Recently, its ability in inhibiting amyloid polimerization has been demonstrated (Narlawar R. et al., 2008), but its poor solubility and stability in water solvents have limited its clinical employment. Therefore, its chemical stabilization and association to NL are required in order to increase its bioavailability at the site of action.

5.3.1 - NL functionalized for BBB targeting and loaded with a tritiated curcumin derivative for amyloid β peptide binding

We tested NL functionalized with ApoE derived peptides and loaded with a chemically stabilized curcumin-derivative ([^{3}H]-curcumin4) (Re F. et al., 2011), and we measured drug cellular uptake and permeability across *in vitro* BBB model, through radiochemical assays.

We demonstrated that [^{3}H]-curcumin4 alone was not internalized by endothelial cells. ApoE functionalized NL, loaded with [^{3}H]-curcumin4, increased the drug cellular uptake. In particular, mApoE functionalization at high density showed the highest internalization. Direct relationship between peptide density on liposome surface and drug cellular internalization was demonstrated with mApoE, but not with dApoE functionalization. The highest enhancement in PE was achieved after drug encapsulation into dApoE functionalized NL at high density, suggesting their greatest ability in increasing the drug flux across the cell monolayer.

Since these results are partially contradictory with our previous data, we might speculate that different dynamics could regulate NL interactions with cellular membrane and NL intracellular fate when NL entrapped a drug payload. This could favour drug passage with dApoE-NL and drug retention by endothelial cells with mApoE-NL. Further investigation are required to assess these issues.

5.3.2 - NL functionalized for BBB targeting and exposing ligands for amyloid β peptide binding

We then considered NL double functionalized for BBB targeting and exposing Aβ binding ligands. Phosphatidic acid (PA) and cardiolipin (CL) have already been demonstrated to bind Aβ peptide with high affinity, and NL carrying these phospholipids were shown to retain this ability (Gobbi M. et al., 2010).

We investigated the internalization and permeability of NL double functionalized for BBB targeting with ApoE peptides (monomer or its tandem dimer) at high density and for Aβ binding with PA and CL phospholipids, by means of CLSM and radiochemical assays.

We demonstrated that mApoE functionalization increased cellular uptake of PA/CL-NL at higher extent compared to dApoE. When considering mApoE functionalized NL, PA-mApoE-NL showed higher uptake compared to CL-mApoE-NL. We also demonstrated that the PE of PA-NL was increased after further mApoE functionalization, but the same did not occur in case of CL-NL.

We might hypothesize that the higher content of negative charges in CL phospholipids could mask positive charges of mApoE peptides, thus interfering with its adsorption onto cellular membrane. It is important to highlight that along with cellular uptake, also NL passage across in vitro BBB models is strictly related to NL-cell interactions. In agreement with our previous data concerning mono-functionalized NL, direct relationship between cellular uptake and PE was again clearly demonstrated with double functionalized NL.

When considering PA-mApoE and PA-dApoE NL, CLSM studies confirmed the staining pattern of those of mono-functionalized mApoE and dApoE-NL. This observation further supports the hypothesis that peptide functionalization regulates NL cellular interaction and, likely, also NL intracellular fate. To further investigate the intracellular fate of double functionalized NL, we performed immunofluorescence assays direct to late endosomes and early lysosomes. No co-localization was detected with mApoE nor with dApoE functionalized PA/CL-NL within these intracellular compartments. This evidence suggests a possible NL escaping mechanism from cellular degradation, likely towards a transcytosis pathway.

Our results related to ApoE and PA/CL double functionalized NL confirm that mApoE functionalization show the best performances, concerning cellular uptake and PE across our *in vitro* BBB models. CL phopsholipid but not PA can interfere with mApoE-mediated cellular interactions, suggesting that positive charge mediated adsorption onto cellular membrane could be responsible for mApoE-NL uptake and transcytosis. Direct relationship between increased NL cellular internalization and PE, along with likely lysosomal escaping and the

absence of cytotoxicity (evaluated by MTT test and sucrose permeability assay) clearly suggest that transcytosis mechanism could account for NL crossing the endothelial cell monolayer.

Finally, we considered a different NL formulation, carrying TAT peptide for BBB targeting and functionalized at the surface with curcumin derivative3 for Aβ binding (Airoldi C. et al., 2011).

We demonstrated that TAT peptide increased cellular uptake and PE of curcumin derivative3-NL, and that no co-localization occurred with the acidic cellular compartments. Cell cytoplasm and perinuclear staining was detected with both single functionalized TAT-NL and double functionalized curcumin derivative3-TAT-NL. Again, no toxicity was detected neither at the cellular nor at the monolayer level.

Taken together, our results concerning curcumin derivative3-TAT-NL suggest that a transcytotic mechanism may occur and account for their passage across cell monolayers. The total amount of internalized NL appeared lower with curcumin derivative3-TAT-NL compared to mono-functionalized TAT-NL. Thus, the functionalization with curcumin derivative3 compound appeared to reduce cellular uptake mediated by TAT peptide. We can speculate that steric hindrance may be responsible for this mechanism, and further experiments will be aimed at disclosing this issue.

5.4 - INVESTIGATION OF THE ENDOCYTIC MECHANISMS LEADING TO NL INTERNALIZATION

In the last part of this study, we investigated the endocytic mechanism mediating NL entry into endothelial cells. Indeed, the endocytic mechanism is strictly related to the intracellular fate of internalized cargoes. Therefore, investigating the uptake mechanism is important when dealing with promising drug and contrast agent delivery vectors, and drug delivery at the specific site of action is fundamental for these new therapeutic approaches.

We started to investigate caveolin1 role, since caveolin1 is the major constituent of caveolae, 50-80 nm sized membrane invaginations that are involved in transcytosis process at the endothelial cells (Candela P. et al., 2008). We stably down-regulated caveolin1 protein in hCMEC/D3 cells by shRNA interfering technique, and we achieved a protein reduction of about 40%. The low efficiency we observed could depend on the selection procedure, since we selected all the transfected cells without performing single clone isolation. We thus achieved a polyclonal population, expressing shRNA targeting caveolin1 at different extent

among different cellular clones. The reduction in protein content is thus the average of caveolin1 content in the mixed population. Further clone isolation will be required to achieve monoclonal populations with the expected less residual protein content (Wadhwa R. et al., 2004).

Preliminary uptake experiments were performed on hCMEC/D3 WT cells and on hCMEC/D3 cells stably down-regulated for caveolin1 protein expression. Cells were incubated with single functionalized mApoE, dApoE and TAT-NL at low peptide density on liposome surface. FACS and CLSM analysis were done to detect NL cellular internalization. hCMEC/D3 WT cells treated with filipin, a cholesterol sequestering agent, were used as control. Since lipid rafts and their associated caveolae are enriched in cholesterol content, filipin is commonly used as specific pharmacological inhibitor of caveolae-mediated endocytosis (Ryoung Kim H. et al., 2007). However, recent studies questioned pharmacological agent employment as specific inhibitors of endocytosis pathways, and problems concerning specificity and cellular toxicity have been raised (Vanden Broeck D. and De Wolf M.J.S., 2006).

Our preliminary results showed about 40% reduction of mApoE-NL cellular uptake after caveolin1 down-regulation. No significant reduction was detected after cell treatment with filipin, at least at the concentration herein utilized. Because of higher filipin concentration displayed cellular toxicity, our results demonstrated that, in our experimental conditions, siRNA technique showed better specificity and less toxicity compared to the common drug based strategy to interfere with caveolae-mediated uptake. No variations in the uptake of dApoE and TAT functionalized NL were detected after caveolin1 down-regulation, nor filipin treatment.

Our preliminary results suggest that caveolin1 dependent endocytic mechanism might account for mApoE-NL entry into brain capillary endothelial cells. We can thus speculate that caveolae-mediated endocytosis could be in part involved in mApoE-NL uptake pathway.

To further assess this hypothesis we co-incubated hCMEC/D3 WT cells with mApoE-NL and Cholera toxin B subunit (CTB), which has long been considered a caveolae-mediated endocytosis marker (Schnitzer J.A. et al., 1996; Shajahan A.N. et al., 2004). We detected partial co-localization between NL and CTB associated fluorescence signals, thus suggesting a common endocytic mechanism accounting for at least partial NL and CTB internalization.

Recent studies demonstrated that different mechanisms could be involved in CTB uptake, such as clathrin mediated endocytosis and clathrin and caveolin independent endocytosis pathways (CLIC/GEEC pathways), and that the CTB uptake mechanism can vary in different cell type (Kirkham M. et al., 2005). We achieved 40% reduction in mApoE-NL

uptake following caveolin1 down-regulation. It remains to be clarified if the residual amount of caveolin1 protein or if other endocytic mechanisms account for the residual 60% of internalized mApoE-NL. Indeed, we detected a partial co-localization between mApoE-NL and CTB and thus we cannot exclude that multiple endocytosis pathways are involved in mApoE-NL uptake. For example, caveolin1 has long been considered necessary and sufficient for caveolae formation but recent studies argue that caveolin1 association with caveolae is not strictly related to caveolin1 involvement in the endocytosis process. Thus, the relationship between caveolin1 and caveolae mediated endocytosis has still to be completely assessed (Doherty G.J. and McMahon H.T., 2009). Finally, endocytosis is a redundant process, and blockade of one pathway can lead to the up-regulation of the others (Doherty G.J. and McMahon H.T., 2009).

Further work will be aimed at reducing caveolin1 residual protein content in hCMEC/D3 cells and at achieving concurrent down-regulation of combinations of proteins specifically involved in distinct endocytosis pathways. Thus, cells concurrently inhibited for mixed combinations of pathways would be developed. Batteries of experiments in these cells might allow a better understanding of the contribution of each single pathway in the internalization of differentially functionalized NL.

6 - CONCLUSIONS

Our results suggest that both PA-mApoE-NL and curcumin derivative3-TAT-NL might offer an attractive mean for both therapy and diagnosis of AD, due to their high capability to bind Aβ and permeability across cerebral microvascular endothelial cell monolayer. PA-mApoE-NL and curcumine deirvative3-TAT-NL might be thus considered promising tools for implementing further strategies for drug and contrast agent delivery to the AD-brain. Moreover, we studied the ability of ApoE-NL to enhance the transport of a drug payload through endothelial brain capillary cell monolayer. The permeability of a tritiated curcumin derivative was enhanced after its entrapment into ApoE-NL, in particular those functionalized with the dimer (dApoE). dApoE-NL appear particularly suitable for implementing further strategies for drug brain targeting.

Due to the limitations of our *in vitro* approaches, further studies, based on in vivo experiments, will be required to evaluate our engineered NL suitability for future clinical exploitation.

Within this study we also investigated the NL cellular uptake mechanisms within BBB derived endothelial cells. According to our preliminary results, caveolae-mediated endocytosis pathway likely account for 40% of mApoE-NL cellular uptake. Further experiments will be required to confirm these data and to assess the involvement of other endocytic mechanisms in the uptake of ApoE and TAT functionalized NL.

7 - ACKNOWLEDGMENTS

I want to thank my PhD tutor, Prof. Guido Cavaletti, for supporting me in these years.

I want to thank Dr. Giulio Sancini, Dr. Francesca Ornaghi, Dr. Roberta Dal Magro, Dr. Sonny Michael Assennato, Dr. Anna Brambilla and all the people who contributed to this thesis. Their work and their constant support has been fundamental for carrying on my research project in these years.

I thank the laboratory of Prof. Masserini, in particular Dr. Francesca Re and Dr. Maria Gregori, for providing nanoliposomes.

I thank Dr. Francesca Farina for Western Blot experiments, Dr. Veronica Sansoni for amplification and purification of plasmidic vectors, and Dr. Roberta Rigolio for FACS analysis.

I thank Prof. Pierre-Olivier Couraud, for providing hCMEC/D3 cell line, and Dr. M. Aschner for supplying RBE4 cell line.

The here outlined investigations were supported by the European Community's Seventh Framework Programme (FP7/2007-2013) under grant agreement n° 212043, NAD Project (Nanoparticles for Therapy and Diagnosis of Alzheimer Disease).

REFERENCES

Airoldi, C., Zona, C., Sironi, E., Colombo, L., Messa, M., Aurilia, D., Gregori, M., et al. (2010). Curcumin derivatives as new ligands of Aβ peptides. *Journal of biotechnology*, *156*(4), 317–24.

Begley, D., & Brightman, M.W. (2003). Structural and functional aspects of the blood-brain barrier. In L. Prokai & K. Prokai-Tatrai (Eds.), Peptide Transport and delivery into the Central Nervous System. *Progress in Drug Research, 61*, 39-78.

Beija, M., Salvayre, R., Lauth-de Viguerie, N., & Marty, J.-D. (2012). Colloidal systems for drug delivery: from design to therapy. *Trends in biotechnology*, *30*(9), 485–96.

Bickel, U. (2005). How to Measure Drug Transport across the Blood-Brain Barrier. *NeuroRx: The Journal of the American Society for Experimental NeuroTherapeutics, 2 (1),* 15-26.

Boado, R. J., Zhang, Y., Zhang, Y., Wang, Y., & Pardridge, W. M. (2008). GDNF fusion protein for targeted-drug delivery across the human blood-brain barrier. *Biotechnology and bioengineering*, *100*(2), 387–96.

Buoso, E., Lanni, C., Schettini, G., Govoni, S., & Racchi, M. (2010). beta-Amyloid precursor protein metabolism: focus on the functions and degradation of its intracellular domain. *Pharmacological research : the official journal of the Italian Pharmacological Society*, *62*(4), 308–17.

Candela, P., Gosselet, F., Miller, F., Buee-Scherrer, V., Torpier, G., Cecchelli, R., Fenart, L., (2008). Physiological Pathway for Low-Density Lipoproteins across the Blood-Brain Barrier: Transcytosis through Brain Capillary Endothelial Cells In Vitro. *Endothelium, 15*, 254-264.

Carthew, R. W., & Sontheimer, E. J. (2009). Origins and Mechanisms of miRNAs and siRNAs. *Cell*, *136*(4), 642–55.

Caruthers, S. D., Wickline, S. a, & Lanza, G. M. (2007). Nanotechnological applications in medicine. *Current opinion in biotechnology*, *18(1)*, 26–30.

Cecchelli, R., Berezowski, V., Lundquist, S., Culot, M., Renftel, M., Dehouck, MP., Fenart, L. (2007). Modelling of the blood-brain barrier in drug discovery and development. *Nature Reviews, 6,* 650-661.

Cestelli, A., Catania, C., D'Agostino, S., Di Liegro, I., Licata, L., Schiera, G., Pitarresi, G. L., et al. (2001). Functional feature of a novel model of blood brain barrier: studies on permeation of test compounds. *Journal of controlled release : official journal of the Controlled Release Society*, *76*(1-2), 139–47.

Cornford, E. M., & Cornford, M. E. (2002). New systems for delivery of drugs to the brain in neurological disease. *Lancet Neurology, 1*, 306–315.

Dartigues, J. F. (2009). Alzheimer's disease: a global challenge for the 21st century. *Lancet neurology*, *8*(12), 1082–3.

De Boer, a G., & Gaillard, P. J. (2007). Drug targeting to the brain. *Annual review of pharmacology and toxicology*, *47*, 323–55.

Dehouck, B., Fenart, L., Dehouck, M. P., Pierce, a, Torpier, G., & Cecchelli, R. (1997). A new function for the LDL receptor: transcytosis of LDL across the blood-brain barrier. *The Journal of cell biology*, *138*(4), 877–89.

Derossi, D., Calvet, S., Trembleau, A., Brunissen, A., Chassaing, G., Prochiantz, A., 1996. Cell internalization of the third helix of the Antennapedia homeodomain is receptor independent. *J. Biol. Chem. 271*, 18188–18193

Dharmawardhane, S., Schürmann, a, Sells, M. a, Chernoff, J., Schmid, S. L., & Bokoch, G. M. (2000). Regulation of macropinocytosis by p21-activated kinase-1. *Molecular biology of the cell*, *11*(10), 3341–52.

Doherty, G. J., & McMahon, H. T. (2009). Mechanisms of endocytosis. *Annual review of biochemistry*, *78*, 857–902.

Dyer, C. a, Cistola, D. P., Parry, G. C., & Curtiss, L. K. (1995). Structural features of synthetic peptides of apolipoprotein E that bind the LDL receptor. *Journal of lipid research*, *36*(1), 80–8.

Engelhardt, B., & Sorokin, L. (2009). The blood-brain and the blood-cerebrospinal fluid barriers: function and dysfunction. *Seminars in immunopathology*, *31*(4), 497–511.

Ferri, C. P., Prince, M., Brayne, C., Brodaty, H., Fratiglioni, L., Ganguli, M., Hall, K., et al. (2005). Global prevalence of dementia: a Delphi consensus study. *Lancet*, *366*, 2112–7.

Ford, M. G. J., Mills, I. G., Peter, B. J., Vallis, Y., Praefcke, G. J. K., Evans, P. R., & McMahon, H. T. (2002). Curvature of clathrin-coated pits driven by epsin. *Nature*, *419*, 361–6.

Gabathuler, R. (2009). Approaches to transport therapeutic drugs across the blood-brain barrier to treat brain diseases. *Neurobiology of disease*, *37*(1), 48–57.

Gobbi, M., Re, F., Canovi, M., Beeg, M., Gregori, M., Sesana, S., Sonnino, S., et al. (2010). Lipid-based nanoparticles with high binding affinity for amyloid-beta1-42 peptide. *Biomaterials*, *31*(25), 6519–29.

Grassart, A., Dujeancourt, A., Lazarow, P. B., Dautry-Varsat, A., & Sauvonnet, N. (2008). Clathrin-independent endocytosis used by the IL-2 receptor is regulated by Rac1, Pak1 and Pak2. *EMBO reports*, *9*(4), 356–62.

Grassart, A., Meas-Yedid, V., Dufour, A., Olivo-Marin, J.-C., Dautry-Varsat, A., & Sauvonnet, N. (2010). Pak1 phosphorylation enhances cortactin-N-WASP interaction in clathrin-caveolin-independent endocytosis. *Traffic (Copenhagen, Denmark)*, *11*(8), 1079–91.

Gumbleton, M., & Audus, K. L. (2001). Progress and limitations in the use of in vitro cell cultures to serve as a permeability screen for the blood-brain barrier. *Journal of pharmaceutical sciences*, *90*(11), 1681–98.

Hawkins, B. T., & Davis, T. P. (2005). The Blood-Brain Barrier / Neurovascular Unit in Health and Disease. *Pharmacological Reviews 57*(2), 173–185.

Hill, M. M., Bastiani, M., Luetterforst, R., Kirkham, M., Kirkham, A., Nixon, S. J., Walser, P., et al. (2008). PTRF-Cavin, a conserved cytoplasmic protein required for caveola formation and function. *Cell*, *132*(1), 113–24.

Hillaireau, H., & Couvreur, P. (2009). Nanocarriers' entry into the cell: relevance to drug delivery. *Cellular and molecular life sciences : CMLS*, *66*(17), 2873–96.

Huber, J. D., Egleton, R. D., & Davis, T. P. (2001). Molecular physiology and pathophysiology of tight junctions in the blood-brain barrier. *Trends in neurosciences*, *24*(12), 719–25.

Kim, H. R., Gil, S., Andrieux, K., Nicolas, V., Appel, M., Chacun, H., Desmaële, D., et al. (2007). Low-density lipoprotein receptor-mediated endocytosis of PEGylated nanoparticles in rat brain endothelial cells. *Cellular and molecular life sciences : CMLS*, *64*(3), 356–64.

Kirkham, M., Fujita, A., Chadda, R., Nixon, S. J., Kurzchalia, T. V., Sharma, D. K., Pagano, R. E., et al. (2005). Ultrastructural identification of uncoated caveolin-independent early endocytic vehicles. *The Journal of cell biology*, *168*(3), 465–76.

Kirkham, M., & Parton, R. G. (2005). Clathrin-independent endocytosis: new insights into caveolae and non-caveolar lipid raft carriers. *Biochimica et biophysica acta*, *1745*(3), 273–86.

Li, G.-H., Li, W., Mumper, R. J., & Nath, A. (2012). Molecular mechanisms in the dramatic enhancement of HIV-1 Tat transduction by cationic liposomes. *FASEB journal : official publication of the Federation of American Societies for Experimental Biology*, *26*(7), 2824–34.

Liberali, P., Kakkonen, E., Turacchio, G., Valente, C., Spaar, A., Perinetti, G., Böckmann, R. a, et al. (2008). The closure of Pak1-dependent macropinosomes requires the phosphorylation of CtBP1/BARS. *The EMBO journal*, *27*(7), 970–81.

Liebner, S., Corada, M., Bangsow, T., Babbage, J., Taddei, A., Czupalla, C. J., Reis, M., et al. (2008). Wnt/beta-catenin signaling controls development of the blood-brain barrier. *The Journal of cell biology*, *183*(3), 409–17.

Lippman, Z., & Martienssen, R. (2004). The role of RNA interference in heterochromatic silencing. *Nature*, *431*, 364–70.

Markoutsa, E., Pampalakis, G., Niarakis, A., Romero, I. a, Weksler, B., Couraud, P.-O., & Antimisiaris, S. G. (2011). Uptake and permeability studies of BBB-targeting immunoliposomes using the hCMEC/D3 cell line. *European journal of pharmaceutics and biopharmaceutics*, *77*(2), 265–74.

Matsuzaki, K. (2007). Physicochemical interactions of amyloid beta-peptide with lipid bilayers. *Biochimica et biophysica acta*, *1768*(8), 1935–42.

Moghimi, S. M., Hunter, a C., & Murray, J. C. (2005). Nanomedicine: current status and future prospects. *FASEB journal : official publication of the Federation of American Societies for Experimental Biology*, *19*(3), 311–30.

Mourtas, S., Canovi, m., Zona, C., Aurilia, D., Niarakis, A., La Ferla, B., Salmona, M., Nicotra, F., Gobbi, M., Antimisiaris, S.G. (2011). Curcumin-decorated nanoliposomes with very high affinity for amyloid-β1-42 peptide. *Biomaterials*, *32*, 1635-1645.

Narlawar, R., Pickhardt, M., Leuchtenberger, S., Baumann, K., Krause, S., Dyrks, T., Weggen, S., et al. (2008). Curcumin-derived pyrazoles and isoxazoles: Swiss army knives or blunt tools for Alzheimer's disease? *ChemMedChem*, *3*(1), 165–72.

Neuwelt, E., Abbott, N. J., Abrey, L., Banks, W. a, Blakley, B., Davis, T., Engelhardt, B., et al. (2008). Strategies to advance translational research into brain barriers. *Lancet neurology*, *7*(1), 84–96.

Nevins, A. K., & Thurmond, D. C. (2006). Caveolin-1 functions as a novel Cdc42 guanine nucleotide dissociation inhibitor in pancreatic beta-cells. *The Journal of biological chemistry*, *281*(28), 18961–72.

Parton, R. G., & Simons, K. (2007). The multiple faces of caveolae. *Nature reviews. Molecular cell biology*, *8*(3), 185–94.

Pelkmans, L., Bürli, T., Zerial, M., & Helenius, A. (2004). Caveolin-stabilized membrane domains as multifunctional transport and sorting devices in endocytic membrane traffic. *Cell*, *118*(6), 767–80.

Pinzón-Daza, M., Garzón, R., Couraud, P., Romero, I., Weksler, B., Ghigo, D., Bosia, a, et al. (2012). The association of statins plus LDL receptor-targeted liposome-encapsulated doxorubicin increases in vitro drug delivery across blood-brain barrier cells. *British journal of pharmacology*, *167*(7), 1431–1447.

Poller, B., Gutmann, H., Krähenbühl, S., Weksler, B., Romero, I., Couraud, P.-O., Tuffin, G., et al. (2008). The human brain endothelial cell line hCMEC/D3 as a human blood-brain barrier model for drug transport studies. *Journal of Neurochemistry*, *107*(5), 1358–1368.

Ray, B., Bishtb, S., Maitrad, A., Maitrab, A., Lahiria, D.K. (2011). Neuroprotective and Neurorescue Effects of a Novel Polymeric Nanoparticle Formulation of Curcumin (NanoCurc™) in the Neuronal Cell Culture and Animal Model: Implications for Alzheimer's Disease. *J Alzheimers Dis.*, 23(1), 61–77.

Re, F., Cambianica, I., Zona, C., Sesana, S., Gregori, M., Rigolio, R., La Ferla, B., Nicotra, F., et al. (2011). Functionalization of liposomes with ApoE-derived peptides at different density affects cellular uptake and drug transport across a blood-brain barrier model. *Nanomedicine: Nanotechnology, Biology and Medicine*, *7*, 551-9.

Redzic, Z. (2011). Molecular biology of the blood-brain and the blood-cerebrospinal fluid barriers: similarities and differences. *Fluids and barriers of the CNS*, *8*(1), 3.

Regina, a, Koman, a, Piciotti, M., El Hafny, B., Center, M. S., Bergmann, R., Couraud, P. O., et al. (1998). Mrp1 multidrug resistance-associated protein and P-glycoprotein expression in rat brain microvessel endothelial cells. *Journal of neurochemistry*, *71*(2), 705–15.

Regina, a, Morchoisne, S., Borson, N. D., McCall, a L., Drewes, L. R., & Roux, F. (2001). Factor(s) released by glucose-deprived astrocytes enhance glucose transporter expression and activity in rat brain endothelial cells. *Biochimica et biophysica acta*, *1540*(3), 233–42.

Rosenthal, J. a, Chen, H., Slepnev, V. I., Pellegrini, L., Salcini, a E., Di Fiore, P. P., & De Camilli, P. (1999). The epsins define a family of proteins that interact with components of the clathrin coat and contain a new protein module. *The Journal of biological chemistry*, *274*(48), 33959–65.

Roux, F., & Couraud, P.-O. (2005). Rat Brain Endothelial Cell Lines for the Study of Blood–Brain Barrier Permeability and Transport Functions. *Cellular and Molecular Neurobiology*, *25*(1), 41–57.

Saitou, M., Furuse, M., Sasaki, H., Schulzke, J. D., Fromm, M., Takano, H., Noda, T., et al. (2000). Complex phenotype of mice lacking occludin, a component of tight junction strands. *Molecular biology of the cell*, *11*(12), 4131–42.

Sanvicens, N., & Marco, M. P. (2008). Multifunctional nanoparticles--properties and prospects for their use in human medicine. *Trends in biotechnology*, *26*(8), 425–33.

Sauer, I., Dunay, I. R., Weisgraber, K., Bienert, M., & Dathe, M. (2005). An apolipoprotein E-derived peptide mediates uptake of sterically stabilized liposomes into brain capillary endothelial cells. *Biochemistry*, *44*(6), 2021–9.

Scherrmann, J. M. (2002). Drug delivery to brain via the blood-brain barrier. *Vascular pharmacology*, *38*(6), 349–54.

Schnitzer, J. E., Oh, P., & Mcintosh, D. P. (1996). Role of GTP Hydrolysis in Fission of Caveolae directly from Plasma Membranes. *Science*, *274*, 239-242.

Selkoe, D. J. (2001). Alzheimer ' s disease results from the cerebral accumulation and cytotoxicity of amyloid β -protein, *Journal of Alzheimer's Disease*, *3*, 75–80.

Shajahan, A. N., Tiruppathi, C., Smrcka, A. V., Malik, A. B., & Minshall, R. D. (2004). Gβγ activation of Src induces caveolae-mediated endocytosis in endothelial cells. *The Journal of biological chemistry*, *279*(46), 48055–62.

Swerdlow, R. H. (2007). Pathogenesis of Alzheimer ' s disease. *Clinical Interventions in Aging*, *2(3)*, 347–359.

Sönnichsen, B., De Renzis, S., Nielsen, E., Rietdorf, J., & Zerial, M. (2000). Distinct membrane domains on endosomes in the recycling pathway visualized by multicolor imaging of Rab4, Rab5, and Rab11. *The Journal of cell biology*, *149*(4), 901–14.

Taddei, A., Giampietro, C., Conti, A., Orsenigo, F., Breviario, F., Pirazzoli, V., Potente, M., et al. (2008). Endothelial adherens junctions control tight junctions by VE-cadherin-mediated upregulation of claudin-5. *Nature cell biology*, *10*(8), 923–34.

Terai, T., Nishimura, N., Kanda, I., Yasui, N., & Sasaki, T. (2006). JRAB / MICAL-L2 Is a Junctional Rab13-binding Protein Mediating the Endocytic Recycling of Occludin. *Molecular Biology of the Cell 17*(May), 2465–2475.

Terasaki, T., Ohtsuki, S., Hori, S., Takanaga, H., Nakashima, E., & Hosoya, K. (2003). New approaches to in vitro models of blood-brain barrier drug transport. *Drug discovery today*, *8*(20), 944–54.

Togo, T., Akiyama, H., Iseki, E., Kondo, H., Ikeda, K., Kato, M., Oda, T., et al. (2002). Occurrence of T cells in the brain of Alzheimer's disease and other neurological diseases. *Journal of Neuroimmunology*, *124*(1-2), 83–92.

Uyttendaele, H., Closson, V., Wu, G., Roux, F., Weinmaster, G., & Kitajewski, J. (2000). Notch4 and Jagged-1 induce microvessel differentiation of rat brain endothelial cells. *Microvascular research*, *60*(2), 91–103.

Vanden Broeck, D., & De Wolf, M. (2006). Selective blocking of clathrin-mediated endocytosis by RNA interference: epsin as target protein. *BioTechniques*, *41*(4), 475–484.

Vazquez, F., Vaucheret, H., Rajagopalan, R., Lepers, C., Gasciolli, V., Mallory, A. C., Hilbert, J.-L., et al. (2004). Endogenous trans-acting siRNAs regulate the accumulation of Arabidopsis mRNAs. *Molecular cell*, *16*(1), 69–79.

Wadhwa, R., Kaul, S. C., Miyagishi, M., & Taira, K. (2004). Know-how of RNA interference and its applications in research and therapy. *Mutation research*, *567*(1), 71–84.

Wang, Y.-J., Zhou, H.-D., & Zhou, X.-F. (2006). Clearance of amyloid-beta in Alzheimer's disease: progress, problems and perspectives. *Drug discovery today*, *11*(19-20), 931–8.

Weiss, N., Miller, F., Cazaubon, S., & Couraud, P.-O. (2009). The blood-brain barrier in brain homeostasis and neurological diseases. *Biochimica et biophysica acta*, *1788*(4), 842–57.

Weksler, B. B., Subileau, E. a, Perrière, N., Charneau, P., Holloway, K., Leveque, M., Tricoire-Leignel, H., et al. (2005). Blood-brain barrier-specific properties of a human adult brain endothelial cell line. *FASEB journal : official publication of the Federation of American Societies for Experimental Biology*, *19*(13), 1872–4.

Wolburg, H., Noell, S., Mack, A., Wolburg-Buchholz, K., & Fallier-Becker, P. (2009). Brain endothelial cells and the glio-vascular complex. *Cell and tissue research*, *335*(1), 75–96.

Zensi, A., Begley, D., Pontikis, C., Legros, C., Mihoreanu, L., Wagner, S., Büchel, C., et al. (2009). Albumin nanoparticles targeted with Apo E enter the CNS by transcytosis and are delivered to neurones. *Journal of controlled release : official journal of the Controlled Release Society*, *137*(1), 78–86.

Zhang, Y., & Pardridge, W. M. (2006). Blood-brain barrier targeting of BDNF improves motor function in rats with middle cerebral artery occlusion. *Brain research*, *1111*(1), 227–9.

Zlokovic, B. V. (2008). New Therapeutic Targets in the Neurovascular Pathway in Alzheimer ' s Disease, *Neurotherapeutics: The Journal of the American Society for Experimental NeuroTherapeutics*, *5*, 409–414.

.